Physico-Chemical Behaviour of Astrochemical Ices

A thesis submitted in partial fulfilment of the requirements for the degree of

Doctor of Philosophy

by

Wafikul Khan

(Roll No: 20330024)

Under the guidance of

Prof. Bhalamurugan Sivaraman

Professor

Atomic Molecular and Optical Physics Division

Physical Research Laboratory, Ahmedabad, India

Discipline of Physics

Indian Institute of Technology, Gandhinagar, India

2025

THESIS APPROVAL

Certified that the thesis titled

Physico-Chemical Behaviour of Astrochemical Ices

Submitted by **Wafikul Khan** (Roll no: **20330024**) to the **Indian Institute of Technology, Gandhinagar,** is approved for the award of the degree of Doctor of Philosophy.

Date-15/10/2025
Place- Ahmedabad, Gujarat,

India

Prof. Rajakumar Balla
External Examiner
Indian Institute of Technology (IIT),
Madras, Tamil Nadu.

Prof. Anirban Mondal
FDC Member
Indian Institute of Technology (IIT),
Gandhinagar, Gujarat

Dr. Rajesh Kumar Kushawaha
DSC and FDC Member
PRL,
Ahmedabad, Gujarat

Dr. Kinsuk Acharyya
DSC and FDC Member
PRL,
Ahmedabad, Gujarat

Dr. Prashant Kumar
DSC and FDC Member
PRL,
Ahmedabad, Gujarat

Prof. Bhalamurugan Sivaraman
PhD supervisor and FDC Member
PRL,
Ahmedabad, Gujarat

Dedicated to my Parents

DECLARATION

I hereby declare that this thesis titled "Physico-Chemical Behaviour of Astrochemical Ices" is carried out by me to fulfil the requirement of PhD degree at Atomic, Molecular and Optical Physics division at Physical Research Laboratory under the supervision of Prof. Bhalamurugan Sivaraman. All information and facts provided in this thesis are correct to the best of my knowledge. I also declare that wherever I have borrowed any ideas or results of someone else, I have properly cited the original sources.

Date-

Wafikul Khan

Roll No- 20330024

Discipline of Physics

Indian Institute of Technology, Gandhinagar,

Gandhinagar, Gujarat-382355

CERTIFICATE

It is certified that the work contained in the thesis titled "Physico-Chemical Behaviour of Astrochemical Ices" by Mr. Wafikul Khan (Roll no: 20330024) has been carried out under my supervision and that this work has not been submitted elsewhere for a degree.

Prof. Bhalamurugan Sivaraman
(Thesis Supervisor)
Professor, Atomic Molecular and Optical Physics Division,
Physical Research Laboratory,
Ahmedabad, India

Acknowledgements:

The Ph.D. journey is a truly transformative experience filled with moments of excitement and passion, yet also accompanied by periods of frustration and daunting challenges. These diverse experiences collectively shape one's evolution into a researcher. Reaching the culmination of this long and enriching path would not have been possible without the unwavering support and contributions of many remarkable individuals. I am deeply thankful to each and every one of you who stood by me, offering your help, encouragement, and guidance throughout this journey.

First and foremost, I am profoundly grateful to my Ph.D. supervisor, Prof. Bhalamurugan Sivaraman. His visionary outlook, deep expertise, and unwavering mentorship have been fundamental in guiding the course of my doctoral research. Throughout this journey, his patience, encouragement, and continuous support have been a constant source of motivation. I am especially thankful for his invaluable advice, constructive feedback, and for nurturing my scientific curiosity. His dedication to fostering a culture of excellence and his ability to instill confidence in his students have had a lasting impact on my academic development and professional aspirations.

I sincerely thank my Doctoral Studies Committee (DSC) members—Dr. Kinsuk Acharyya, Dr. Rajesh Kumar Kushawaha, and Dr. Prashant Kumar—for their insightful suggestions and steady support throughout my Ph.D. journey. Their critical feedback and thought-provoking inputs during the DSC seminars helped me to view my work from broader and more nuanced perspectives. A heartfelt

thanks to Prof. R. P. Singh for his ever-helpful and encouraging attitude, both in academic and personal matters; his warmth and positivity have always uplifted me. I express my deepest gratitude to Prof. Anil Bhardwaj, Director of PRL, and Prof Nigel Mason for their constant support and encouragement throughout my doctoral journey. I am also grateful to Prof. Pallamraju, Dean of PRL; Dr. Bhushit Vaishnav, Head of Academic Services; and the entire academic committee of PRL. I deeply appreciate the contributions of various administrative divisions—accounts, purchase, library, administration, CNIT, dispensary & transport— whose support made my research smooth and efficient. A special mention to the Thaltej canteen, particularly Rahul bhai, for always ensuring meals are available even at odd hours, and to the housekeeping team for their tireless work in maintaining a clean and healthy campus and hostel environment.

I am immensely thankful to all my teachers from Bankura Banga Vidyalay, Bankura Christian College and The University of Burdwan. Your guidance and faith in my potential have inspired me throughout my academic life.

To my friends back there in Bankura and Burdwan: Imran, Rajesh, Enamul, Rajdip, Animesh, Pallabi, Nawshad, Motahar, Asutosh, Roupya, Soumen, Arabinda, Anjan, Debraj and Suvendu- Thank you for your unwavering love, care and support throughout.

A Ph.D. journey is not just about research and perseverance, it is also about the people who walk beside you, making the experience unforgettable. Over the past five years, my time at the PRL Thaltej Hostel has been deeply enriched by the

wonderful friendships I have made and the vibrant community I have been fortunate to be a part of. I extend my heartfelt thanks to my incredible friends, Arup Chakraborty (Arup C), Trinesh & Debashis for their constant presence in my PhD life. Arup C's sharp wit and dark humor, Debashis's affectionate nature, and Trinesh's thoughtful care made the tough times easier and the good times even better. I am grateful to my other batch mates- Sanjay, Arup M, Aditya, Guru Bhai, Kamran, Dharmendra, Malika, Ananya, Sandeep, Mansi, Akansha, and Chandrima for their friendship and positivity they shared throughout this journey. My research would not have taken shape the way it did without the support of an excellent work environment. Thanks to my amazing lab members I have worked with—Dr. Vijayan, Jaya Krishna Meka (JK), Dr. Arijit, Dr. Surendra Sir, Dr. Ragav, Dr. Dipen, Shivanshi, Ganapathy, Aswin & Dr. Bratati, thank you for your invaluable guidance, camaraderie, and encouragement. A heartfelt special thanks to JK whose unwavering presence and support through every phase of my time in PRL meant more than words can express. A big thank–you to Rutuj and Pooja Ma'am for all the joyful memories, tasty food, and great companionship. A huge shout out to my seniors Ayan da, Shefali di, Madhu bhaiya, Ankit bhaiya (fitness expert), Sana Di, Vikas bhai, Soumya, Shantanu, Vineet, Kimi, Vardaan, Birendra, Tanmoy Da, Supriya Da, and Ramanuj Da, Sudipta Da for creating such a lively, welcoming, and fun-filled atmosphere at PRL. To my enthusiastic and energetic juniors- Narendra, Chahat, Varsha, Kiran, Satyendra, Sahil, Nitin, Aarti, Rachita, & Soumik, thank you for adding an extra spark to my everyday life with your presence and positivity.

To my beloved parents and family, words cannot adequately express my gratitude. Your unwavering love, constant encouragement, tireless support, and countless sacrifices have been the foundation of my strength throughout this entire journey. A special thanks to my elder brother Toufikul whose sacrifices and encouragement have helped shape the person I am today. And to my beloved wife, Mukulika thank you for being my pillar of strength and constant companion. Your support has enabled me to pursue and achieve everything I have dreamed of. The prayers and blessings of my family have carried me through the most challenging times.

Last but certainly not least, to all those individuals whom I may have unintentionally overlooked in this acknowledgement, please know that your support has been deeply appreciated and was instrumental in the successful completion of this thesis.

Thank you for being a part of this incredible and meaningful journey.

Abstract:

The interstellar medium (ISM), the space between the stars within a galaxy, is a chemically rich environment where more than 330 molecules have been identified. The molecules range from simple diatomic molecules to complex ones, such as fullerene (C_{60}/C_{70}). Within the ISM, there exist molecular clouds where the physical conditions (density, temperature, radiation) are such that molecules can exist in both the ice phase and the gas phase. These molecular ices include water (H_2O), carbon monoxide (CO), carbon dioxide (CO_2), ammonia (NH_3), methanol (CH_3OH), and even complex molecules like ethylene glycol [$(CH_2OH)_2$]. These ices have been detected not only in the ISM but also in various solar system bodies such as outer solar system planets, their moons, and in comets. The presence of these simple to complex molecular ices has been confirmed for a long time; the James Webb Space Telescope (JWST) is providing even finer details about their morphology. One of the fundamental questions in the field of astrochemistry is the synthesis of complex molecules in these cold environments.

The morphology and stability are the key parameters that govern the reactions in these harsh environments. The amorphous ice, being more porous possess greater diffusion of other molecules inside it and react more efficiently than the crystalline one. The morphological phase behaviour and stability of ice like pure water ice is well characterized at different temperatures relevant to the astrochemical conditions. But in reality the ices are mixed with other ices, some even capable of interacting with each other. Inspite of this the effect of intermolecular interactions like hydrogen bonding between molecules on the stability and morphology of molecular ices have been least explored. On the other hand, there exist molecules

such as pure NH_3, whose morphological phase is under debate since the last seven decades and awaiting a clear picture in these environments.

In the ISM, the energetic processing results in the formation of complex molecular ices from the simple ones. Still, an intriguing puzzle is the formation of Polycyclic Aromatic Hydrocarbon (PAHs) at this low temperature. Although the formation of PAHs is well established in high-temperature environments, such as carbon-rich stars or Earth, their presence in various environments, including low-temperature environments, raises questions about their formation pathways in these environments. The known pathways at low temperatures are neither very effective for the formation of PAHs, nor do they account for their high abundance. So some alternative pathways must exist in this environment.

Laboratory simulation is one of the key processes for studying the behaviour of molecules under astrochemical conditions. We have used the Simulator for Astromolecules at Low Temperature (SALT) setup which can mimic the low temperature astrochemical conditions. We have studied the behaviour of the molecular ices from 10 K to their sublimation temperature using in-situ IR spectroscopy. Electron irradiation experiments were carried out in ASTRID2 synchrotron facility in Aarhus University, Denmark. CO ice was irradiated with 2 keV electrons and the resultant ice after irradiation was heated up to room temperature, the ice was studied in situ in VUV/UV spectroscopy. The residue on the substrate after irradiation was studied using High Resolution Transmission Electron Microscopy (HRTEM).

A major finding of the thesis is the strong effect of hydrogen bonding between water and ethylene glycol (EG) on the phase and sublimation of water ice. In a

coexistence scenario of EG and water, water ice is seen to be present at a temperature 60 K higher than its own sublimation temperature in an amorphous phase. This is applicable to the cometary ices where water ice will be present in comets at a lower distance than previously known, that too in an amorphous phase which is more reactive. So, water can take part in reactions in an elevated temperature.

Another major finding was the effect of diols such as EG and 1,3-propanediol on the condensation temperature of water ice. Water ice could be condensed at a temperature more than its sublimation temperature on to the grains where a preexisting layer of diol is present. The formed water ice has been stable up to the sublimation temperature of the diols. This phenomena makes it important to consider water ice freezing out on the dust grains at elevated temperatures.

This thesis also presents a new and novel pathway for low temperature formation of PAHs from the second most abundant ice, CO ice upon electron irradiation at 10 K. The VUV/UV spectrum and the imaging of residue have confirmed the synthesis of ring containing graphite/graphene. This can serve as an efficient pathway for PAH formation at low temperature.

A comprehensive investigation into the phase behaviour of NH_3 ice across a range from 10 K to its sublimation temperature revealed that the morphology of the NH_3 ice depends on the deposition temperature and thermal processing. The ice can be in the amorphous, metastable and crystalline phases depending on the thermal history. This provides a strong framework for interpreting astronomical observations on NH_3 ice in the ISM and solar system ices.

The thesis advances our knowledge on the molecular interactions, ice morphology, and energetic processing of ices in the astrochemical conditions.

Table of Contents

List of Figures:

List of Tables:

List of Abbreviations:

A	Band strength (infrared spectroscopy)
ALMA	Atacama Large Millimeter/submillimeter Array
ASTRID2	Aarhus Storage Ring in Denmark 2 (Synchrotron facility)
CNM	Cold Neutral Medium
DIB	Diffuse Interstellar Band
eV	Electron Volt
FIR	Far Infrared
FTIR	Fourier Transform Infrared (Spectroscopy/Spectrometer)
GHz,MHz	Gigahertz, Megahertz (frequency unit)
HIM	Hot Ionized Medium
HR-TEM	High-Resolution Transmission Electron Microscopy
IR	Infrared
ISM	Interstellar Medium
JIRAM	Jovian Infrared Auroral Mapper (Juno mission)
JWST	James Webb Space Telescope
K	Kelvin (temperature unit)
LiF	Lithium Fluoride (substrate)
mbar	Millibar (pressure unit)
MCT	Mercury Cadmium Telluride (detector)
NIR	Near Infrared
NIRSpec	Near-Infrared Spectrograph (JWST instrument)
OFHC	Oxygen-Free High Conductivity (Copper)
PRL	Physical Research Laboratory

PMT	Photomultiplier Tube
PAHs	Polycyclic Aromatic Hydrocarbon(s)
ROSINA	Rosetta Orbiter Sensor for Ion and Neutral Analysis
SALT	Simulator for Astromolecules at Low Temperature
UHV	Ultrahigh Vacuum
UV	Ultraviolet
VUV	Vacuum Ultraviolet
WIM	Warm Ionized Medium
WNM	Warm Neutral Medium
ZnSe	Zinc Selenide (substrate)

Chapter 1 Introduction

1.1 Astrochemistry:

Astrochemistry is the study of the chemical processes occurring in space, particularly those that govern the formation, evolution, and destruction of molecules in various astrophysical environments. If we begin with a brief history, up to 1930s, it was well known that clouds of gas exist in the space between the stars, commonly referred to as interstellar medium (ISM), but whether these clouds contained molecules or not was unclear. In fact, Eddington in 1926 speculated that the possibility of finding molecules in these harsh environments is nearly zero (Eddington, 1988). However, this view changed dramatically in 1937 with the first molecular detection in the ISM, the methylidyne (CH) radical (Dunham Jr, 1937, Swings and Rosenfeld, 1937). This breakthrough sparked an accelerated search for interstellar molecules. Today, over 330 molecules have been identified in the interstellar and circumstellar medium, ranging from simple diatomic species to large and complex structures such as fullerenes (C_{60}, C_{70}), as catalogued by the Cologne Database for Molecular Spectroscopy[1]. Another interesting identification was the diffuse interstellar bands (DIBs) (Heger, 1922) , which is a series of hundreds of absorption features in the near ultraviolet and mid infrared spectra of stars when their light passes through the diffuse interstellar medium. It was believed that the large carbon containing molecules like fullerenes and polycyclic aromatic hydrocarbons (PAHs) can be the source of these DIBs

[1] https://cdms.astro.uni-koeln.de/

(Herbig, 1995, Ehrenfreund, 1999). Campbell et al., 2015 and Linnartz et al., 2020 have attributed a DIB to the big molecule C_{60}+, the source of hundreds of other DIBs is yet to be understood.

The study of the chemical behaviour of the molecules and the processes associated which give rise to the formation of such complex molecules in the ISM is covered in the field of astrochemistry.

1.2 Interstellar medium:

The ISM is the matter and radiation that exist in the space between stars. It is mainly made up of 99% gas (atomic, molecular and ionized) and 1% dust (silicate, carbonaceous particles). This material is distributed inhomogeneously throughout the galaxy, creating regions with vastly different physical and chemical conditions. The ISM is predominantly composed of neutral hydrogen (93.38%) and helium (6.49%), while heavier elements—often referred to as "metals" in astronomical terminology, including oxygen, carbon, and nitrogen—make up only about 0.11% (Kaiser, 2002). To better understand the diverse environments within the ISM, it is commonly classified into three main phases:

1. **Cold Neutral Medium (CNM)** – often referred to as molecular or atomic clouds;
2. **Warm Neutral/Ionized Medium (WNM/WIM)** – transitional zones with partially ionized or neutral gas;
3. **Hot Ionized Medium (HIM)** – highly ionized, low-density gas also known as coronal gas.

Among these, the CNM plays a particularly important role in astrochemistry, as it harbours molecular clouds, which vary widely in density, temperature, and radiation exposure. The densest of these, known as dark molecular clouds or dense molecular clouds, are shielded from ultraviolet (UV) radiation by interstellar dust, allowing complex chemistry to proceed. Conversely, diffuse clouds are exposed to ambient starlight, while translucent clouds occupy an intermediate regime.

A summary of the typical physical conditions and molecular composition across different types of molecular clouds is given in Table 1.1:

Table 1.1 Molecular clouds in ISM (Kaiser, 2002, Snow and McCall, 2006)

Molecular Clouds	**Density (cm^{-3})**	**Temperature (K)**	**Molecules**
Diffuse Atomic Clouds	1-100	30-100	Atoms (H, C+), no stable molecule
Diffuse Molecular Clouds	$10 – 10^2$	30-100	simple molecules H_2,CH+, CH, CN, C_2, OH, CO, HCO+, HCN

Translucent Clouds	$10^2 – 10^3$	10-50	simple molecules H_2,CH+, CH, CN, C_2, OH, CO, HCO+, HCN, C_3
Dense Molecular Clouds	$10^2 – 10^6$	10–50	carbon-rich, linear and cyclic molecules with up to 13 atoms

1.2.1 Diffuse Atomic Clouds:

These are the clouds that are fully exposed to the interstellar radiation field, so all the molecules in these clouds are destroyed by photodissociation. Hydrogen remains in the neutral form while other atoms are mostly ionized, thereby providing abundant electrons. It can be expected that the chemistry in this region should be less, but surprisingly, most of the DIB bands seem to be developed in this region. The temperature of this region is known to be 30-100 K.

1.2.2 Diffuse Molecular Clouds:

These are the clouds where the interstellar radiation field is attenuated sufficiently such that a significant amount of molecular hydrogen remains in the molecular form. However, there is still enough interstellar radiation in these clouds to break up CO molecules and ionize atomic carbon, thereby increasing the presence of C^+. Because diffuse molecular clouds contain a large amount of H_2, chemical reactions can occur more actively. Many molecules are detected in these clouds (e.g CO, CH, CN, C_2, C_3, H_3^+, HCO^+, OH, C_2H etc). The typical

temperatures is of the orders of 30-100 K and the typical molecular density is $10\text{-}10^2$ cm^{-3}.

1.2.3 Translucent clouds:

When interstellar radiation is blocked sufficiently, carbon starts changing from its ionized form (C^+) to either neutral carbon (C) or carbon monoxide (CO). The chemistry in this stage is quite different from that in diffuse molecular clouds because there are fewer free electrons and more highly reactive neutral carbon (C) atoms available. These are known to contain H_2, CH, CH^+, CS, CN, C_2, OH, and CO, along with larger species HCN, HNC, C_2H, HCO^+, and H_2CO, etc. The typical temperature in these regions varies from 10-50 K, and the particle density is 10^2–10^3 cm^{-3}.

1.2.4 Dense Molecular clouds:

In the diffuse and translucent clouds, the chemistry is driven by photochemistry and photoionization. In the dense molecular cloud, the submicron sized dust grains shield the molecules from the interstellar radiation field. With the increasing extinction of the interstellar radiation field, carbon now becomes mostly molecular (Snow and McCall, 2006). Here the chemistry is again very different due to the presence of very less abundance of electrons and the reactive C is replaced by CO. These clouds are self-gravitating with densities of the order of 10^4 cm^{-3}. The typical temperature of these clouds are 10-50 K. these clouds are known to contain from very simple molecule like CO, H_2O, CO_2 and complex molecules like CH_3OH, ethylene glycol, PAHs etc.

The classification of molecular clouds based on their physical and chemical properties is summarized in Table 1.1, while an illustrative representation of the

chemical transitions occurring across different types of clouds is provided in Figure 1.1.

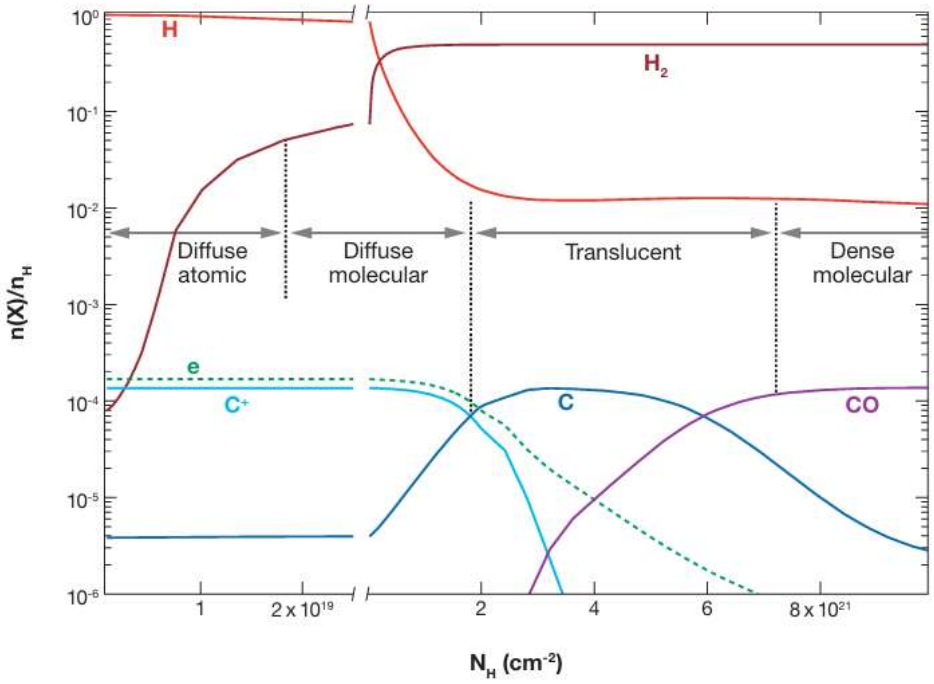

Figure 1.1 Plot of the ratio of number density of a species X to that of hydrogen vs. the column density of hydrogen. Adapted from (Snow and McCall, 2006).

In Figure 1.1, the relative abundance of various species—atomic hydrogen (H), molecular hydrogen (H_2), ionized carbon (C^+), neutral carbon (C), carbon monoxide (CO), and free electrons (e^-)—is plotted as a function of the column density of hydrogen (N_H)**.** The quantity on the y-axis, $n(X)/n_H$ represents the fractional abundance of a particular species X relative to hydrogen, and is shown across increasing values of N_H x-axis. This provides a visual summary of how the chemical composition evolves from diffuse atomic to dense molecular clouds.

As shown in the Figure 1.1, atomic hydrogen dominates at low column densities, characteristic of diffuse atomic clouds. As N_H increases, hydrogen

gradually transitions into its molecular form (H_2), indicating the onset of diffuse molecular clouds. Simultaneously, C^+ is initially abundant due to photoionization but declines as it is converted into neutral carbon (C), and eventually into carbon monoxide (CO) in well-shielded dense molecular regions. CO becomes the dominant carbon-bearing species in these dense environments where photo dissociating radiation is effectively blocked.

Various molecules detected in the ISM so far is given in Table 1.2.

Table 1.2 List of molecules detected so far in the ISM

Number of Atoms	Molecules Detected
2 atoms	CH^+, CH, CN, OH, CO, H_2, SiO, CS, SO, SiS, NS, C_2, NO, HCl, NaCl, KCl, AlCl, AlF, PN, SiC, CP, NH, SiN, SO^+, CO^+, HF, SiH, FeO, O_2, CF^+, PO, AlO, OH^+, CN^-, SH^+, SH, HCl^+, TiO, ArH^+, N_2, NO^+, NS^+, HeH^+, PO^+, SiP, FeC, MgS, NaS
3 atoms	C_3, C_2H, C_2O, C_2S, CH_2, HCN, HCO, HCO^+, HCS^+, HOC^+, H_2O, H_2S, HNC, HNO, MgCN, MgNC, N_2H^+, N_2O, NaCN, OCS, SO_2, c-SiC_2, CO_2, NH_2, H_3^+, SiCN, AlNC, SiNC, HCP, CCP, AlOH, H_2O^+, H_2Cl^+, KCN, FeCN, HO_2, TiO_2, C_2N, Si_2C, HS_2, HCS, HSC, NCO, CaNC, NCS, MgC_2, HSO, CaC_2
4 atoms	c-C_3H, l-C_3H, C_3N, C_3O, C_3S, C_2H_2, NH_3, HCCN, $HCNH^+$, HNCO, HNCS, $HOCO^+$, H_2CO, H_2CN, H_2CS, H_3O^+, c-SiC_3, CH_3, C_3N^-, PH_3, HCNO, HOCN, HSCN, H_2O_2, C_3H^+,

	HMgNC, HCCO, CNCN, HONO, MgC_2H, HCCS, HNCN, H_2NC, $HCCS^+$, CH_3^+, HCNS, $HOCS^+$, HNSO
5 atoms	**C_5, C_4H, C_4Si, l-C_3H_2, c-C_3H_2, H_2CCN, CH_4, HC_3N, HCCNC, HCOOH, H_2CNH, H_2C_2O, H_2NCN, HNC_3, SiH_4, H_2COH^+, C_4H^-, HC(O)CN, HNCNH, CH_3O, NH_4^+, H_2NCO^+, $NCCNH^+$, CH_3Cl, MgC_3N, NH_2OH, HC_3O^+, HC_3S^+, H_2C_2S, C_4S, HC(O)SH, HC(S)CN, HCCCO, NaCCCN, MgC_3N^+, HC_3N^+ , HC_3S , NC_3S**
6 atoms	**C_5H, l-H_2C_4, C_2H_4, CH_3CN, CH_3NC, CH_3OH, CH_3SH, HC_3NH^+, HCCCHO, NH_2CHO, C_5N, l-HC_4H, l-HC_4N, c-H_2C_3O, H_2CCNH, C_5N^-, HNCHCN, SiH_3CN, C_5S, MgC_4H, CH_3CO^+, C_3H_3, H_2C_3S, HCCCHS, C_5O, C_5H^+, $HCCNCH^+$, c-C_3C_2H, HC_4S, $HMgC_3N$, MgC_4H^+ , $H_2C_3H^+$, H_2C_3N , $(HO)_2CO$, H_2CNCN, NCHCCS , c-H_2C_3S**
7 atoms	**C_6H, CH_2CHCN, CH_3C_2H, HC_5N, CH_3CHO, CH_3NH_2, c-C_2H_4O, H_2CCHOH, C_6H^-, CH_3NCO, HC_5O, $HOCH_2CN$, HCCCHNH, HC_4NC, c-C_3HCCH, l-H_2C_5, MgC_5N, CH_2C_3N, NC_4NH^+, MgC_5N^+, HC_5N^+, HNC_5, $CH_2(CN)_2$, HCCCHCN, CH_3CHS**
8 atoms	**CH_3C_3N, HC(O)OCH_3, CH_3COOH, C_7H, C_6H_2, CH_2OHCHO, l-HC_6H, CH_2CHCHO, CH_2CCHCN, H_2NCH_2CN, CH_3CHNH, CH_3SiH_3, $H_2NC(O)NH_2$, $HCCCH_2CN$, HC_5NH^+, CH_2CHCCH, MgC_6H, $C_2H_3NH_2$, $(CHOH)_2$, $HC_2(H)C_4$, C_7N^-, CH_3CHCO, MgC_6H^+, Z-$(CH)_2(CN)_2$**

9 atoms	**CH_3C_4H, CH_3CH_2CN, $(CH_3)_2O$, CH_3CH_2OH, HC_7N, C_8H, $CH_3C(O)NH_2$, C_8H^-, C_3H_6, CH_3CH_2SH, CH_3NHCHO, HC_7O, HCCCHCHCN, H_2CCHC_3N, $H_2CCCHCCH$, HOCHCHCHO, HC_7N^+, $CH_2(CCH)_2$, $(CH_3)_2S$**
10 atoms	**CH_3C_5N, $(CH_3)_2CO$, $(CH_2OH)_2$, CH_3CH_2CHO, CH_3CHCH_2O, CH_3OCH_2OH, c-C_6H_4, H_2CCCHC_3N, C_2H_5NCO, $C_2H_5NH_2$ (?), HC_7NH^+, E-$CH_3CHCHCN$, Z-$CH_3CHCHCN$, $CH_3C(CN)CH_2$, CH_2CHCH_2CN, $HOCH_2C(O)NH_2$, CH_3CH_2CCH**
11 atoms	**HC_9N, CH_3C_6H, C_2H_5OCHO, $CH_3OC(O)CH_3$, $CH_3C(O)CH_2OH$, c-C_5H_6, $HOCH_2CH_2NH_2$, H_2CCCHC_4H, $C_{10}H^-$, $H_2C(CH)_3CN$**
12 atoms	**c-C_6H_6*, n-C_3H_7CN, i-C_3H_7CN, $C_2H_5OCH_3$, 1-c-C_5H_5CN, 2-c-C_5H_5CN, CH_3C_7N (?), n-C_3H_7OH, i-C_3H_7OH, $(CH_3)_2C=CH_2$**
>12 atoms	**C_{60}*, C_{70}*, C_{60}^+*, c-C_6H_5CN, $HC_{11}N$, 1-$C_{10}H_7CN$, 2-$C_{10}H_7CN$, c-C_9H_8, 1-c-C_5H_5CCH, 2-c-C_5H_5CCH, c-$C_5H_4CCH_2$, 2-C_9H_7CN, C_6H_5CCH, $CH_3OCH_2CH_2OH$, 1-$C_{12}H_7CN$, 5-$C_{12}H_7CN$, 1-$C_{16}H_9CN$, 2-$C_{16}H_9CN$, 4-$C_{16}H_9CN$**

1.3. Molecular ices in the ISM:

In the interstellar medium, dust particles appear to be composed of either silicates or carbon, depending upon the star from which the material originates. These dust particles play a key role in the formation of molecules. Inside the dense clouds, the sub-micron grain particles shield newly synthesized molecules

in gas phase from the energetic UV radiation field. The grains in the dense molecular clouds have a temperature of ~10 K. Once molecules, radicals, or atoms from the gas phase collide with solid particles, they are accreted on the grain surface resulting in an amorphous icy mantle. At such ultralow temperatures, all species except H, H_2, and He hold sticking coefficients of unity, meaning that each collision of gas phase species with a cold surface leads to adsorption and thickening of the ice layers. Water ice is the most abundant constituent of the icy mantles. Other molecules present are carbon monoxide (CO), carbon dioxide (CO_2), ammonia (NH_3) etc along with organic molecules like methane (CH_4), methanol (CH_3OH) and others. Figure 1.2 shows the ice spectrum recorded by the James Webb Space Telescope (JWST) towards NIR38 (A_v~60 mag) in the molecular cloud region Chameleon I (McClure et al., 2023). The spectrum shows the presence of ice features like H_2O, stretching, bending, the liberation band, along with other molecular features for CO, NH_3, CO_2, CH_4, complex molecules like CH_3OH, and even features appearing from the mixture of different molecular ices. Figure 1.2 (b), highlights the specific part of the spectrum showing the presence of dangling bond of water around 3650 cm^{-1} a characteristic feature of the porous nature of the water ice. These features not only validate the presence of ices in the molecular cloud, but also give crucial information about the morphology of the ice. Even the broad infrared features of the molecules also validate their amorphous morphology. Very recently HDO ice has been detected in the low mass protostar by JWST (Slavicinska et al., 2025). Also, Rocha et al., 2024 reported the first observational indication of the presence of complex organic molecular ices in through JWST. So ice is an integral and important part of the ISM.

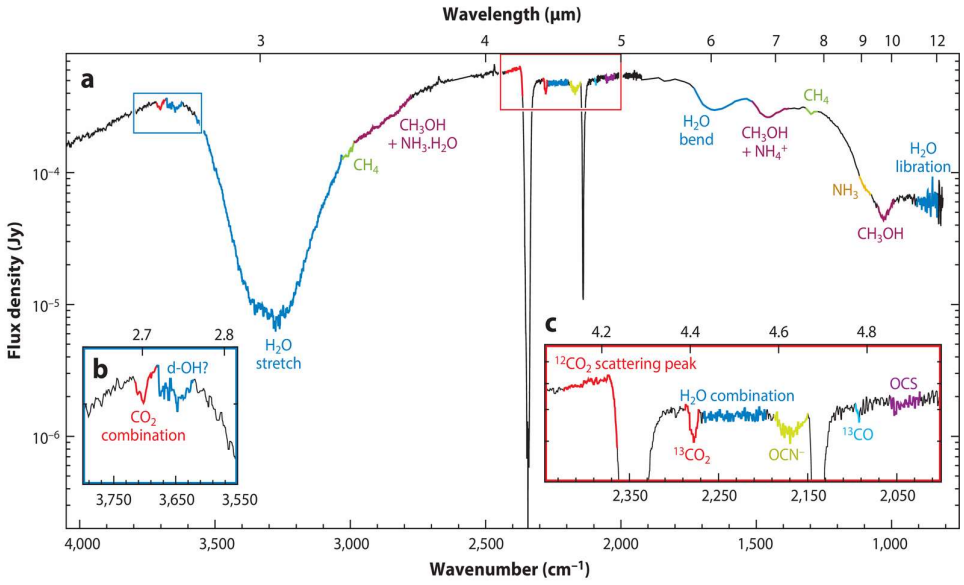

Figure 1.2 Mid-IR spectrum recorded by JWST towards NIR 38. Image adopted from Cuppen et al., 2024, the original image was modified from the McClure et al., 2023.

In reality, ices become observable in the translucent clouds (Whittet et al., 1988) because the interstellar radiation field dissociates molecules slower than its formation. During the transition from translucent to dense molecular cloud, the gas phase species are mostly atomic. The O, N, C atoms freeze out onto the grains upon collision and become hydrogenated by hydrogen addition reaction. It gives rise to the formation of H_2O rich ice layer along with the formation of NH_3, CH_4 etc. At this stage, the oxygen is mostly reserved in the form of water. In the gas phase it reacts with C and form CO. This CO can further react with oxygen and form CO_2. So the main gas phase species present in dense molecular cloud is now CO alongside H_2. This CO can again freeze out at the low temperature forming a rich layer of CO on the water rich icy layer. Therefore, the dense molecular cloud forms an onion-like structure with the inner layer consisting of amorphous solid water along with NH_3, CO_2, CH_4 and the outer layer mainly dominated by CO. This layer then gets hydrogenated and forms

other molecules like H_2CO, CH_3OH, and other complex organic molecules like glycolaldehyde, ethylene glycol etc (Tielens and Hagen, 1982) (Fedoseev et al., 2015) .

1.4 Ices in the solar system:

Our solar system is known to contain a variety of molecules in different planetary bodies, their moons, asteroid in comets. However, as this thesis focuses on astrochemical ices, the discussion is limited to the molecular ices detected on various solar system bodies. Interestingly the ices are not only found on the cold outer solar system bodies, but also are present in the inner solar system planets except Venus.

1.4.1 Ice on Mercury:

Despite being the closest planet to the Sun, water ice has been observed in the permanently shadowed region near Mercury's North Pole. The permanently shadowed craters are not exposed to direct sunlight, hence their temperature does not rise much, preventing the sublimation of water ice (Paige et al., 2013). Additionally, the energetic cosmic rays have been suggested to contribute to the formation of other molecular ices in Mercury (Delitsky et al., 2017)

1.4.2 Ice on Mars:

Mars exhibits seasonal and permanent ices, primarily composed of H_2O and CO_2. H_2O and CO_2 ices are found in the permanently shadowed regions of the poles (Kieffer et al., 1976, Phillips et al., 2011). Even atmospheric CO_2 freezes out to form seasonal CO_2 frost at the poles (Kelly et al., 2006).

1.4.3 Ice on Earth:

On planet Earth, the most common molecular ice is H_2O ice. It typically exists in its hexagonal crystalline form, which is stable under Earth's pressure and

temperature conditions. However, other crystalline phases may form under the diverse thermodynamic conditions present on different planetary bodies.

1.4.4 Outer solar system objects:

The cold temperature of the outer solar system bodies allows a broader range of molecules to exist in the ice phase. The surface temperature of Jupiter's satellites can vary from 80-130 K while that for Saturn can be as low as 35 K to 200 K and same to the other satellites of Uranus, Neptune and of the Pluto, Charon. Water ice is the most abundant ice on all these bodies while other simple to complex molecular ice, CO, CO_2, SO_2, NH_3, CH_4, CH_3OH etc have also been detected (Dalton, 2010). The common molecules detected in the satellites Jupiter and Saturn are in the magnetosphere of these planets, where charged particles can interact with these ices to form other complex molecules. The ultraviolet photolysis and radiolysis have been observed to be important for the complex molecules' formation in these icy bodies.

The icy satellites of Jupiter, mainly Europa, Ganymede, Callisto contain the most abundant water ice, both in the crystalline and amorphous form. Very recently Cartwright et al., 2025 showed the presence of 3.1 micron crystalline H_2O ice Fresnel peak in Europa using the JWST NIRSpec data. The other detected molecules are SO_2, CO_2, H_2O_2, O_2, hydrates of H_2SO_4, $MgSO_4$ and Na_2SO_4. Ozone (O_3) has long been observed in Ganymede, and recent studies demonstrated that irradiation of SO_2 ice on Callisto could lead to O_3 formation, highlighting the impact of energetic processing on surface chemistry (Ramachandran et al., 2024b). Even salts like hydrated sodium chloride, ammonium chloride and sodium/ammonium carbonate along with organic compounds including aliphatic aldehydes have been detected in Ganymede

using the Jovian Infrared Auroral Mapper (JIRAM) spectrometer onboard Juno mission (Tosi et al., 2024).

The known ices in the Saturnian satellites are mostly water-rich with the presence of other molecules like CO_2, CH_4, NH_3, and various organic molecules and possible phosphates (Postberg et al., 2018). Titan, Saturn's largest moon, features lakes of CH_4 and C_2H_6 on its surface. Its atmosphere hosts Nitriles (e.g., HCN, HC_3N), CO, CO_2, benzene, and tholins (López-Puertas et al., 2013) . Very recently, using JWST, methyl radical has been found in the atmosphere of Titan, which is a key to the formation of ethane and other heavier molecules (Nixon et al., 2025). While other moons of Saturn are known to contain H_2O, CO_2, O_3, in a recent study, Elowitz et al., 2021 showed the presence of Hydrazine in Rhea and explained the chemical ways of their production on the icy surfaces.

Pluto and Charon, due to their extremely low temperatures, support ices with even lower sublimation temperatures like N_2, CH_4, CO, etc, alongside the ubiquitous water ice. The impact basin Sputnik Planitia on Pluto is known to contain large deposits of N_2 ice. Charon's surface is dominated by crystalline H_2O ice and NH_3-bearing compounds (Dalle Ore et al., 2018). Recently, JWST detected both CO_2 and H_2O_2 on Charon, suggesting radiolytic or photolytic processing of surface ices under cosmic irradiation. Notably, the CO_2 was found in its crystalline form (Protopapa et al., 2024). A detailed list of molecules in the icy bodies of the solar system can be found in Table 1.3

Table 1.3 Molecules observed in the icy bodies of the outer Solar System along with their temperature,(Collated from (Dalton, 2010) & Cosmic ice laboratory[2]

Body	Temperature (K)	Ices Present
Mercury		H_2O
Mars		H_2O, CO_2
Earth		H_2O
Io (Jupiter)	80 - 130	SO_2, SO_3, SH, H_2S, H_2O,silicates
Europa (Jupiter)	86 - 132	H_2O, SO_2, SH, CO_2, O_2, HC, XCN, H_2O_2, H_2SO_4, carbonate salt, hydrates of H_2SO_4, $MgSO_4$ and Na_2SO_4
Ganymede (Jupiter)	90 - 160	H_2O, SO_2, SH, CO_2, HC, XCN, O_2, O_3, hydrated and hydroxylated minerals
Callisto (Jupiter)	80 - 158	H_2O, SO_2, SH, CO_2, HC, XCN, O_3, hydrated and hydroxylated minerals
Mimas (Saturn)	73	H_2O, CO_2
Enceladus (Saturn)	33 - 85 ; 120 - 160 at hot spots	H_2O, NH_3 CO, $NH_3 \cdot H_2O$,H_2O_2, CH_3OH
Tethys (Saturn)	86	H_2O, CO_2, $NH_3 \cdot H_2O$

[2] https://science.gsfc.nasa.gov/691/cosmicice/sol-sys.html

Dione (Saturn)	87	H_2O, CO_2, HC, O_3
Rhea (Saturn)	53-99	H_2O, CO_2,HC, O_3, CH_4
Hyperion (Saturn)	60-115	H_2O, CO_2, CN
Iapetus (Saturn)	40-130	H_2O, CO_2, C, HC, CN, H_2S, $NH_3 \cdot H_2O$
Phoebe (Saturn)	72-113	H_2O, CO_2, CN, CH
Titan (Saturn)	70-200	H_2O, $C_2(CN)_2$, CO,CO_2,CH_4, CH_3D,C_2H_2,C_2H_4, C_2H_6,C_3H_8,HCN, HC_3N,C_4H_2,C_2N_2, C_3H_4,C_6H_6
Rings (Saturn)		H_2O, HC?
Miranda (Uranus)	80-86	H_2O, NH_3 (NH_3 hydrate?), hydroxylated silicates
Ariel (Uranus)	60-84	H_2O, CO_2, OH?
Umbriel (Uranus)	64	H_2O, CO_2
Titania (Uranus)	60-64	H_2O, C, HC, CO_2, OH?
Oberon (Uranus)	73	H_2O, C, HC, OH?
Triton (Neptune)	30-39	N_2, CH_4, CO, CO_2, H_2O
Nereid (Neptune)	60	H_2O
Pluto	38-63	N_2, CH_4, CO, H_2O, CO_2
Charon	40-53	N_2, H_2O, NH_3 (NH_3 hydrate?)
Kuiper belt objects		H_2O, NH_3, CH_4, C_2H_6

1.5 Molecules detected in comet:

Comets, often referred to as "dirty snowballs," are icy bodies that orbit the Sun. They originate from two primary reservoirs: The Kuiper Belt and the distant Oort Cloud. Their nuclei consist of a complex mixture of ices and dust, preserving some of the most pristine material from the early solar system. These ices are not just frozen water but include a wide variety of volatile compounds that provide valuable insights into the physical and chemical processes occurring during the early stages of solar system formation.

The most abundant molecule detected in cometary ices is water (H_2O). Alongside water, CO**,** CO_2, and NH_3 are commonly found (Mumma and Charnley, 2011). Observations have revealed a chemically rich inventory of molecules in cometary comae, including: different molecules like hydrocarbons - CH_4, C_2H_6, C_2H_2, C_2H_4, etc, alcohols, aldehydes, acids, nitrogen-bearing compounds like N_2, HCN, HNC, CH_3CN etc, inert gases –Ar, Kr, Xe, different halides like HCl, HBr, HF along with other molecules have been detected in the coma of the comets. A detailed review of the presence of molecules in the cometary atmosphere is presented in Biver et al (Biver et al., 2022). The volatiles present in comets are known to be formed and reserved at large distance at very low temperature. So they are the least altered object. They are thought to contain the record of the physical and chemical processes in the early stages of the solar system.

A detailed list of molecules detected in comets can be found in Table 1.4.

Table 1.4 Molecules detected in comets adopted from the astrochymist website [3]

Number of Atoms	Molecules Detected
2 atoms	C_2, CN, N_2^+, CO^+, CH, NH, OH, CH^+, OH^+, CO, CS, CN^+, S_2, NO, SO, NS, H_2, N_2, O_2, HF, HCl, HBr, PO
3 atoms	C_3, NH_2, CO_2^+, H_2O^+, HCN, HCO, H_2S^+, CO_2, H_2O, NCN, H_2S, HNC, HCO^+, OCS, HDO, SO_2, CS_2, S_3, CO_2^{2+}, CH_2^+, NH_2^+, HDO^+
4 atoms	NH_3, H_2CO, C_3H^+, H_3S^+, H_3O^+, C_2H_2, H_2CS, HNCO, S_4, CH_3^+, NH_3^+, H_3O^+, $C_2H_2^+$, $HCNH^+$, NCCN, PH_3
5 atoms	CH_4, HC_3N, HCOOH, H_2CCO, NH_4^+, CH_3Cl, $C_2H_3^+$, H_2COH^+, i-C_3H_2, c-C_3H_2
6 atoms	CH_3CN, c-$C_3H_3^+$, CH_3OH, NH_2CHO, CH_3SH, NH_4CN, NH_4Cl, $C_2H_4^+$, CH_3OH^+, NH_4F
7 atoms	$HCOCH_3$, CH_3NH_2, CH_3NCO, NH_4OCN, $C_2H_5^+$, $CH_3OH_2^+$, NH_4SH, c-C_2H_4O
8 atoms	C_2H_6, $HCOOCH_3$, CH_2OHCHO, NH_4OCN
9 atoms	C_2H_5OH, CH_3CONH_2, C_2H_6S, NH_4HCOO
10 atoms	$HOCH_2CH_2OH$, $C_2H_5NH_2$, $(CH_3)_2CO$, C_2H_5CHO, $C_2H_5NO_2$
>12 atoms	$C_{14}H_{10}$, $C_{16}H_{10}$, NH_4CH_3COO

[3] https://www.astrochymist.org/astrochymist_comet.html

1.6 Sublimation temperature of molecular ices in the astrochemical conditions:

In astrochemical environments, the sublimation temperature of a molecule is the temperature at which it transitions directly from the solid (ice) phase to the gas phase under the low-pressure conditions typical of space. The stability and presence of a molecular ice on planetary bodies, comets, or interstellar grains is governed primarily by this parameter. For instance, H_2O ice, with its relatively high sublimation temperature, can be stable on bodies which have a temperature less than 170-180 K. In contrast, CO ice, which sublimates at much lower temperatures, is observed only in the outer solar system or cold interstellar environments. Thus, understanding sublimation temperatures is essential not only for interpreting observations but also for designing laboratory simulations that mimic the astrophysical conditions.

Table 1.5 summarizes the sublimation temperatures of several key molecules detected in comets and other icy bodies. These values are particularly relevant in deciding the temperature windows for laboratory studies, understanding radial ice distributions in disks and solar system bodies, and modelling volatility gradients in astrophysical ices.

The sublimation temperature of some of the common molecules are listed in Table 1.5.

Table 1.5 Sublimation temperature of some selected astrochemical molecules

Molecule	Sublimation temperature (K)	References

Molecular hydrogen (H_2)	6	(Seligman and Laughlin, 2020)
Molecular Nitrogen (N_2)	27	(Bisschop et al., 2006)
Molecular Oxygen (O_2)	37-43	(Sivaraman et al., 2007)
Ozone (O_3)	62-66	(Sivaraman et al., 2007)
Argon (Ar)	46	(Hama et al., 2017)
Neon (Ne)	11	(Hama et al., 2017)
Carbon Monoxide (CO)	29	(Caro et al., 2016)
Carbon Dioxide (CO_2)	85	(Ehrenfreund et al., 1996)
Sulfur Dioxide (SO_2)	120	(Schriver-Mazzuoli et al., 2003)
Ammonia (NH_3)	113	(Luna et al., 2014)
Hydrogen Sulfide (H_2S)	90	(Mifsud et al., 2024)
Water (H_2O)	170	(Fraser et al., 2001)
Methane (CH_4)	60	(Tamai et al., 2023)
Methanol (CH_3OH)	140	(Öberg et al., 2009)
Formaldehyde (HCHO)	95	(Ioppolo et al., 2011)
Formic acid (HCOOH)	165	(Ioppolo et al., 2011)
Methylamine (CH_3NH_2)	140	(Hudson et al., 2022b)
Acetone (CH_3COCH_3)	150	(Hudson et al., 2018)
Formamide ($HCONH_2$)	>200	(Sivaraman et al., 2013)
Benzene(C_6H_6)	150	(Hudson and Yarnall, 2022)

Pyridine(C_6H_5N)	160	(Hudson and Yarnall, 2022)
Ethanethiol (CH_3CH_2SH)	130	(Pavithraa et al., 2017)

1.7 Processing of ices:

In the previous sections, we have discussed the presence of various simple to complex molecules in low-temperature environments such as the interstellar medium (ISM) and bodies across our solar system. A fundamental question in astrochemistry remains: how are complex molecules formed under such cold conditions? The chemical evolution of molecular ices is governed by a combination of non-energetic and energetic processing mechanisms. There are five major pathways through which interstellar ices undergo processing:

- **Non-energetic processes**:
    - *Thermal processing*
    - *Atom-addition reactions*
- **Energetic processes**:
    - *Shock-induced chemistry*
    - *Photochemistry (UV/visible photons)*
    - *Radiation chemistry (ions, electrons, X-rays, γ-rays)*

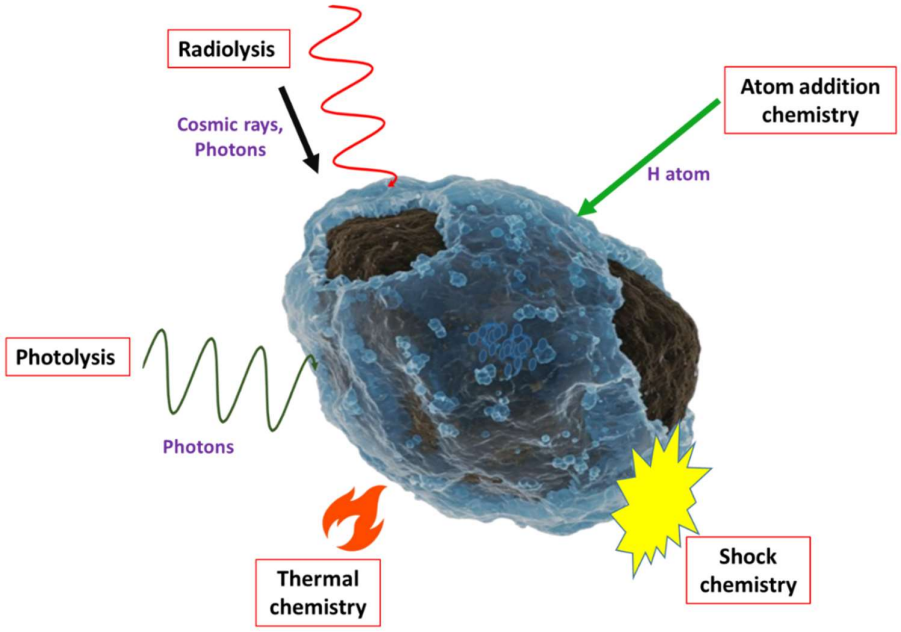

Figure 1.3 Different processes for chemical evolution of ices.

Ices made up of H_2O, CO, CO_2, CH_3OH, NH_3 are ubiquitous in the cold dark clouds as well as different solar system bodies depending on the temperature of the body. The processing of these common abundant ice can give rise to the formation of other complex molecules.

Thermal processing of astrochemical ices, including heating and annealing, plays a significant role in driving phase transitions, promoting sublimation, and enabling thermally activated chemical reactions. This form of processing has proven effective in facilitating the formation of new molecular species. For instance, the reaction between HCOOH and NH_3 during thermal processing leads to the formation of the salt $NH_4^+HCOO^-$ (Theulé et al., 2013). Kaňuchová et al., 2017 demonstrated that heating a mixture of H_2O and SO_2 from 30 K to 120 K resulted in the formation of various sulfates and bisulfates. More recently,

Marks et al., 2023 observed the formation of carbamic acid from a thermally processed mixture of NH_3 and CO_2.

Atom addition reactions, particularly the hydrogenation of CO, are another important non-energetic pathway for forming complex molecules at low temperatures. These reactions lead to the formation of key prebiotic molecules such as methyl formate ($HCOOCH_3$), glycolaldehyde ($HOCH_2CHO$), and ethylene glycol ($HOCH_2CH_2OH$). A comprehensive review of atom addition reactions and their relevance to the synthesis of complex organic molecules in interstellar ices is provided by Linnartz et al., 2015.

Processes involving energetic particles play a critical role in the formation of complex molecules in astrochemical environments. Photolysis (or photochemistry) refers to the interaction of interstellar ices with visible and ultraviolet (UV) photons, which leads to electronic excitation, bond dissociation, and subsequent bond reformation. In contrast, radiolysis involves the interaction of ices with high-energy particles capable of ionizing matter. Ionizing radiation in interstellar chemistry includes a wide range of sources such as cosmic rays (MeV to TeV), and high-energy photons, including vacuum ultraviolet (VUV, 6.2–12.4 eV), extreme ultraviolet (EUV, 12.4–124 eV), X-rays (>124 eV), and gamma rays (100 keV to 1 TeV).

Energetic processing has been shown to initiate radical formation within the ice matrix, where these reactive intermediates can subsequently combine with neighbouring species to form new, often more complex, molecules. Numerous studies have demonstrated that UV photolysis and keV electron irradiation of molecular ices yield comparable radicals and molecular products. This

similarity in product composition suggests that the chemical evolution of interstellar ices is more dependent on the total energy deposited into the system than the specific nature of the energy source (Gerakines et al., 2004, Islam et al., 2014, Maté et al., 2015, Mullikin et al., 2021). Laboratory studies have shown that simple molecules such as N_2, CH_4, and CO, when subjected to photon and electron irradiation at astrochemically relevant temperatures, can yield a diverse range of complex organic compounds. These include alcohols, carboxylic acids, ketones, aldehydes, amines, nitriles, and even urea (Materese et al., 2015, Materese et al., 2014). Organic molecules such as methyl formate ($HCOOCH_3$), dimethyl ether (CH_3OCH_3), glycolaldehyde ($HOCH_2CHO$), acetic acid (CH_3COOH), and methoxymethanol (CH_3OCH_2OH) have been detected as irradiation products of methanol ice (Bennett et al., 2007, Bennett and Kaiser, 2007, Modica and Palumbo, 2010, Palumbo et al., 1999, Mason et al., 2014, Moore et al., 1996). Comparative studies have further shown that methanol ice irradiated with both high-energy electrons (1 keV) and low-energy electrons (<20 eV) produces similar sets of molecular products (Boyer et al., 2016, Sullivan et al., 2016). A similar observation was reported for ammonia (NH_3) ice, where irradiation with electrons ranging from 7 eV to 1 keV resulted in minimal differences in the final product distribution (Shulenberger et al., 2019). These findings support the widely accepted view that high-energy irradiation in ices predominantly operates via reactions initiated by cascades of low-energy secondary electrons. These electrons are generated along the path of primary high-energy particles as they pass through the solid matrix. The detailed role of these low-energy electrons will be discussed in the next chapter.

Besides these simple and complex molecules, another important class of molecules exist in the ISM known as Polycyclic Aromatic Hydrocarbons (PAHs). PAHs, 1-cyanonapthalene and 2-cyanonapthalene (McGuire et al., 2021), indene (Burkhardt et al., 2021, Cernicharo et al., 2021a), 1-cyanopyrene (Wenzel et al., 2024a), 2-cyanopyrene and 4-cyanopyrene (Wenzel et al., 2024b) have been detected in the low temperature region of the ISM. Also the presence of PAHs has been confirmed in meteorites (Sabbah et al., 2017, Lecasble et al., 2022), as well as in the comet 81P/Wild 2 (Clemett et al., 2010), also in the samples in the asteroid Ryugu (Zeichner et al., 2023). Yet a clear pathway for the formation of PAHs in the low temperature astrochemical conditions in scarce in the literature.

Another important aspect of astrochemical ice processing is the formation of non-volatile/ refractory residue upon energetic particle irradiation. When ice is formed at low temperature (~10 K) and irradiated with energetic particles, in some cases it has been observed that some leftover is there on the substrate even when it is heated up to room temperature, which can further be seen by naked eye when the substrate is taken out from the experimental chamber. The residue has been a topic of research for a long time and has been crucial in explaining different interstellar spectral features (Moore and Donn, 1982). Recently N-graphene was synthesized in the astrochemical ices by irradiating benzonitrile and heating it to room temperature (Sivaraman et al., 2023). Additionally the shape of the interstellar dust was explained by studying the residue after irradiating benzene in the astrochemical conditions (Rahul et al., 2020).

In an earlier study, Melcher et al., 1982 and Moore, 1984 reported that MeV F^+, He^+, and H^+ ion sputtering of SO_2 ice produced a yellow, non-volatile residue, initially presumed to be sulfur-rich. However, Rutherford Backscattering Spectrometry (RBS) revealed the residue to be oxygen-rich, underscoring the importance of rigorous compositional analysis to correctly interpret the nature and astrochemical relevance of such residues.

Table 1.6 List of molecules used in the thesis and their presence in the ISM/ Comets

Molecules used in the thesis	**Region**	**Detection in gas / ice phase**	**Reference**
D_2O (used as a proxy of water)	ISM	Gas phase	(Butner et al., 2007)
	Comets	Gas phase	(Altwegg et al., 2017)
Ethylene Glycol (EG)	ISM	Gas phase	(Hollis et al., 2002)
	Comets	Gas phase	(Crovisier et al., 2004)
1,3 propanediol (used due to similar chemical properties of EG)	ISM	ISM	-
	Comets	Comets	-
CO	ISM	Gas & Ice phase	(Wilson et al., 1970) (Whittet et al., 1985)
	Comets	Gas & Ice phase	(Feldman and Brune, 1976) (Feldman, 1986)
	ISM	Gas & Ice phase	(Cheung et al., 1968) (Knacke et al., 1982)

NH_3	Comets	Gas Phase	(Altenhoff et al., 1983)

1.8 Thesis Motivation:

Astrochemical ices can remain in different morphological/structural phases depending on the environmental temperature. The most common ice, water (H_2O), is typically found in a hexagonal crystalline form (I_h) on Earth. However, the same water ice can have different morphologies at different temperatures in astrochemical conditions. Under interstellar or outer solar system conditions (~10 K), water and other molecular ices generally exist in an amorphous phase. As the temperature increases, these ices undergo phase transitions—for instance, amorphous water ice transitions to cubic crystalline ice (I_c) around 125 K and then to hexagonal ice (I_h) at ~150 K (Watanabe and Kouchi, 2008) while further heating causes the ice to sublime after 170 K (Fraser et al., 2001). The morphology of the ices has been observed to play a crucial role in the reactivity and hence chemistry of the molecular ice. The phase transition affects the porosity and diffusion within the ice, thereby altering the chemical behaviour. It has been observed that due to increased diffusion in porous ice, the chemical reactivity and products formed can be different in the amorphous and crystalline ice (Zheng et al., 2007, Grieves and Orlando, 2005, Bag et al., 2013). The amorphous → crystalline phase change temperature for the simple molecules like CO is found to be at 23 K (Gerakines et al., 2023), for CO_2, it has been observed to be at 30 K (Escribano et al., 2013), for complex molecule like CH_3OH it is around 112-113 K (Carrascosa et al., 2023). On the other hand, for another important constituent of astrochemical ice, NH_3, it has a controversial

and complex crystallization behaviour. The phase of NH_3 ice was reported first by Reding and Hornig, 1951 showing the crystalline spectrum of NH_3 ice upon deposition around 83 K, few years later Staats et al., 1959 reported the formation of two metastable phases around 77 K and 112 K. Such debate on the morphological behaviour of NH_3 ice had been discussed by several studies (Pipes et al., 1978, Ferraro et al., 1980, Holt et al., 2004). Later, Zheng and Kaiser, 2007 discarded the presence of metastable phase in NH_3 and reported the crystallization of NH_3 ice around when deposited at 10 K and heated to higher temperature is around 57 K. Meanwhile, Dawes et al., 2007 reported the presence of a metastable phase and the formation of crystallites. This debate highlights the need for a comprehensive experimental study of ammonia ice morphology across its entire thermal range (10–115 K).

The presence of a specific molecular ice in a given environment can often be predicted from the characteristic sublimation temperature of that pure molecular ice (Table 1.5). However, volatile species can also be trapped within the porous/amorphous water ice matrices and remain stable at higher temperatures than their own sublimation temperature (Collings et al., 2004). Despite progress in characterizing pure ices, intermolecular interactions in mixed ices—such as hydrogen bonding—are rarely explored, especially regarding their influence on condensation, morphology, and thermal stability.

On another side, PAHs are known to be ubiquitous in the interstellar medium (ISM). They are known to contain nearly 20% of the carbon atoms in the ISM and Milky Way (Tielens, 2013, Allamandola et al., 1987) and also in other galaxies (Smith et al., 2007). On the Earth, and carbon rich star they form at

high temperatures (Pascoli and Polleux, 2000) , recent studies have revealed ring-containing molecules and PAHs in cold molecular clouds (McGuire et al., 2021, Cernicharo et al., 2021a, Burkhardt et al., 2021, Wenzel et al., 2025, Wenzel et al., 2024a). Isotopic analyses of Ryugu asteroid samples further confirm PAH formation at low-temperature (Zeichner et al., 2023). The known pathways involve the reactions between small molecules to form a benzene ring which can grow further to form different PAHs. A detailed review on the formation pathway can be found in (Reizer et al., 2022). The smallest molecule which is considered as a precursor is acetylene. However, the known pathways take longer time to produce PAHs than it gets destroyed by the energetic radiations present in the ISM, so there is an unexplained pathway for PAHs formation at low temperature. Also very recently Kocheril et al., 2025 showed that the known bottom up formation pathway from acetylene terminates at $C_6H_5^+$, making it difficult to contribute to the formation of aromatic molecules/ PAHs in the astrochemical conditions. These findings indicate the need to look for alternative formation pathways of PAHs at low temperature.

1.9 Objective of the thesis:

As explained in the preceding section, astrochemical ices can exist in different morphologies depending on the temperature which in turns affect their reactivity. However, most of the studies on the astrochemical ices so far has considered the ices to be pure. On the other hand, in reality, the astrochemical ices are not pure, they are mixed with other ices. Although we have the knowledge about the structural properties of pure ices, but the effect on these properties in the presence of other molecules is scarce in the literature.

Previous investigations into molecular stability have primarily considered either pure ices or mixtures involving inert, porous matrices. But the chemical interaction between different molecules have not been considered. Furthermore, there exist a gap in our understanding of the formation pathway of aromatic molecules at low temperature. So the objectives of the thesis are

1. To simulate the low temperature astrochemical conditions (ultrahigh vacuum ~10^{-9} mbar & 10 K) in the laboratory using the experimental system Simulator for Astromolecules at Low Temperature (SALT).
2. To study the behaviour of molecular ices in the presence of other molecules capable of forming strong chemical interactions (mainly Hydrogen bonding) with the said molecular ice.
3. To investigate how such intermolecular interactions, influence the condensation, sublimation and morphology of the ice of the interest in the astrochemical environments.
4. To explore alternative formation pathways for the formation of aromatic molecules beyond the known pathways in the astrochemical conditions.
5. To understand a clear picture of the structural morphology of NH_3 ice through an extensive experimental investigation.

1.10 Thesis Structure:

Chapter-1 introduces the field of astrochemistry and outlines the scientific context for the thesis. It covers the composition and structure of the interstellar medium (ISM), including its density, temperature, and chemical complexity. A detailed list of molecules identified in the ISM and recent JWST findings on molecular ices are discussed. The occurrence and distribution of molecular ices

across solar system bodies, including planets, moons, and comets, are reviewed, along with sublimation temperatures to understand ice behaviour in various environments. The morphology of pure molecular ices is explored in relation to temperature, followed by a discussion on energetic processing mechanisms that drive chemical evolution. Finally, the chapter introduces the formation of aromatic molecules and outlines the thesis motivation, objectives, and structure.

Chapter 2 presents the spectroscopic methods used to probe ice morphology under astrochemical conditions. It introduces the fundamentals of electromagnetic radiation, vibrational spectroscopy (with harmonic and anharmonic treatments), and VUV/UV spectroscopy based on molecular orbital theory and the Franck-Condon principle. Instrumental setups for IR and VUV/UV spectroscopy are described. The interaction of energetic electrons with molecular ices and their chemical effects are also examined.

Chapter 3 describes the experimental techniques and systems, particularly the SALT setup designed to simulate interstellar conditions. It describes the substrates used for IR/UV experiments and their spectral suitability. Electron irradiation experiments carried out at Aarhus University are described, including details on the electron gun and experimental parameters.

Chapter 4 examines how ethylene glycol (EG), a molecule found in the ISM and comets, influences the phase behaviour and sublimation of D_2O ice. Layered and mixed ices were studied using IR spectroscopy. Results indicate that EG inhibits the crystallization of D_2O and delays its sublimation, highlighting the role of hydrogen bonding in stabilizing water, with implications for water retention in comets near the Sun.

Chapter 5 explores the interaction between diols (EG and 1,3-propanediol) and D_2O. D_2O was found to condense and remain stable above its typical sublimation temperature when deposited over diol ice, suggesting that strong hydrogen bonding can stabilize water in warm regions. The results support the possibility of water formation and retention on warm dust grains.

Chapter 6 proposes a new PAH formation mechanism from CO ice under electron irradiation at 10 K. VUV/UV spectroscopy and HRTEM confirm the presence of aromatic structures and graphitic residues, suggesting CO as a viable PAH precursor under ISM conditions.

Chapter 7 investigates the phase of ammonia ice in the astrochemical conditions. The morphological phase of ammonia ice was studied when it was deposited over a range of temperatures starting from 10 K to 100 K. The findings resolve ambiguities in structural phases of ammonia ice and their dependence on deposition temperature.

Chapter 8 summarizes the thesis findings, including new insights into ice morphology, stability, and reactivity under astrochemical conditions. It also proposes future directions based on the outcomes, including further studies of molecular interactions and the formation of complex organics at low temperatures.

Chapter 2 Molecular spectroscopy and energetic irradiation

Chapter Overview:

Interstellar molecules, specifically diatomic radicals, were first identified in the 1930s through their electronic transitions in the visual and near-UV regions of the spectrum. The diffuse interstellar bands (DIBs), a collection of approximately 400 interstellar absorption lines in the visible and far-red regions of stellar spectra, were discovered even earlier. The detection of interstellar molecules in the infrared became possible only after the development of sensitive detectors and the advancement of infrared observation capabilities in the 1970s. The pace of new molecular identifications increased significantly with the commencement of Atacama Large Millimeter/submillimeter Array's (ALMA) operational phase. So, spectroscopy has been an essential tool to detect molecules using ground and space based telescopes. When an electromagnetic wave passes through a molecule, it can excite the molecule to its higher excited rotational, vibrational and electronic state which can be analysed using the characteristic spectrum of the sample. In this thesis, I have used ultraviolet (UV) and infrared (IR) spectroscopy to characterize the properties of the ices. In this chapter, I will discuss the basic principles of the spectroscopic techniques.

2.1 Interaction of electromagnetic radiation with molecules:

Electromagnetic waves are a form of energy that propagates through space in the form of electromagnetic fields. They consist of oscillating electric and magnetic fields that are perpendicular to each other and to the direction of propagation. These waves can travel through vacuum, unlike mechanical waves. Electromagnetic waves travel at the speed of light in a vacuum, approximately 3×10^8 meters per second. They include various forms such as radio waves, microwaves, infrared (IR), visible light, ultraviolet (UV), X-rays, and gamma rays.

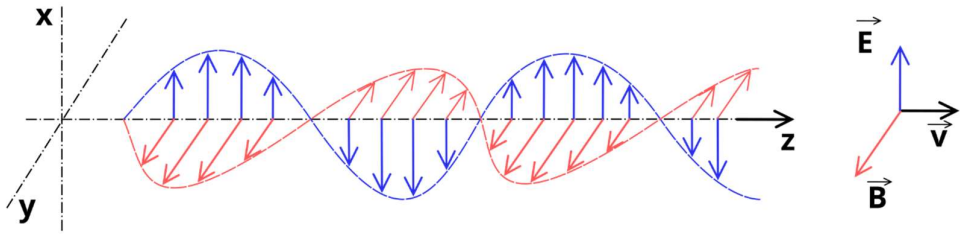

Figure 2.1 Visual representation of electromagnetic wave image source- Wikipedia[4].

The wavelength (λ), frequency (ν) and the velocity (c) of the electromagnetic wave are related with the equation

$$c= \lambda\nu$$

The energy of the wave can be expressed as,

$$E= h\nu$$

Where h is the Plank's constant having a value 6.626×10^{-34} J.s

2.2 Molecular spectra:

Molecules, like atoms can exist in both the ground state as well as in the exited states. The absorption and emission spectra of molecules arise from transitions

[4] https://en.wikipedia.org/wiki/Electromagnetic_radiation

between the allowed energy states. The energy structure of a molecule is significantly more complicated than that of atoms. In atoms, we can neglect the nuclear motion or incorporate it through the concept of reduced mass. In contrast for molecules, as an example of a diatomic molecule, the nuclei can vibrate about their equilibrium nuclear separation and the entire molecule can rotate about its centre of mass. The energy in each of these motions are quantized and hence we can expect many more energy levels in molecules compared to atoms.

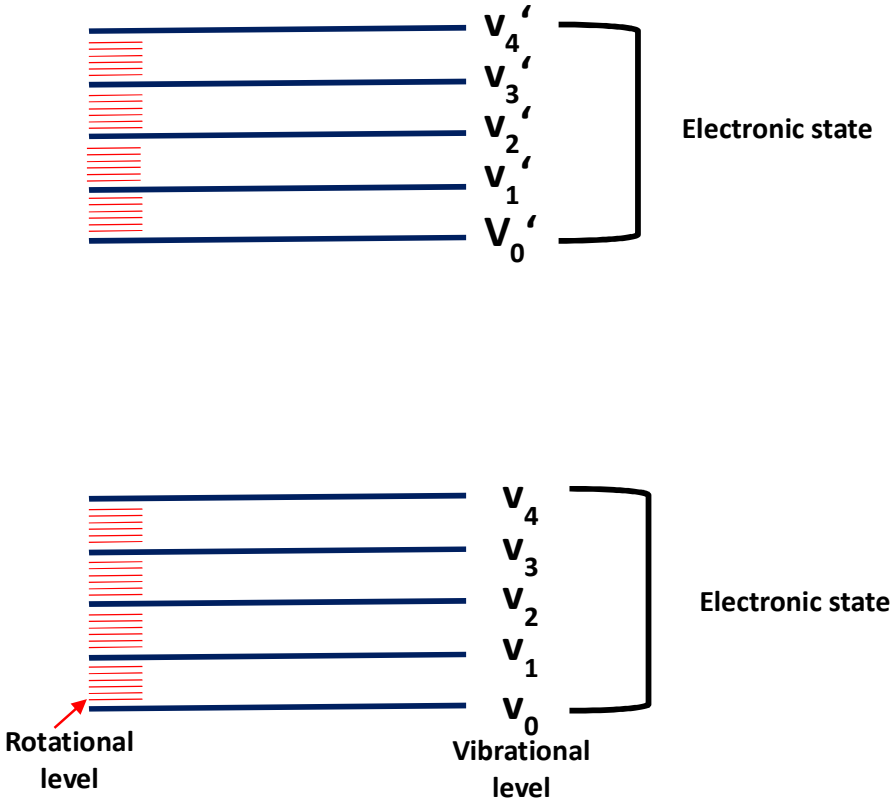

Figure 2.2 Molecular energy level diagram showing the electronic, vibrational and rotational energy levels.

The total energy of a molecule is composed of three principal components: electronic, vibrational and rotational energy levels. The molecular energy levels are grouped into widely separated sets, called electronic energy levels. Within each

electronic state, there exist multiple vibrational levels**,** which are further subdivided into rotational levels, creating a fine structure (see Figure. 2.2).

2.3 Principles of spectroscopy:

Spectroscopy is the study of the interaction between electromagnetic radiation and matter. It is a powerful tool to probe the internal structure of the molecules. When an electromagnetic wave interacts with molecules, it can excite the system to a higher energy state and the interacted photons can characterize the internal properties of the molecules, this is the heart of the underlying theory of spectroscopy. Depending on the energy of the wave, there can be various processes Figure 2.3. The lower energy photons, in the radio wave region can affect the orientation of spin, while the microwave and infrared can change the orientation and configuration/vibration of the molecule respectively. The visible and X- ray photons can change the electron distribution while the gamma rays can even affect the nuclear orientation of the molecule.

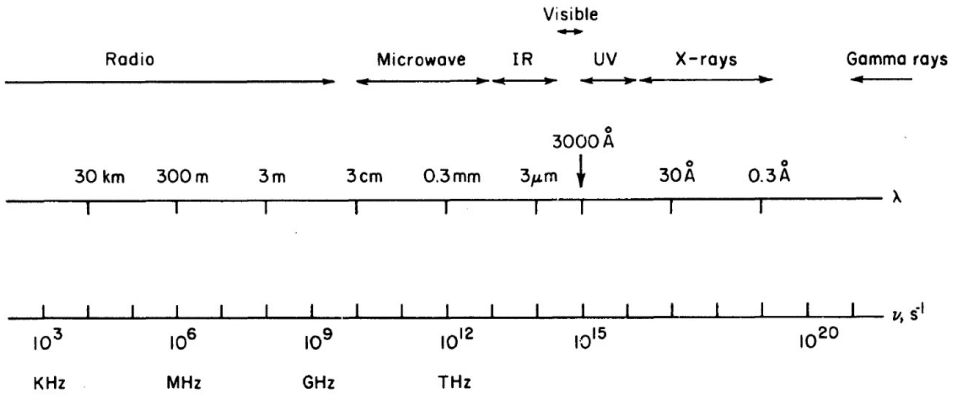

Figure 2.3 The electromagnetic spectrum. IR and UV are acronyms for infrared and ultraviolet, respectively; the abbreviations kHz, MHz, GHz, and THz stand for kilohertz, megahertz, gigahertz, and terahertz. (Adopted from (Struve, 1989); John Wiley & Sons).

The spectra of a molecule can change significantly depending on the region of the electromagnetic spectrum involved. Visible and ultraviolet (UV) light possess

sufficient energy to alter the distribution of electrons within a molecule, changing its electronic potential energy. This redistribution causes electrons to move to different energy levels, leading to excitation, de-excitation, or even ionization of the molecule. As a result, spectroscopy involving visible and UV light is referred to as electronic spectroscopy. Infrared light is capable of exciting molecules from one vibrational energy level to another. As a result, infrared spectroscopy is often referred to as vibrational spectroscopy. The rotational excitation corresponds to the microwave region of the spectrum. Since all the works presented in this thesis deal with molecular ices, which are solid molecules, they are rotationally constrained, so more emphasis will be given to infrared and electronic spectroscopy in the next sections.

2.4 Vibrational Spectroscopy:

In a simple diatomic molecule, the atoms are connected to each other by a bond that behaves like a spring. The compression or expansion of the bond obeys Hooke's law where the restoring force is given by

$$F = -kx$$

Where k is the force constant of the bond and x is the displacement from equilibrium.

If the equilibrium internuclear separation is r_{eq}, then for the compression or expansion of the molecule, the force can be given as

$$F = -k\,(r - r_{eq})$$

Where r is the internuclear separation.

The potential energy function under whose influence the nuclei vibrate is parabolic in nature and can be written as

$$V = \frac{1}{2} k (r- r_{eq})^2$$

This system is modeled as a quantum harmonic oscillator. The reduced mass μ of the molecule composed of atoms with masses m1 and m2 is given by

$$\mu = \frac{m1m2}{m1+m2}$$

The angular frequency and linear frequency of the oscillator is given by

$$\omega_0 = \sqrt{\frac{k}{\mu}} \quad \text{rad s}^{-1}, \; \nu_0 = \frac{1}{2\pi} \sqrt{\frac{k}{\mu}} \quad \text{Hz}$$

The corresponding wavenumber is,

$$\nu_0 = \frac{1}{\lambda} = \frac{\nu 0}{c} = \frac{1}{2\pi c} \sqrt{\frac{k}{\mu}} \quad \text{cm}^{-1}$$

The quantized vibrational energy levels of the harmonic oscillator are,

$$E_v = (v+\frac{1}{2}) h\nu_0$$

Where v= 0,1,2,3……. v is the vibrational quantum number

Even at 0th vibrational level has an energy $\frac{1}{2} h\nu_0$ - known as zero point energy.

So the energy levels are equally spaced having values, $\frac{1}{2} h\nu_0, \frac{3}{2} h\nu_0, \frac{5}{2} h\nu_0, \frac{7}{2} h\nu_0$…

During a transition between two vibrational energy levels v' (higher level) and v" (lower level), the energy absorbed or emitted can be given by

$$\Delta E = (v'+\frac{1}{2}) h\nu_0 - (v"+\frac{1}{2}) h\nu_0$$

$$= (v'-v") h\nu_0$$

For a vibrational transition to be IR-active, the dipole moment of the molecule must change with respect to bond length $\frac{dp}{dx} \neq 0$, and this leads to a selection rule $\Delta v = \pm 1$,

Therefore the transition will include only a single frequency ν_0 following the selection rule and the spectrum will also consist of a single band positioned at frequency ν_0. But in reality vibrational spectrum consists of a strong fundamental band at around ν_0 along with other bands (overtones) at frequencies lesser and lesser than $2\nu_0$, $3\nu_0$ ....

So the strict selection rule is not obeyed, and the transitions for $\Delta v>1$ also take place. Also, the appearance of the overtones not exactly at $2\nu0$, $3\nu0$ …. also indicates that the potential energy of the molecules is not exactly parabolic. The spacing between energy levels become lower and lower as we reach the higher energy states and converge slowly.

Anharmonic oscillator and Morse potential

The more realistic potential curve is given by a Morse potential expressed as-

$$V = D_e [1 - \exp\{a(r_{eq} - r)\}]^2$$

Where $a=\sqrt{\frac{k}{2De}}$ is a molecule specific constant and D_e well depth of the potential.

The corresponding energy levels are:

$$E = \hbar\omega [(\nu + ½) - \chi_e (\nu + ½)^2]$$

χ_e is the anharmonicity constant which has a small positive value ($\chi_e \sim 0.01$).

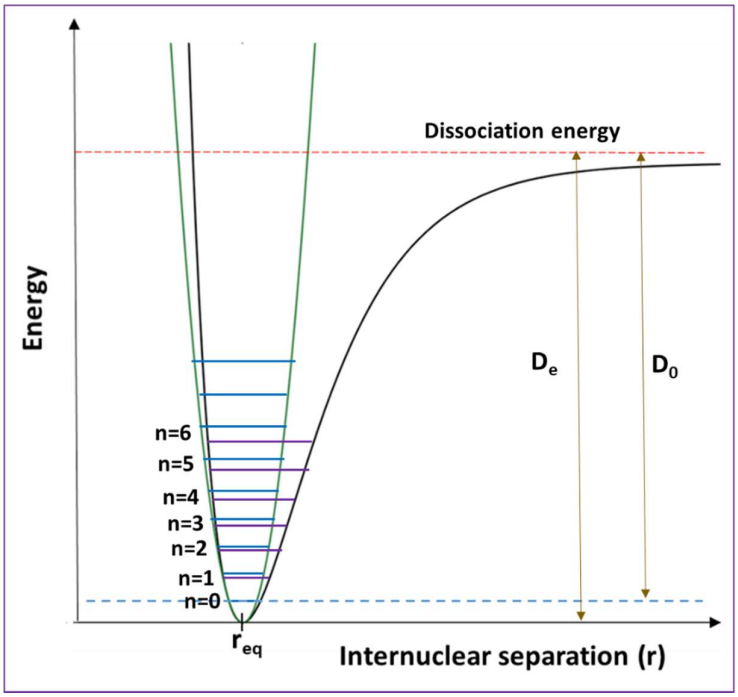

Figure 2.4 The potential energy curve of a diatomic molecule as a function of interatomic distance. Green- Harmonic, Black- Morse potential.

The selection rule for the anharmonic oscillator allow:

$$\Delta v = \pm 1, \pm 2, \pm 3, \ldots.$$

The intensity due to $\Delta v = \pm 1$ being the most intense and the overtones ($\Delta v > 1$) appear with progressively lower intensity.

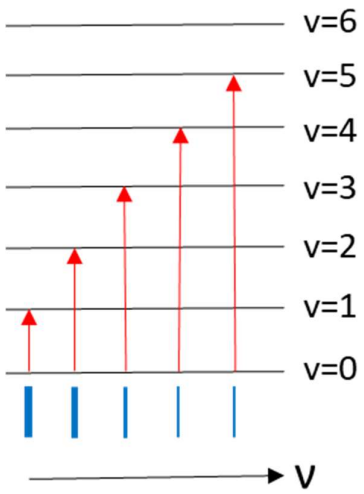

Figure 2.5 The fundamental ($\Delta v = \pm 1$) and the overtones ($\Delta v = \pm 2$, $\Delta v = \pm 3$..). The intensity of the corresponding lines are given in blue colour.

2.5 Vibrations in polyatomic molecule:

A complex molecule has many different modes of vibrations. A polyatomic molecule having N atoms has 3N degrees of freedom. These degrees of freedom correspond to the translational, vibrational, and rotational degrees of freedom. The translation of the molecule can be specified by noting the position of its centre of gravity while its rotation can also be resolved using three perpendicular axis. So a nonlinear molecule has 3N-6 degrees of freedom. For a linear molecule, since there is no rotation possible along the bond axis so it will have 3N-5 different degrees of freedom.

In the case of water ice, being a nonlinear molecule, it will have be 9-6=3 degrees of freedom. Whereas a linear molecules CO2 will have 9-5=4 degrees of freedom.

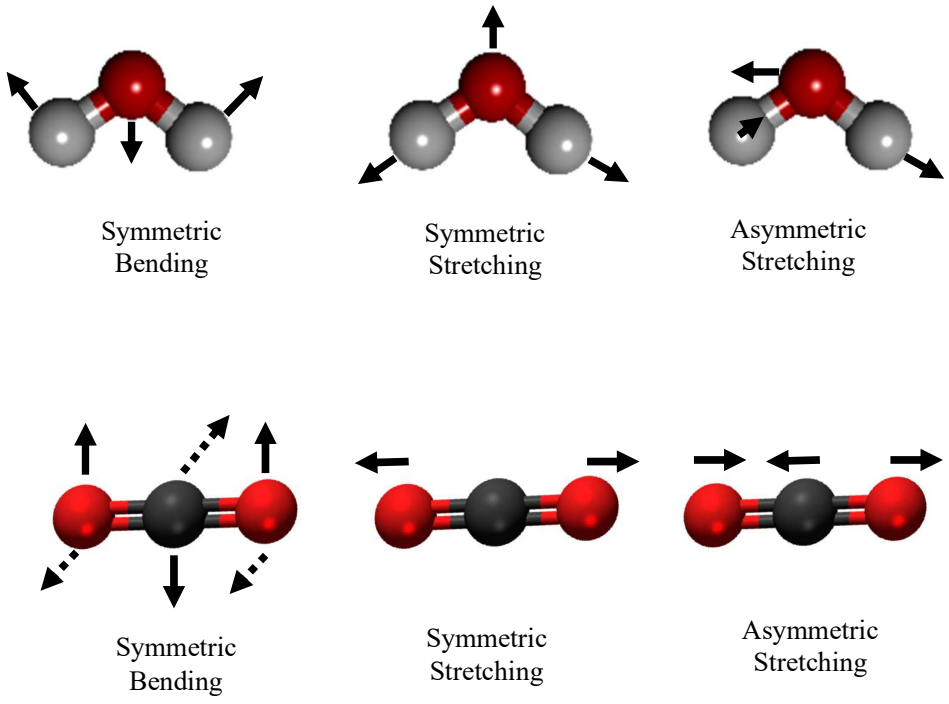

Figure 2.6 Normal mode of vibration of H_2O and CO_2 molecule.

As shown in the Figure 2.6, we can see the normal modes of vibration of H_2O and CO_2 molecule. The symmetric bending can happen in two perpendicular planes. In this case, we should note that for symmetric stretching, the overall charge distribution will not change and the molecular symmetry will be maintained. So the symmetric stretching mode will not absorb the infrared radiation and this mode is not IR active. For the other modes, there is a change in the distribution and so they are infrared active.

It should be noted that the energy required to stretch a molecule is more than that to bend it. So the spectral features corresponding to the stretching vibration will appear at higher frequency/wavenumber than that of bending. Also, in the case of carbon - carbon bonds, the spectral feature corresponding to triple bond will be at higher frequency than that of double bond which in turn have higher frequency than that of single bond. This is because the force constant increases with bond multiplicity.

2.6 Infrared Spectroscopy:

The vibrational characteristics of molecules, discussed in the earlier section, are effectively probed using Infrared (IR) spectroscopy. As we know, if there is a change in the dipole moment of the molecules, the infrared features will be active. The heteronuclear diatomic molecules such as CO, HCl are always infrared active because their permanent dipole moment due to the charge imbalance in the constituent atoms. But homonuclear diatomic molecules like N_2, O_2 do not have any infrared active features. Another example is CO_2, which we discussed in the previous section. It might not have a permanent dipole moment, but some of its vibrations (e.g, asymmetric stretching or bending) give rise to the change in dipole

moment, and those vibrations become IR active. It is also important to understand that the infrared spectral features vary significantly depending on the physical state of the molecule. For example, gaseous molecules typically show sharp peaks due to the absence of intermolecular interactions. In contrast, solid molecules exhibit broadened features as a result of interactions with surrounding molecules in the matrix. For instance, the symmetric stretching mode of water vapor appears around 3600 cm^{-1}**,** while the same mode in solid water ice is broadened, forming a peak spanning 3000–3600 cm^{-1}. In liquid water, this peak is even broader, extending from 2900–3700 cm^{-1} (De Ninno et al., 2013). Moreover, the surrounding chemical environment can shift the positions of the vibrational features.

Molecular vibrations can be broadly categorized into stretching vibrations, where bond lengths change, and bending vibrations, where bond angles change**.** Stretching vibration can be divided into 2, symmetric and asymmetric stretching, while bending vibration can be divided into categories like twisting, wagging, rocking, scissoring etc.

2.7 FTIR spectroscopy:

The most commonly used instrument for IR spectroscopy is the Fourier Transform Infrared (FTIR) spectrometer. A typical FTIR system consists of –

- An IR source
- A Michelson interferometer
- A sample compartment
- A detector

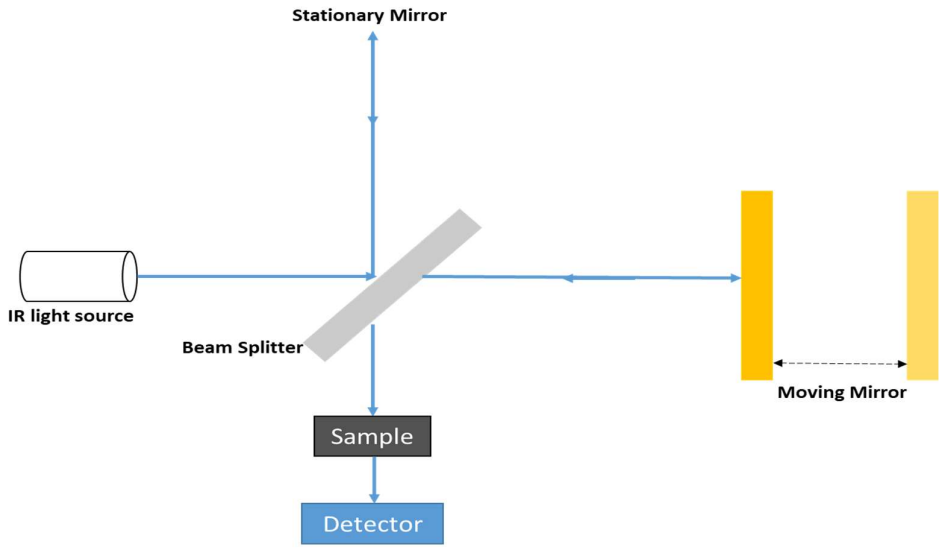

Figure 2.7 Schematic diagram of FTIR spectrometer.

The schematic diagram of an FTIR setup is shown in Figure 2.7. The core component of the FTIR is the Michelson interferometer. The interferometer consists of a beam splitter and two mirrors, one of which is fixed and the other is movable. IR radiation is collimated onto the beam splitter. The beam splitter allows 50% of the beam to transmit and fall on the fixed mirror while the other 50 % to fall onto the moving mirror. Both the beams are reflected from the mirrors and then recombines at the beam splitter where half of the beam is passed through the sample and then recorded by the detector. The other part of the recombined beam is transmitted back to the source. Changing the distance of the movable mirror will create a change in the path length of the two beams thereby interfering differently depending on the path difference between the two reflected beams. These two beams passing through the sample appears to the detector with two different path lengths and interfere with all the information of the sample inside with it and creates an interferogram. That interferogram is decoded with a mathematical operation,

Fourier transform which gives us the final spectrum of the sample which is absorbance or transmittance vs. the wavenumber.

For our experiments, we have used a Thermo Nicolet iS50 FTIR spectrometer. The source of the spectrometer is a Polaris IR source, which emits a wide range of infrared radiation, 9600-20 $cm^{-1.}$ For our experiment, we utilize the mid-IR region (4000-400 cm^{-1}), which is relevant for identifying the vibrational features of the ices. Our experimental system uses Potassium Bromide (KBr) as the beam splitter and deuterated, L-alanine doped triglycine sulphate (DLaTGS) as a detector, which has a spectral resolution better than 0.09 cm^{-1} , allowing us to resolve fine features in the vibrational spectrum.

2.8 VUV/UV Spectroscopy:

Unlike infrared (IR) spectroscopy, which probes vibrational transitions caused by the interaction of photons with molecular vibrational modes**,** ultraviolet (UV) and vacuum ultraviolet (VUV) spectroscopy probe electronic transitions. The interaction of UV photons with molecules gives rise to the excitation of the valence electron from a lower energy state to a higher energy state. In IR spectroscopy, a change in dipole moment is required for a vibrational transition to be IR active. This is why homonuclear diatomic molecules such as N_2 or H_2, which do not possess a permanent or fluctuating dipole moment during vibration, are infrared inactive**.** However, this restriction does not apply in the same way to UV or VUV spectroscopy. Electronic transitions involve the redistribution of electron density, which is always associated with a change in the dipole moment**.** As a result, even homonuclear diatomic molecules like N_2 and H_2 exhibit electronic absorption features in the UV and VUV regions. These transitions are often allowed by electric

dipole selection rules and can be observed spectroscopically, even if the molecules are IR inactive.

Most common electronic transitions include

- σ → σ* (high-energy transitions)
- n → σ* (non-bonding to antibonding)
- π → π*
- n → π*

In Figure 2.8, different allowed electronic transitions in a molecule are shown. The transition from σ→ π* and π → σ* are forbidden by the symmetry, so they are not observed in the standard UV-Vis spectrum.

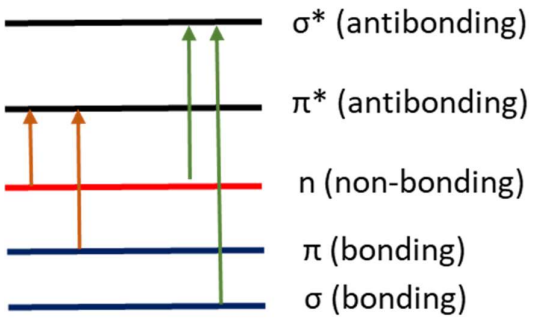

Figure 2.8 Diagram of electronic transition (not to scale).

2.9 Molecular orbitals:

Molecular Orbital (MO) is a region around a molecule where the probability of finding an electron is high. MOs arise from the linear combination of atomic orbitals, which is an approach where the atomic orbitals from the constituent atoms combine to form delocalized orbitals over the entire molecule. Since by Heisenberg

uncertainty principle, the position and momentum of an electron cannot be defined with 100% precision, the atomic orbitals are often given as 3D shapes, governed by the quantum numbers, n (principal quantum number), l (orbital angular momentum quantum number), m_l (magnetic quantum number) and s (spin quantum number).

Now let us consider a case of the H_2 molecule, the molecular orbitals will be formed by the combination of the two 1S atomic orbitals of the two hydrogen atoms. One orbital will be formed from the addition of the mathematical functions of the atomic orbitals and another will be by subtracting them two.

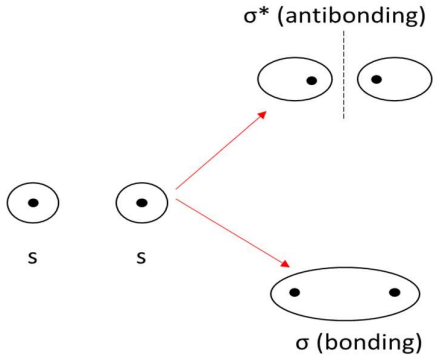

Figure 2.9 Combination of two s atomic orbitals.

Figure 2.9 shows the formation of σ molecular orbitals from the combination of two atomic orbitals. When two atomic orbitals are in phase, they will form one type of molecular orbital, while when the atomic orbitals are out of phase, a new molecular orbital is formed. One of the orbitals is known as a bonding molecular orbital (σ) because the electrons in this orbital spend most of the time in the region between two nuclei. On the other hand, in the antibonding molecular orbital (σ*), the electrons will spend most of their time away from the two nuclei. The energy level diagram for the two molecular orbitals is given in Figure 2.10.

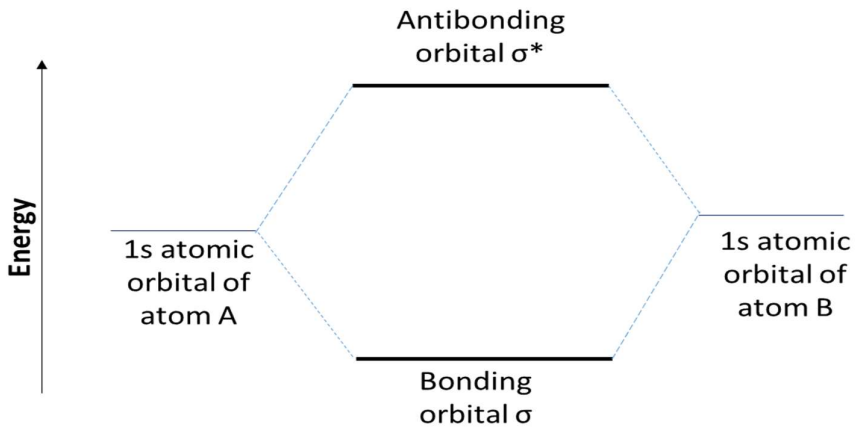

Figure 2.10 Energy level diagram of the two molecular levels.

In case of bonding molecular orbital, it has a lesser energy than that of the individual atomic orbitals while the antibonding molecular orbitals have an energy greater than that of the individual atomic orbitals.

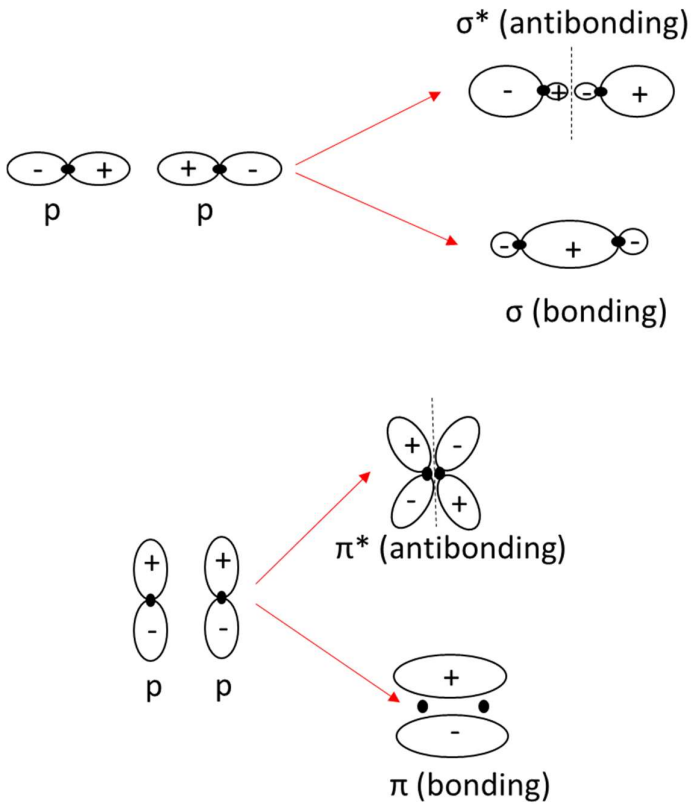

Figure 2.11 Overlap of p molecular orbitals, forming σ & π bonds.

In a similar way, the overlap of the p molecular orbitals, can give rise to the formation of different bonding and antibonding molecular orbitals. Figure 2.11 shows the formation of different bonding and anti-bonding orbitals because of the overlap of p molecular orbitals. For p orbitals in head on overlap, depending on in phase or out of phase overlap between the lobe structures, they can form bonding and antibonding orbital**,** σ orbitals. Whereas when there is a side-on overlap between two p orbitals, similarly depending on in phase or out of phase overlap between the orbitals, they will form bonding or antibonding, π molecular orbital.

2.10 Vibrational progression and Frank-Condon principle:

In a simplistic picture, one might expect that an electronic transition corresponds to a sharp line in the UV spectrum, as suggested schematically in Figure 2.8. However, as will be shown in Chapter 6, electronic transitions often appear as broad features or vibrationally-resolved bands. This is because an electronic transition is frequently accompanied by a change in vibrational energy level, resulting in what is known as a vibronic transition. The intensity and the shape of the vibronic transitions can be explained using Frank-Condon principle. The Frank-Condon principle states that the electronic transition is faster than the nuclei can respond because the timescale of electronic motion ($\sim 10^{-15}$ s) is much shorter than that of nuclear motion ($\sim 10^{-12}$ s). As a result, during the transition, the vibrating molecule will not change its internuclear distance. So only vertical transitions from a lower electronic energy state to higher electronic exited state will occur. Figure 2.12 shows transitions between two electronic states with 4 different situations.

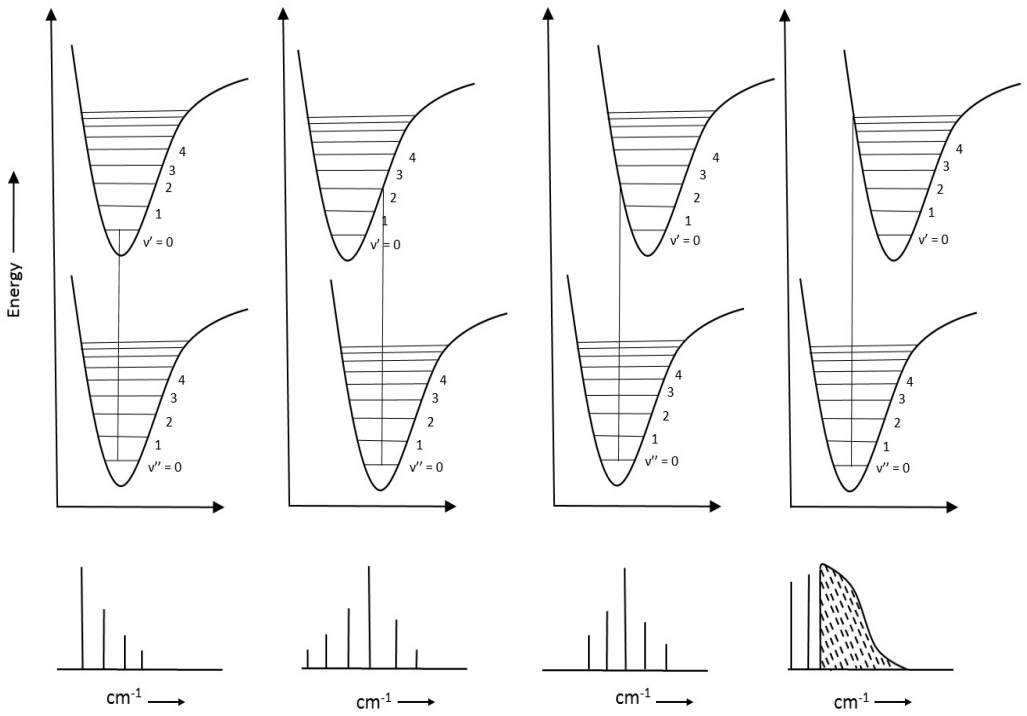

Figure 2.12 The intensity of the lines by Frank –Condon principle (a) internuclear distance of the exited state is (a) same (b) smaller (c) slightly greater (d) considerably greater than the ground state. Adopted from Banwell and McCash, 2017.

In (a), the internuclear distance are almost equal in both the ground and the exited electronic state, the most probable transition occurs from the vibrational ground state v"=0 of the lower electronic state to the vibrational ground state to v'=0 of the excited state**,** since this does not change the internuclear distance of the molecule. Hence, the strongest spectral line will be the (0,0) band, accompanied by weaker bands like (1,0),(2,0)… with rapidly decreasing intensity.

In (b), the internuclear distance of the ground state is greater than that of the exited state. Here the most probable transition will occur from v"=0 → v'=2. So here the weak bands will appear for the other transitions. This leads to a shifted vibrational progression with a different intensity profile.

In (c) the internuclear distance of the ground state is smaller than that of the exited state. Here also the results are similar to that of (b). Here starting from (0,0) band, first the intensity will grow up to (2,0) then start decreasing. A similar vibrational progression will be seen for CO in Chapter 6.

In (d) the internuclear separation is much greater in the exited state. The transition can promote the molecule into the continuum of the excited state's potential energy surface, leading to dissociation**.**

2.11 UV spectrometer:

The schematic diagram of a dispersive VUV spectrometer is shown in Figure 2.13. A typical VUV spectrometer consists of the following key components

- A light source,
- A monochromator (with entrance and exit slit)
- Sample compartment and
- A detector.

A synchrotron is used as a light source for the VUV spectroscopy. The light emitted from the synchrotron source enters the monochromator through an entrance slit, which narrows the beam to a suitable size**.** Inside the monochromator, a diffraction grating disperses the polychromatic light into its individual wavelengths based on the grating equation. By adjusting the angle of the grating and the exit slit, a specific wavelength (monochromatic light) can be selected. The selected monochromatic beam is then directed into the sample compartment, where it interacts with the sample. The transmitted or absorbed intensity is then measured by the detector, and the resulting spectrum is

recorded. The VUV spectroscopic study presented in Chapter 6 was carried out using the Aarhus STorage RIng in Denmark 2 (ASTRID2) synchrotron beamline facility in Aarhus University, Denmark. ASTRID2 is a third-generation synchrotron light source that provides high-resolution and high-flux radiation in the vacuum ultraviolet region, making it ideal for precise electronic spectroscopy of gas-phase and condensed-phase samples.

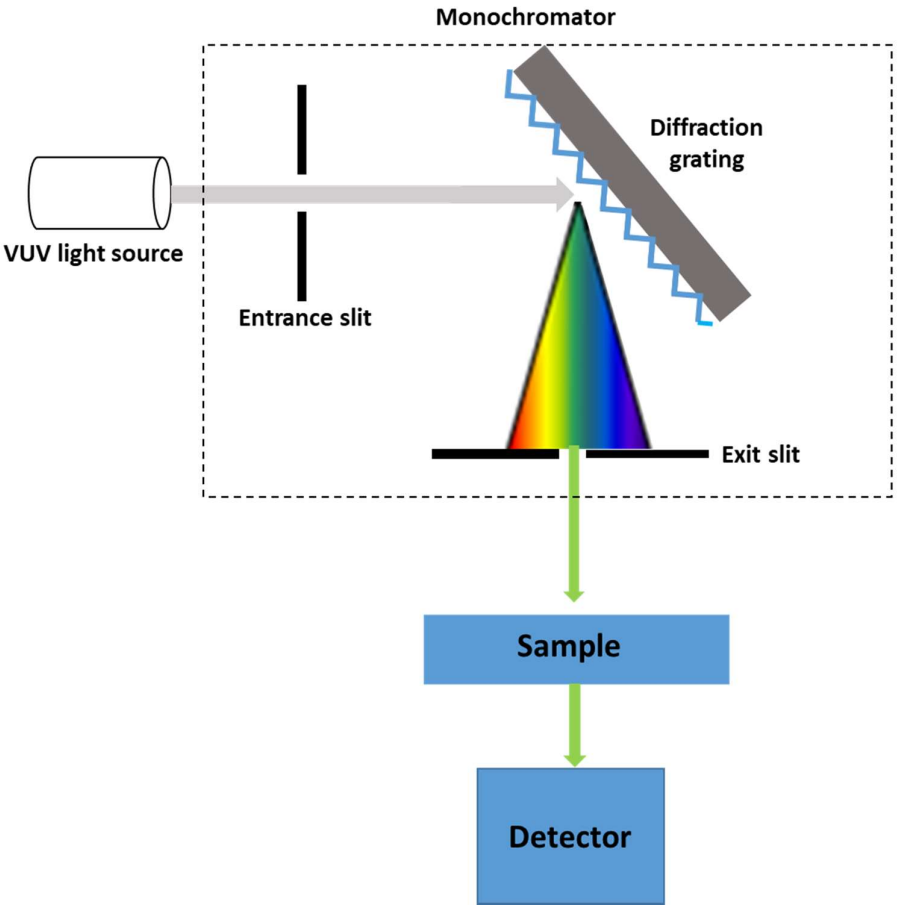

Figure 2.13 Schematic diagram of UV spectrometer.

2.12 Beer Lambert Law:

The physical process by which electromagnetic radiation is absorbed by a sample can be quantitatively described using the Beer–Lambert Law. This law relates the intensity of transmitted light to the number density of absorbers in the medium. Mathematically, it is expressed as:

$$I = I_0 \cdot e^{-\sigma n l}$$

Where;

- I_0 is the intensity of the incident radiation,
- I is the intensity of the transmitted radiation,
- n is the number density (concentration) of absorbing molecules (in cm^{-3}),
- l is the optical path length through the sample (in cm),
- σ is the absorption cross-section of the molecule (in cm^2).

The absorbance is defined as

$$\alpha = (\sigma n l / 2.303)$$

It is also commonly expressed using the logarithmic ratio of the incident to the transmitted intensity

$$\alpha = \log (I_0 / I)$$

The transmittance T is given by

$$T = I / I_0$$

Thus, absorbance and transmittance are related by

$$\alpha = -\log(T)$$

2.12 Chemistry by energetic electron irradiation:

The interaction of energetic electrons with molecules plays a crucial role in the chemical evolution in molecular ices. In general, when a high energy (keV) electron interacts with a molecular ice, it generates a cascade of low energy secondary electrons which can trigger the complex chemical reactions for the formation of larger molecule. It is now well accepted that the low-energy secondary electrons contribute to the chemistry of the interstellar molecular ices (Arumainayagam et al., 2010, Arumainayagam et al., 2019, Boyer et al., 2016).

There are several processes which can drive the chemistry as discussed below

- **Electron ionization:**

When an electron of sufficient energy interacts with a molecular ice, it can knock out the electron from the molecule and leave a radical cation behind

$$M + e^- \rightarrow M^{\bullet +} + 2e^-$$

It has been observed previously that the mixture of binary ices CO/NH_3, C_2H_4/H_2O, C_2H_4/CH_3OH when irradiated by electron irradiation with an energy greater than the threshold for ionization energy of the molecule, it ionizes the molecules and the resulting ion interacts with other molecules present in the neighborhood and result in the formation of formamide, ethanol and ethyl methyl ether respectively (Warneke et al., 2015, Bredehöft et al., 2017, Schmidt et al., 2018).

- **Electronic excitation:**

The colliding electron can excite the molecule to a neutral excited state.

$$M+e^- \rightarrow M^*+e^-$$

In a binary mixture of CO/CH_3OH ices, formaldehyde forms with an electron energy of 7 eV which is known to be the excitation energy of the CH_3OH ices (Schmidt et al., 2021b).

- **Electron attachment:**

When an incoming electron attach to a molecule, it can form a radical anion.

$$M+e^- \rightarrow M^{\bullet -}$$

Electron attachment to CO at 4 eV in CO/H_2O mixed ices leads to the formation of $CO^{\bullet -}$ anion which can undergo proton transfer with H_2O yielding $HCO^{\bullet}$ and HO^- (Schmidt et al., 2019) , Then $HCO^{\bullet}$ reacts with the nearby H_2O to form of formaldehyde (H_2CO) . Similarly C_2H_4 in C_2H_4/H_2O mixed ices at energies below 5-6 eV produces the $C_2H_4^{\bullet -}$ radical anion, initiating the formation of ethanol (Warneke et al., 2015).

Dissociative processes:

The above described processes have assumed that the molecule remains intact. However, the molecules can dissociate because of electron irradiation.

- **Neutral dissociation:**

- The parent molecule can undergo dissociation because of the incoming electrons. These dissociated products can react with the neighbouring molecules to form different products.

$$M+e^- \rightarrow A^\bullet + B^\bullet + e^-$$

The product formation from neutral dissociation has been observed in many cases starting from

$NH_3 \rightarrow H^\bullet + NH_2^\bullet$ (Schmidt et al., 2022)

$H_2O \rightarrow H_2 + O$ (Schmidt et al., 2019)

$\rightarrow H^\bullet + HO^\bullet$ (Warneke et al., 2015)

$CH_4 \rightarrow H^\bullet + CH_3$ (Schmidt et al., 2022)

$CH_3OH \rightarrow CH_3^\bullet + HO^\bullet$ (Schmidt et al., 2021a)

- **Dissociative electron attachment:**

In this case, as an effect of the electron irradiation, a radical anion is produced along with a neutral fragment.

$$M+e^- \rightarrow A^- + B^\bullet$$

- **Dissociative ionization:**

In this case the molecule will be dissociated forming a cation and at least one neutral product.

$$M+e^- \rightarrow A^+ + B^\bullet + 2e^-$$

The states a molecule or the fragments can occupy after the interaction with the electron can be more reactive. If these molecules are in contact with other molecules, it can further react with them and chemical enrichment can happen.

2.13 Morphology of molecular ice:

In the interstellar medium, molecules colliding with dust grains at extremely low temperatures (~10 K) adhere to the surface, forming molecular ice. The molecular ices as explained in Chapter-1, are present in different planets, their moons, comets or ISM can have different structures depending on the temperature of the environment. On the other hand, the molecular ices can be mixed or layered. In all these cases, the molecules can have both amorphous and crystalline structure depending on the physical conditions in the surrounding medium.

For example, water ice can exhibit different structural phases based on the formation conditions. When water molecules freeze from the liquid phase, they generally form hexagonal crystalline ice (ice I_h). However, when water vapor condenses directly onto a cold surface, the resulting ice can be either amorphous or crystalline depending on the substrate temperature. At temperatures around, vapor-deposited ice—whether water or another volatile species—typically forms an amorphous solid due to insufficient molecular mobility. Upon warming, molecular mobility increases, enabling reorganization of the structure. For water ice, amorphous ice begins to crystallize near 130 K, forming cubic crystalline ice (ice Ic). Further heating leads to a transition into the more stable hexagonal crystalline phase (ice I_h) around 150 K (Watanabe and Kouchi, 2008).

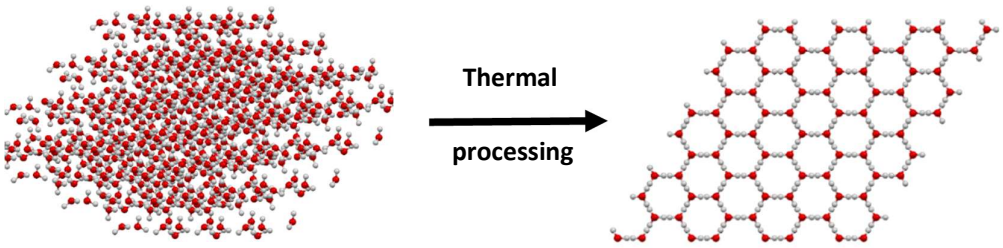

Figure 2.14 Change of morphology from amorphous to crystalline during the thermal processing.

The morphology plays a significant role in the chemistry of the molecules in the low temperature. Amorphous ice being more porous become chemically more active towards any reaction than its crystalline counterpart. The morphology of the molecular ice present in the ISM or the icy bodies in the solar system has been studied by many experiments (Mason et al., 2006, Pavithraa et al., 2017). Infrared spectroscopy has been proven to be a powerful tool for probing structural changes in the ices. For instance, Hofmann et al., 2025 showed the changes in the infrared spectral features appearing due to the change of morphology of the water at different temperatures from 15 K to 150 K.

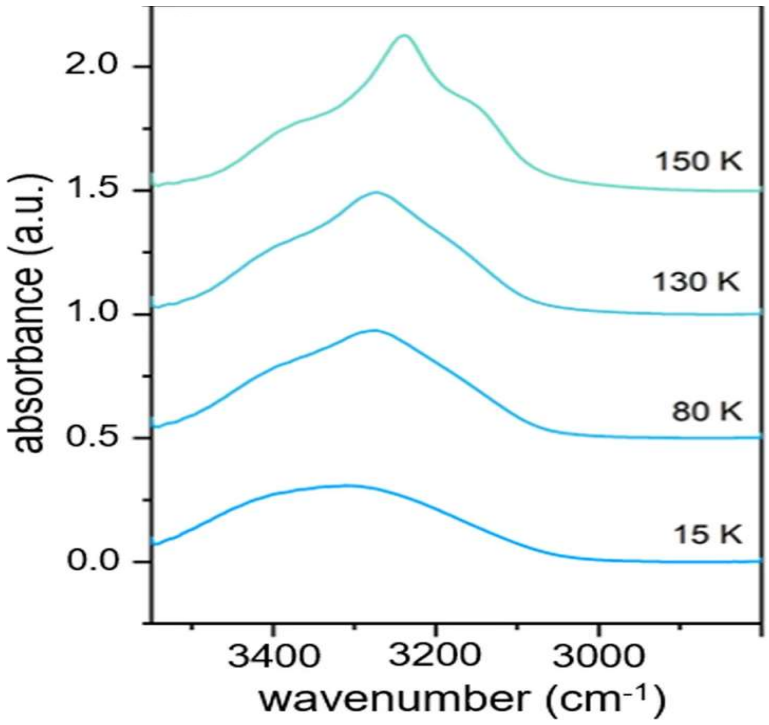

Figure 2.15 Change of amorphous water ice (10 K) to crystalline water ice (150) with the IR spectra (Hofmann et al., 2025).

On the other hand, once the ice becomes crystalline, it is known to remain crystalline until its sublimation when heated to higher temperature. Contrary to this, Pavithraa et al., 2017 reported the reversible phase change in the astrochemical ices and it is shown that when the ice was heated further from crystalline phase, it went back to the amorphous form. Besides, the change in morphology of molecular ice from crystalline to amorphous can also happen by the irradiation of energetic particles (Famá et al., 2010).

Amorphous molecular ices, due to their porous structure, have the ability to trap volatile molecules within their matrix. These trapped species, even if more volatile than the host molecule, can remain embedded in the ice at temperatures higher than their typical sublimation points (Collings et al., 2004). This entrapment enables

them to participate in chemical reactions that would otherwise be unlikely. Therefore, the morphology of ice plays a crucial role in governing chemical reactivity in the interstellar medium and on planetary bodies.

2.14 Conclusion:

This chapter explains the necessary details of the basics of molecular spectroscopy. We have discussed the IR, UV spectroscopy, and the details of the underlying technique in the spectrometers used. The chapter also includes the role of spectroscopy in determining the morphological phase of the ices. The role of electron irradiation has been covered in the discussion.

Chapter 3 Experimental setup and methodology

Chapter Overview:

This chapter provides a detailed description of the experimental set up used for the experiments. Each component has been discussed, highlighting its function and significance. The spectrometers used for IR and VUV measurements have been thoroughly explained. The chapter concludes with a brief explanation of the electron gun system used for the irradiation experiments.

3.1 Introduction:

The experiments presented in this thesis were conducted using two distinct experimental facilities: The Simulator for Astromolecules at Low Temperature (SALT) setup in Physical Research Laboratory, Ahmedabad, India and another the Aarhus Storage Ring in Denmark 2 (ASTRID2) synchrotron facility in Aarhus University, Denmark. In order to replicate the physical and chemical conditions present in the cold astrophysical environments which are characterized by very low temperature (~10 K) and ultrahigh vacuum, laboratory experiments are typically conducted inside an ultrahigh vacuum (UHV) chamber coupled with a closed cycle helium cryostat. Within the chamber, a substrate is mounted on the cold head of the cryostat. The cryostat can reach a temperature as low as 6 K within the chamber with a pressure 10^{-10} mbar. Molecular ices are grown by depositing the molecules on to the substrate at low temperature. A resistive heater connected to the cold head can be used to control the temperature enabling it to do thermal processing. On the other hand, when the ices are formed, they can be subjected to energetic processing that mimics the conditions in space such as irradiation of ultraviolet (UV) photons,

ions to electrons. In this thesis, we have simulated the processing of ices using the electron gun.

3.2 Vacuum chamber:

The experiments are carried out in a vacuum chamber maintained at pressure approximately 10^{-10} mbar which corresponds to a molecular density of ~ 10^{6} cm^{-2}. At very low temperature (~10 K) the sticking coefficient of most of the gas phase species approaches nearly unity, implying that the molecules colliding with the cold substrate will adsorb on to that and form an ice layer. However, if the chamber pressure is not sufficiently low, at a temperature ~10 K, the gas molecules (contaminants) present inside the chamber can also condense and form unwanted layers of ice on the substrate. The time to form one monolayer of contaminant ices onto the substrate can be approximately calculated from the impingement rate of the molecules.

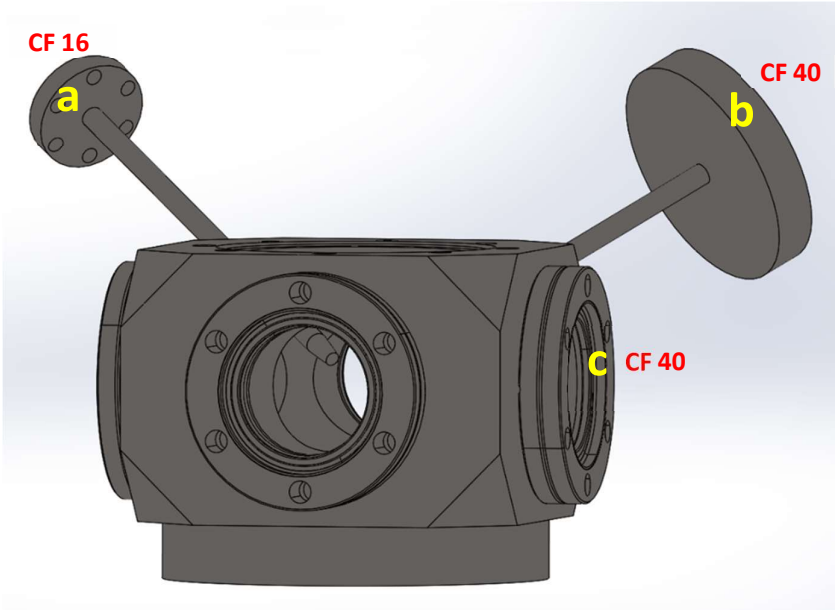

Figure 3.1 Vacuum chamber made of stainless steel. (a) CF-16 flange for gas inlet, (b) CF-40 flange additional gas inlet port, (c) CF-40 ports for IR probing.

It can be shown that for ~10^{-6} mbar, the time to form one monolayer (~10^{15} molecules cm^{-2}) of contaminant ice is approximately 2.5 seconds, which shifts to approximately 2000 seconds when the chamber pressure is ~10^{-9} mbar. Therefore ultrahigh vacuum is a necessary part of our experiments to mimic the conditions as well as to minimize the contaminations.

Furthermore, stainless steel is known to have the lowest outgassing rate, making it an ideal material for constructing the vacuum chamber. The UHV chamber (Figure 3.1) used in the experimental setup is made of stainless steel (SS304) in order to achieve ultrahigh vacuum pressures.

3.3 Cryostat:

The Simulator for Astromolecules at Low Temperature (SALT) set up at Physical Research Laboratory consists of a closed cycle helium cryostat (ARS, USA model CS204AB-FMX-6-450) capable of cooling down the temperature of the substrate as low as 6 K. A schematic diagram of the cryostat is shown in Figure 3.2. The operating principle of the cryostat is based on the well-known Gifford-McMahon cycle, in which high pressure helium gas (Purity 99.999%) is compressed and directed into the cold head, the He gas expands and contribute to the cooling of the experimental system. It is a two stage cryocooler where the first stage reduces the temperature from room temperature to a colder value bearing the maximum heat load while the second stage cools it down more efficiently and can reach at very low temperature ~6 K.

The lower part of the cryostat is known to be the cold finger, is constructed from oxygen free high conductivity copper (OFHC). A substrate typically 25 mm in diameter and 2 mm in thickness is mounted at the tip of the cold finger using indium foil as an interfacial layer. Indium being both ductile and thermally conductive helps

to maintain efficient thermal contact between the substrate and the cold finger (Figure 3.3). To monitor and control the temperature, a silicon diode temperature sensor is attached to the substrate along with a resistive heater to heat the substrate to any desired value. A Lakeshore 335 temperature controller is used for precise temperature regulation. It is useful in the temperature range 1.4 K to 500 K where the ramp rate can be fixed from 0.1 $Kmin^{-1}$ to 100 $Kmin^{-1}$. On the cold head, two gas transfer lines, made of stainless steel is used to flow the He gas from the compressor to the cryostat and bring it back to the compressor.

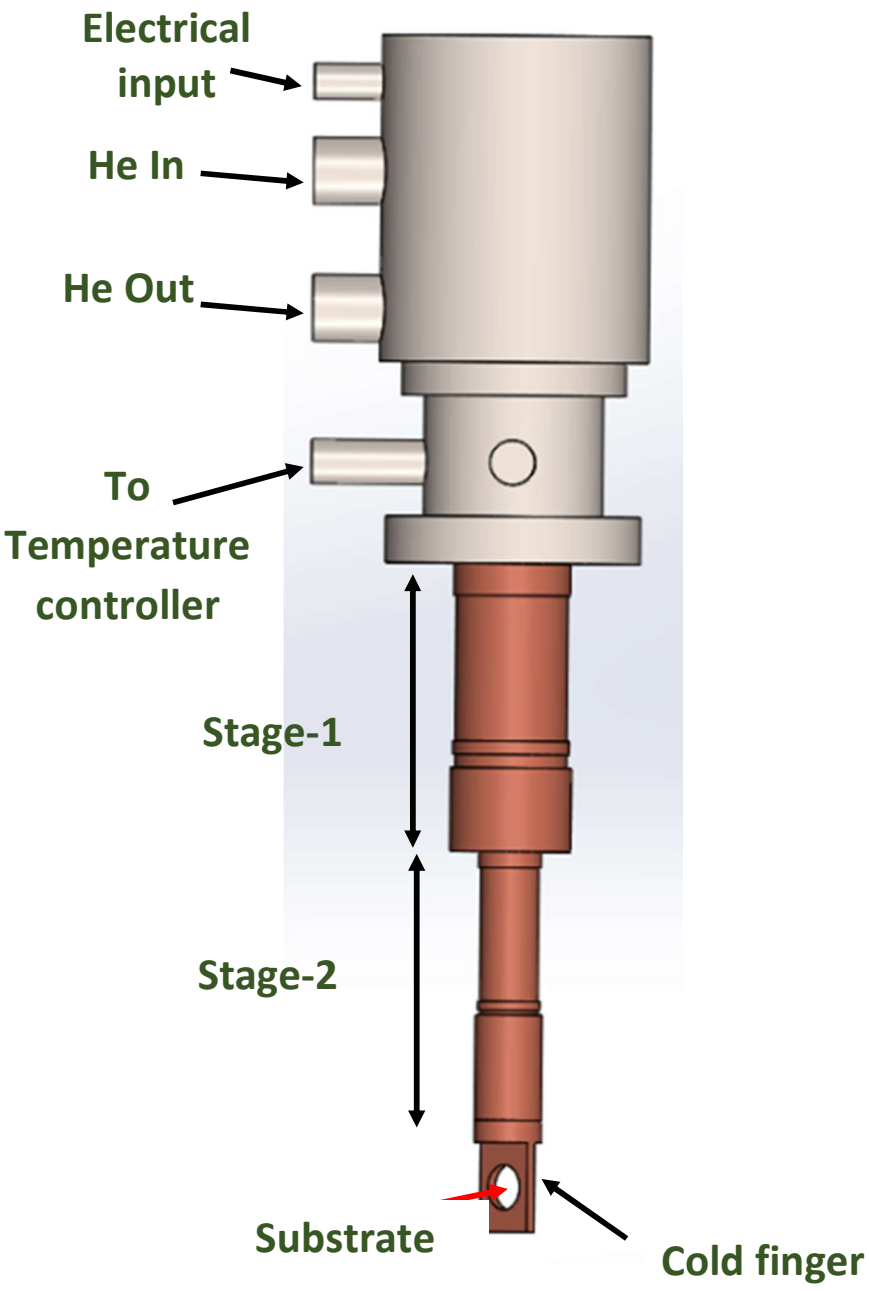

Figure 3.2 Closed cycle He cryostat.

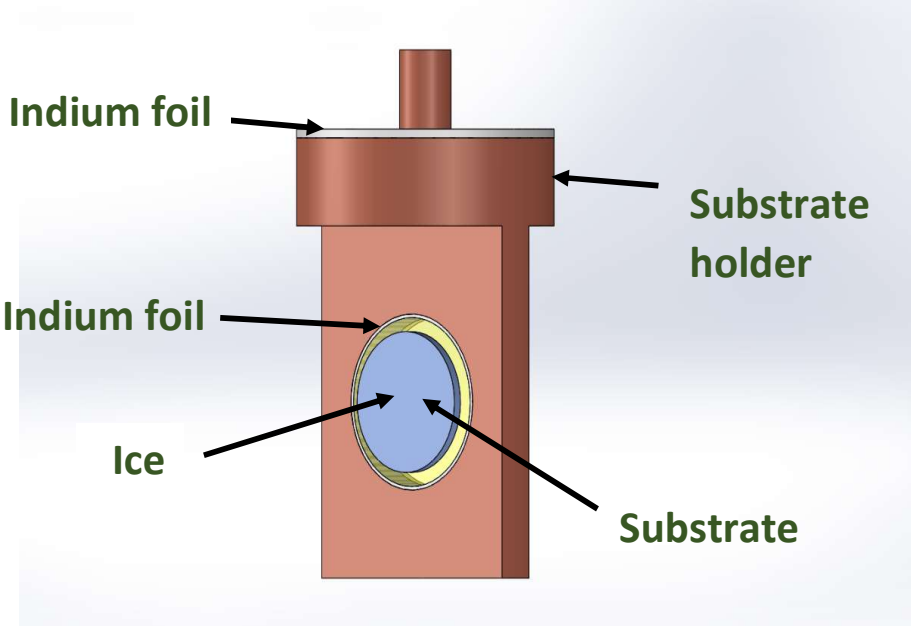

Figure 3.3 OFHC substrate holder with indium foil (shown in grey) containing substrate (shown in yellow) and ice (shown in blue) on top of the substrate.

The cryostat is connected to the vacuum chamber, a turbo molecular pump and gauges by a cross flange. The turbo molecular pump is backed by a scroll pump ensuring the molecular flow present inside the chamber for an efficient performance of the turbomolecular pump. Sample containers are connected to the chamber through stainless steel gas lines. These gas lines are typically evacuated to a pressure ~10^{-3} mbar prior to sample introduction to ensure the removal of the atmospheric contamination. The samples used in the experiments are mostly liquid and gas which have sufficient vapor pressure at room temperature. The liquid samples are kept in a quartz sample holder and gets processed using freeze-pump-thaw cycles to remove any dissolved atmospheric gases from the sample. After purifying the liquid sample, the vapor is directed towards the chamber through the gas line. For the gas sample, they are directly introduced to the gas line from the gas cylinders.

Once the substrate is cooled to a temperature ~10 K, the vapor of the liquid or gaseous molecules are introduced to the chamber using an all metal leak valve allowing controlled deposition on to the cold substrate and form the molecular ices. An assembly of different parts explained till now is shown in Figure 3.4.

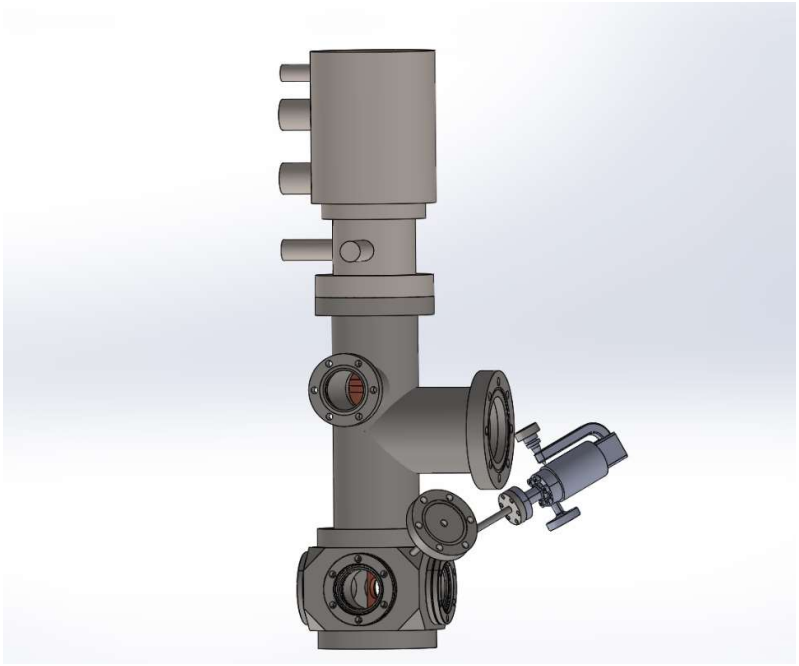

Figure 3.4 Assembly of different parts of the cold head and vacuum chamber.

In the experiments described in Chapter-4 and 5, three types of sample configuration is used- pure, layered and mixture of samples. For layers, first the gas line is evacuated to a level 10^{-3} mbar. Then the vapor of the sample liquid/gas was introduces in the gas line and then deposited on to the substrate making the first molecular ice layer. After that the gas line was again evacuated and the previous molecules were taken out of the gas line. Again the second molecule was allowed to enter into this gas line and deposited onto the previously deposited ice making it

another layer. For mixture of molecules, they are first mixed inside a mixing chamber and then deposited together on to the cold substrate

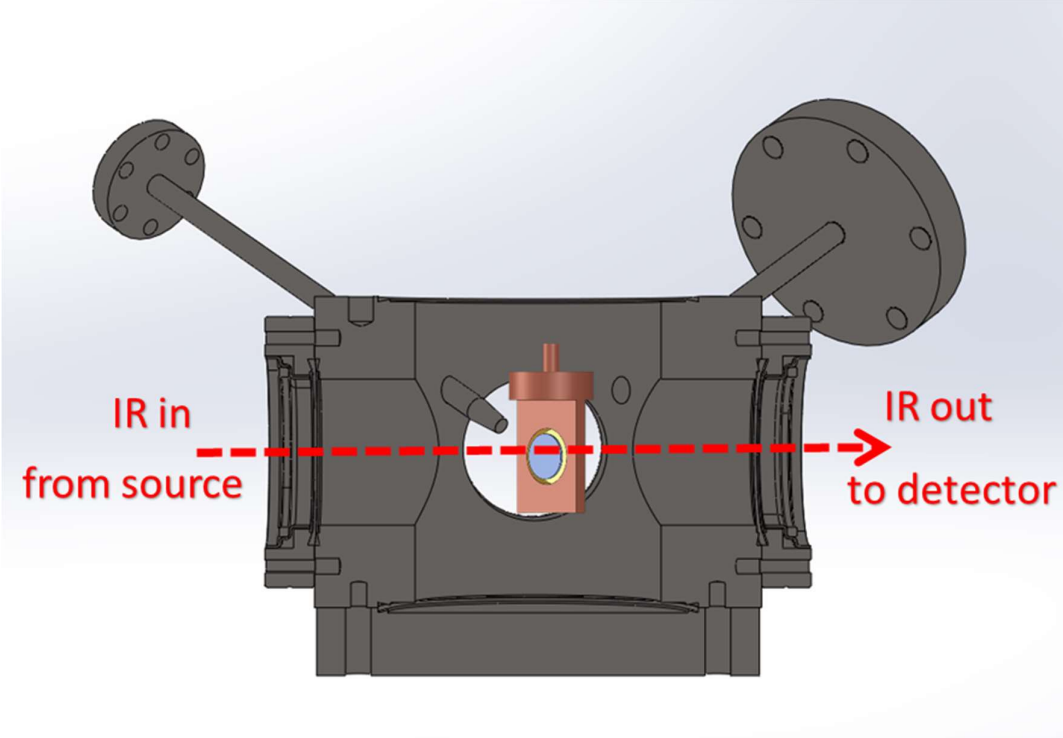

Figure 3.5 IR beam from source to detector via the cold substrate.

After the molecules are deposited on to the cold surface, the molecular ices are characterized using various spectroscopic technique. The chamber is equipped with optical windows made of materials that are transparent to the desired regions of the electromagnetic spectrum allowing spectroscopic measurements such as infrared (IR) and vacuum ultraviolet (VUV) transmission spectroscopy. In these techniques, IR/VUV light is passed through the sample and the transmitted light reaches the detector. By studying the characteristic of the transmitted light, we can analyse important information about the molecular composition of the as explained in Chapter-2.

The thickness of the molecular ice films can be calculated using different techniques. One such method is laser interference which takes into account the variation of light intensity during the growth of the film due to the interference between the light reflected in the boundaries of vacuum-ice and ice-substrate interface. Another well-known technique involves calculating the column density of the molecules in the ice using the band area of a specific vibrational absorption peak and the corresponding band strength (A value) of that particular vibration. In PRL, we use the second technique.

3.4 Choice of Substrate:

Choosing an appropriate substrate is a critical aspect of the ice spectroscopy experiments. In Chapter 6, we have used Lithium Fluoride (LiF) as a substrate for the vacuum ultraviolet (VUV) spectroscopy of CO ices, while in other chapters with infrared (IR) as probing technique, the substrate chosen was Zinc Selenide (ZnSe). The main reason behind the choice of substrates is their transparency region. Some substrates are transparent in a particular range in the electromagnetic spectrum while other is transparent at a different region. Another important aspect is its interaction with the molecular ice. ZnSe has been mostly used in different astrophysical ices experiments because of its insolubility in water. On the other hand, there are other substrates like Sodium Chloride (NaCl), Cesium Iodide (CsI), , Potassium Bromide (KBr) etc which are very hygroscopic, LiF being less but hygroscopic are avoided although they are well transparent in the IR region as well.On the otherhand, LiF being transparent in the VUV region was used in the spectroscopy of CO ices. There exist many substrates commonly used for these experiments. A list of the substrates and their transparency is given in Table 3.1.

Table 3.1 Some commonly used substrates for the ices experiments

Material	Transparency Range (Wavelength)	Transparency Range (Wavenumber, cm^{-1})	Remarks
Lithium Fluoride (LiF)	120 nm – 6 μm	83300 – 1666	VUV, UV, and IR
Magnesium Fluoride (MgF_2)	130 nm – 7.0 μm	76923 – 1429	VUV to IR
Calcium Fluoride (CaF_2)	130 nm – 10 μm	76923 – 1000	VUV to IR
Barium Fluoride (BaF_2)	150 nm – 12 μm	66667 – 833	VUV to IR
Fused Silica	180 nm – 2.2 μm	55556 – 4545	UV to NIR
Sapphire (Al_2O_3)	170 nm – 5.5 μm	58823 – 1818	UV to IR
Potassium Bromide (KBr)	230 nm – 25 μm	43478 – 40	UV to IR, hygroscopic

Potassium Chloride (KCl)	210 nm – 20 μm	47619 – 500	UV to IR
Sodium Chloride (NaCl)	200 nm – 15 μm	50000 – 666	UV to IR, hygroscopic
Cesium Iodide (CsI)	250 nm – 55 μm	40000 – 182	UV to FIR
Zinc Selenide (ZnSe)	600 nm – 21 μm	16666 – 476	Visible to IR
Zinc Sulfide (ZnS)	370 nm – 13.5 μm	27027 – 740	Visible to IR
Germanium (Ge)	1.8 μm – 23 μm	5555 – 434	IR only
Silicon (Si)	1.2 μm – 15 μm	8333 – 666	IR only

3.5 FTIR spectrometer:

The spectroscopy of the molecular ice after their formation on to the cold substrate were carried out as shown in Figure 3.5. At PRL, we have used a Thermo Scientific Nicolet IS50 Fourier Transform Infrared (FTIR) spectrometer. The fundamental working principle of the spectrometer is based on interferometry and described in detail in Chapter-2. The core of the spectrometer is a Vectra interferometer with

precise alignment of the optical components which give high stability and precision in measurements. This spectrometer is capable of working in the far infrared (10 cm^{-1}) to visible (up to 27000 cm^{-1}) region of the electromagnetic spectrum. It has two internal sources, one is Polaris IR source which spans a range 10 cm^{-1} to 9600 cm^{-1} useful for the far and mid-IR spectroscopy, and another is tungsten halogen source with a range 2000 cm^{-1} to 27000 cm^{-1} useful for near IR and visible applications. The beam path can be configured with a variety of beam splitters. The IR source is typically paired with beam splitters as KBr (7800-350 cm^{-1}) and XT-KBr (11000-375 cm^{-1}), while the white light source is used with Calcium Fluoride (CaF_2) (14500-1200 cm^{-1}), quartz (27000-2800 cm^{-1}), for visible and near IR applications. For far IR applications, beam splitters like Cesium Iodide (CsI) (6400-200 cm^{-1}) and solid substrate (700-50 cm^{-1}) are available. This is important to note that CsI is extremely hygroscopic (sensitive to moisture) and fragile. There is another optional IS50 ABX automated beam splitter exchanger which can allow up to three beam splitters to be mounted and exchanged thereby making smooth transition between different wavelength ranges.

A key component in the iS50 spectrometer is the helium- neon (He-Ne) laser with a wavelength 632.8 nm (15798 cm^{-1}). The laser beam is directed through the interferometer alongside the IR beam serving as a precise reference for mirror position and velocity. This reference allows the instrument to maintain a constant mirror speed and phase during the scans. Also it dynamically aligns the interferometer's fixed and moving mirrors providing an exceptional wavenumber accuracy (better than 0.005 cm^{-1}) and precision (0.0008 cm^{-1}).

After passing through the sample, the IR beam is directed to detectors. There is a dedicated DLaTGS **(**deuterated, L-alanine doped triglycine sulphate**)** detector with

a KBr window that covers 12000-700 cm^{-1} while it has many other detectors like Mercury Cadmium Telluride (MCT)-High D* (11,700–800 cm^{-1}), MCT-A (11,700–600 cm^{-1}), MCT-B (11,700–400 cm^{-1}), InGaAs (12,000–3,800 cm^{-1}), InSb (11,500–1,850 cm^{-1}), Lead Selenide (PbSe) (11,000–2,000 cm^{-1}), silicon (27,000–8,600 cm^{-1}), DLaTGS-CsI (6,400–200 cm^{-1}), and bolometers or photoacoustic detectors for the far-IR (down to 10 cm^{-1}). This spectrometer can offer a high optical resolution better than 0.09 cm^{-1} which is important to resolve fine spectral features in the complex molecular ices.

For the experiments reported in this thesis, the mid-IR region has been used and for that we have used Polaris IR as a source and DLaTGS-KBr as a detector.

3. 6 VUV Beamline:

The VUV spectroscopy of the molecular ices was carried out in Aarhus Storage Ring in Denmark 2 (ASTRID2). As explained in the previous section, the principle involves passing VUV/UV light through the sample and analyzing the transmitted light using a detector. The schematic diagram of a typical VUV/UV spectrometer is shown in Chapter-2.

Electrons are initially produced in a 100 MeV track microtron and subsequently injected into the ASTRID booster ring where they are accelerated to 580 MeV. The electrons are then transferred via a dedicated beamline into ASTRID2 where they are injected at the storage energy of 580 MeV.

This set-up enables a constant electron current typically around 180-200 mA with a stable photon output for experiments. Once circulating in the storage ring, the electrons emit synchrotron radiation as they are deflected by the ring's bending magnets and insertion devices. The VUV light produced are then passed thorough

different mirror systems and redirected towards the monochromator. The AU-UV beamline is equipped with toroidal grating monochromators offering two interchangeable gratings: a low energy grating with 1000 groves/mm which gives higher flux covering 200-700 nm range and a high energy grating with 2000 grooves/mm which is optimized for high resolution and cover 100-350 nm range. Both the gratings have a major radius of 1 m and minor radius of 0.7755 m. The entrance and exit slits of the monochromator are selectable with fixed sizes (e.g., 50, 100, 200, 500 µm for the entrance; 100, 200, 500, 1000 µm for the exit). Since LiF is an excellent optical material for the VUV region (Table-3.1), we have formed CO ice at 10 K and studied the VUV spectroscopy of the ice.

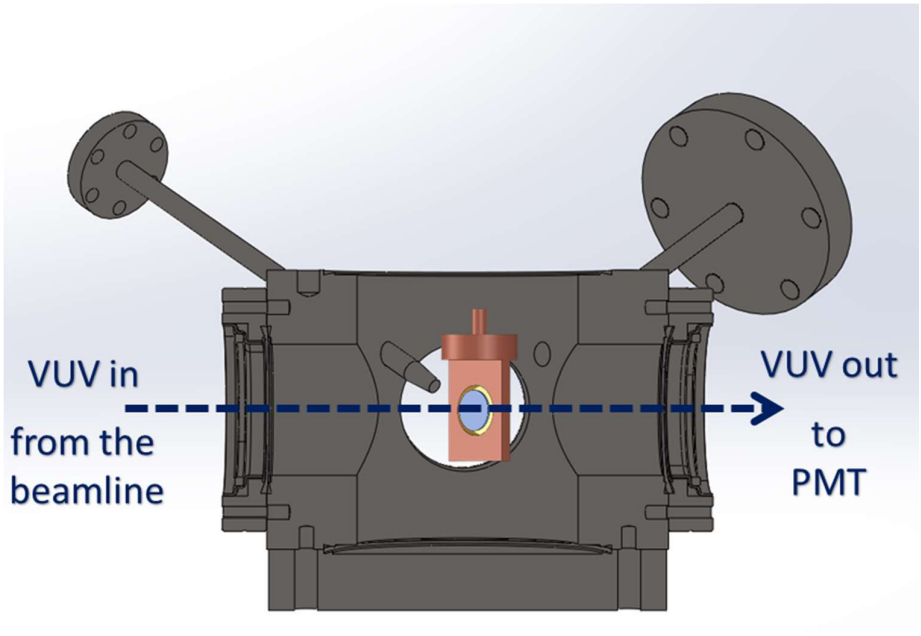

Figure 3.6 VUV beam from source to the PMT detector via the cold substrate.

In our experiments for this thesis we have used the high energy grating covering the range from 100-350 nm for spectroscopy of CO ice. The VUV light is then

passed through the molecular ice and reaches to the photomultiplier tube (PMT) aligned with the detector (Figure 3.6).

3.7 Electron Gun:

The molecular ices are known to be processed through various energetic particles that causes the evolution of other complex molecules in the ice phase. In chapter-6, we have used electrons of keV energy to process CO ice and study the molecular evolution.

The electron gun used in the experiments is SPECS EQ 22/35 from SPECS GmbH which is a stable electron source capable of generating electrons up to 5 keV. The working principle begins with heating a tungsten hairpin filament, which is held at a negative potential corresponding to the desired electron energy. This heating causes electrons to be emitted. These emitted electrons are then accelerated towards the anode.

For stable operation, the EQ 22/35 requires pressure conditions below 10^{-6} mbar. The electron beam can be optimized either for maximum beam current or for minimum diameter. Typical operational parameters include a Wehnelt voltage of -30 to -100 V, a Focus voltage of 0.7 to 0.8 times the energy voltage, and a Filament operating at 2 to 3 V with 2.2 A. The electron emission ranges from 0.01-250 µA, the typical range used is in between 1-20 µA. The spot size can be adjusted down to 50 µm, and the optimized beam diameter varies from 400 µm at approximately 100 eV beam energy to 50 µm at 5 keV beam energy. It also allows for scanning over a maximum range of about 10x10 mm^2. The energy resolution of the beam is typically smaller than 1 eV, primarily defined by the thermal broadening of the energy width.

In our experiments, we have used an electron energy 2 keV at a beam current 0.1 mA to irradiate CO ices with beam raster of 5x5 mm^2. The electron irradiated sample is probed using VUV spectroscopy. The VUV spectra of the sample pre and post irradiation are recorded, usually at 10 K where irradiation was carried out.

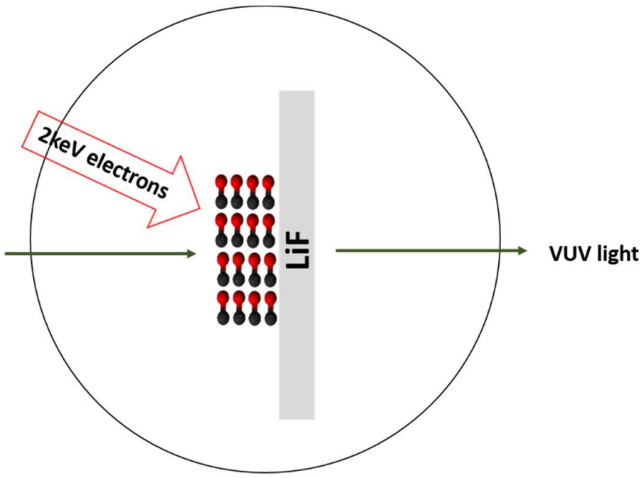

Figure 3.7 Schematic of the configuration used for VUV probing of the molecular ice pre and post electron irradiation.

3.8 Conclusion:

The experimental system described in this chapter, an ultrahigh vacuum chamber with cold head and ports of pumping and sample handling, was used for the experiments in PRL and in VUV beamline at ASTRID2. The spectroscopy techniques employed are complimentary to each other where the characteristic absorptions of molecules and complex residues from irradiation can be studied. In addition, to the spectroscopy the use of high resolution transmission electron microscope (as an end user) enabled us to understand the physical nature of the residues that are obtained from the experiments. The experiments carried out and the results obtained are provided in detail in the following chapters.

Chapter 4 Effect of ethylene glycol on the phase and sublimation of water ice in the astrochemical conditions

Chapter overview:

Water ice is the most abundant ice in the solar system as well as in the interstellar medium (ISM), making it a key component in the chemical evolution of astrophysical environments. The stability and morphology (amorphous or crystalline) of water ice are crucial factors that influence its reactivity and interaction with other species. While the phase and sublimation behaviour of pure H_2O are well established under astrochemical conditions, the real interstellar ices are complex mixture of various other molecules. Despite this, the effect of the molecular interaction, mainly hydrogen bonding between molecules, on the phase and sublimation of water ice is poorly understood. In this chapter, we investigate the influence of the hydrogen bonding interaction between ethylene glycol (EG) and water in the solid phase. Our results show that in the ice phase EG can restrict the known phase transition of water. Also, it can elevate the sublimation temperature of water ~50 K higher than that for pure water ice. These results can have great implications on the chemistry in comets and ISM.

4.1 Introduction:

Water (H_2O) ice is known to be the most common molecular ice both in the interstellar medium (ISM) and in the inner solar system. In addition to water, a

variety of complex molecular ices have been detected in the ISM. The dense molecular cloud is known to be made up of a layered structure. The inner layer is mostly made of amorphous solid water and other components like carbon dioxide (CO_2), ammonia (NH_3) and methane (CH_4) while the outer layer is mostly made up of carbon monoxide (CO) (He et al., 2021). H-atom addition reaction in the CO-rich layer leads to the formation of various molecular species and radicals like HCO, H_2CO, CH_2OH, CH_3O, and CH_3OH. The recombination reaction between the radicals are known to form complex molecules like glycolaldehyde ($HOCH_2CHO$), the simplest sugar and ethylene glycol $(CH_2OH)_2$. Both these molecules are known to be detected in the ISM by (Hollis et al., 2000, Hollis et al., 2002). Ethylene glycol (EG), often referred to as "*interstellar antifreeze*" has been observed in several environments including the hot core of Orion (Brouillet et al., 2015) , the low mass protostar NGC 1333-IRAS2A (Maury et al., 2014),the intermediate-mass protostar NGC 7129 FIRS 2 (Fuente et al., 2014) and also in the MM1 core of NGC63341 (McGuire et al., 2017). EG can also be formed through several pathways – by the hydrogenation of glycolaldehyde, (Leroux et al., 2021), via the barrierless radical-radical reactions between two hydroxymethyl (CH_2OH) radicals, (Zhu et al., 2019) or through energetic processing of mixture of methanol (CH_3OH) and water (Hudson and Moore, 2000) . The presence of both CH_3OH and H_2O in the protoplanetary disks (Walsh et al., 2016, Hogerheijde et al., 2011) suggests that complex organic molecules such as EG may also be present, although EG itself has not been definitively detected in such environments. EG has been detected in seven comets in the solar system with various abundances (Biver et al., 2022) , also in meteorites especially in carbonaceous chondrites (Cooper et al., 2001). Table 4.1

lists the comets where EG has been detected and their respective abundances relative to water.

Table 4.1 Long and short period comets containing ethylene glycol in relative abundances to water

Comet	Abundance relative to water	Reference
C/1995 O1 (Hale-Bopp)	0.25 %	(Crovisier et al., 2004)
C/2012 F6 (Lemmon),	0.24 %	(Biver et al., 2014)
C/2013 R1 (Lovejoy)	0.35%	(Biver et al., 2014)
C/2014 Q2 (Lovejoy)	0.07%	(Biver et al., 2015)
67P/Churyumov–Gerasimenko	0.011%	(Rubin et al., 2019)

On Earth, EG is known as an *"antifreeze"* as it does not allow water to freeze at its normal freezing point. This effect arises from hydrogen bonding between these two molecules. Both EG and water contain hydroxyl (–OH) groups, in which the electronegative oxygen atom pulls electron density toward itself, creating partial negative and positive charges. These dipolar interactions between molecules lead to strong intermolecular coupling, which depresses the freezing point of water. Since EG and water are expected to co-exist within ices within the icy mantles present on the dust grains in the ISM and on comets, it is possible that EG may also

influence the physical behaviour of water on these bodies. However, to date, the effect of molecular interactions between EG and water molecules at the low temperatures of the ISM and on comets is poorly studied. Therefore, we have studied the MIR spectroscopy of mixture and layered ices of diols and water (deuterated water) in the low temperature.

4.2 Experimental Methodology:

All the experiments are performed using the experimental setup, SALT. The detail of the experimental setup is given in Chapter 3. Here we have used EG (≥99% purity, Merck) and deuterated water (D_2O) (≥99% purity, Fisher Scientific), both of which are available in liquid form. Vapors of these molecules were deposited on to the ZnSe substrate at 10 K at a base pressure 10^{-9} mbar. The behaviour of the ices are studied *in-situ* using FTIR spectroscopy in the mid IR range 4000-650 cm^{-1}. In all our experiments we have used D_2O instead of H_2O to avoid the overlap between the –OH stretching modes of H_2O and EG. The most intense vibrational feature of D_2O, i.e, OD stretching band, appears around 2434 cm^{-1}, which is spectroscopically clean for EG. Therefore, the changes in the spectrum of D_2O because of the presence of EG can be observed distinctly when we replace H_2O by D_2O. The presence of D_2O has been confirmed in the ISM (Butner et al., 2007), also with high mass resolution and sensitivity of the Rosetta Orbiter Sensor for Ion and Neutral Analysis (ROSINA), in comet 67P C-G with D/H ratio of the order of 10^{-4} (Altwegg et al., 2017).

To investigate the effect of EG on water, experiments are carried out with both the molecules separately as well as in three different configurations,

- **D_2O on top of EG**- EG was deposited at 10 K, followed by the deposition of D_2O on top of it at 10 K. A visual representation can be found in Figure 4.1
- **EG on top of D_2O**- D_2O was deposited at 10 K, and EG was deposited on top of it at the same temperature. The configuration is illustrated in Figure 4.2
- **Mixture of EG and D_2O**- where both the molecules were mixed in the gas line and deposited together on the substrate at 10 K. A visual representation can be found in Figure 4.3.

After the ices were deposited, they were heated at a constant ramp rate 5 K min^{-1} until the molecules sublimated completely. For every experiment, we took 32 scans and averaged to get the final spectra. The resolution was 4 cm^{-1} for all the spectra.

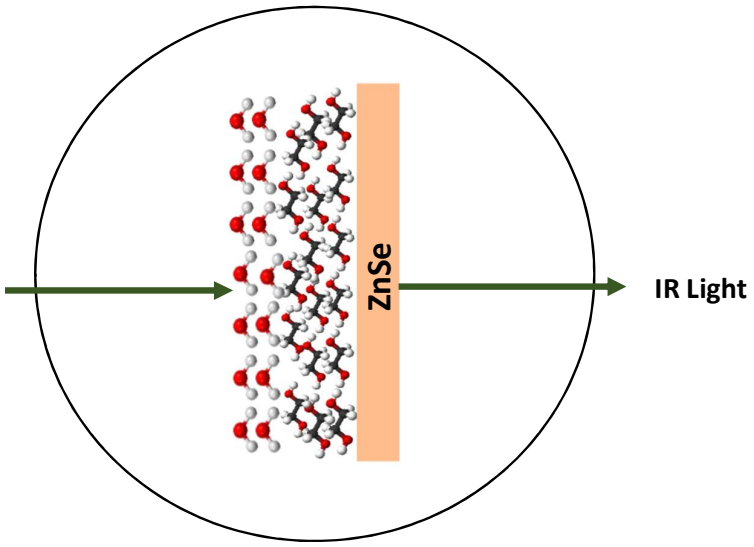

Figure 4.1 D_2O on top of EG, both the molecules are deposited at 10 K.

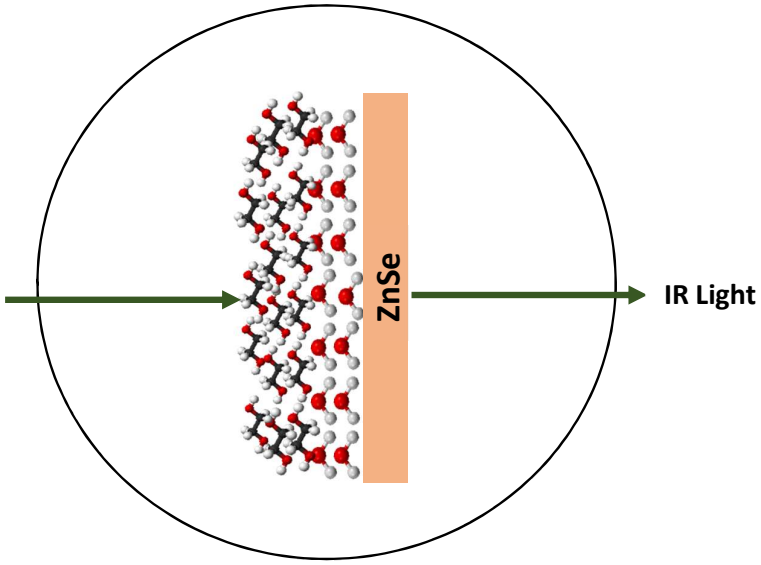

Figure 4.2 EG on top of D_2O both the molecules are deposited at 10 K.

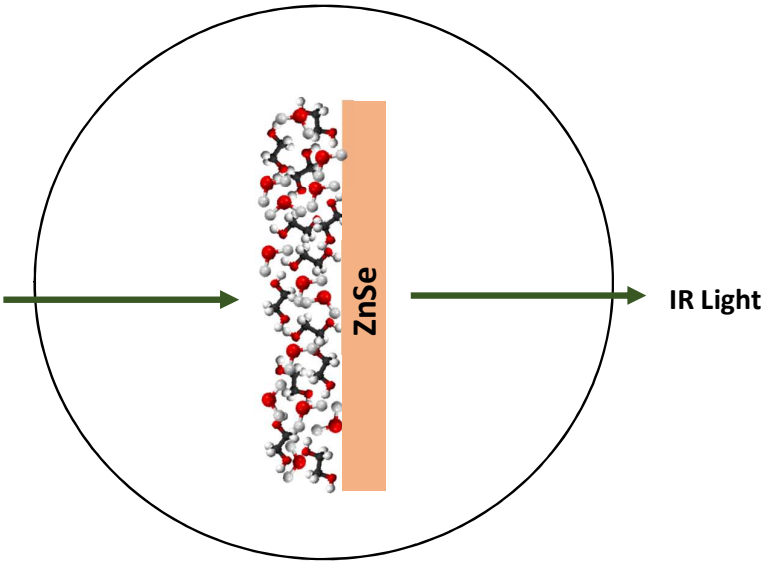

Figure 4.3 Mixture of EG and D_2O, both the molecules are deposited at 10 K.

4.3 Results and Discussion:

4.3.1 Pure ethylene glycol and water ice:

As discussed earlier, we performed temperature dependent mid-IR spectroscopic study of both EG and D_2O to characterize their independent spectral features. The

mid- IR spectra of pure EG, deposited at 10 K and subsequently warmed to higher temperatures at a ramp rate 5 $Kmin^{-1}$ are shown in Figure 4.6. The characteristic absorption features of ethylene glycol are positioned at 1048 cm^{-1} which corresponds to C-C stretching mode, 1092 cm^{-1} which corresponds to C-O stretching mode, 2941 cm^{-1} band which corresponds to C-H stretching band, and 3313 cm^{-1} corresponding to O-H stretching mode. The spectra when compared to the ones present in the literature (Hudson et al., 2005, Leroux et al., 2021) show a very good agreement. A comprehensive list of the peak positions, after deposition and at different temperatures corresponding to crystalline and amorphous ice is given in Table 4.2.

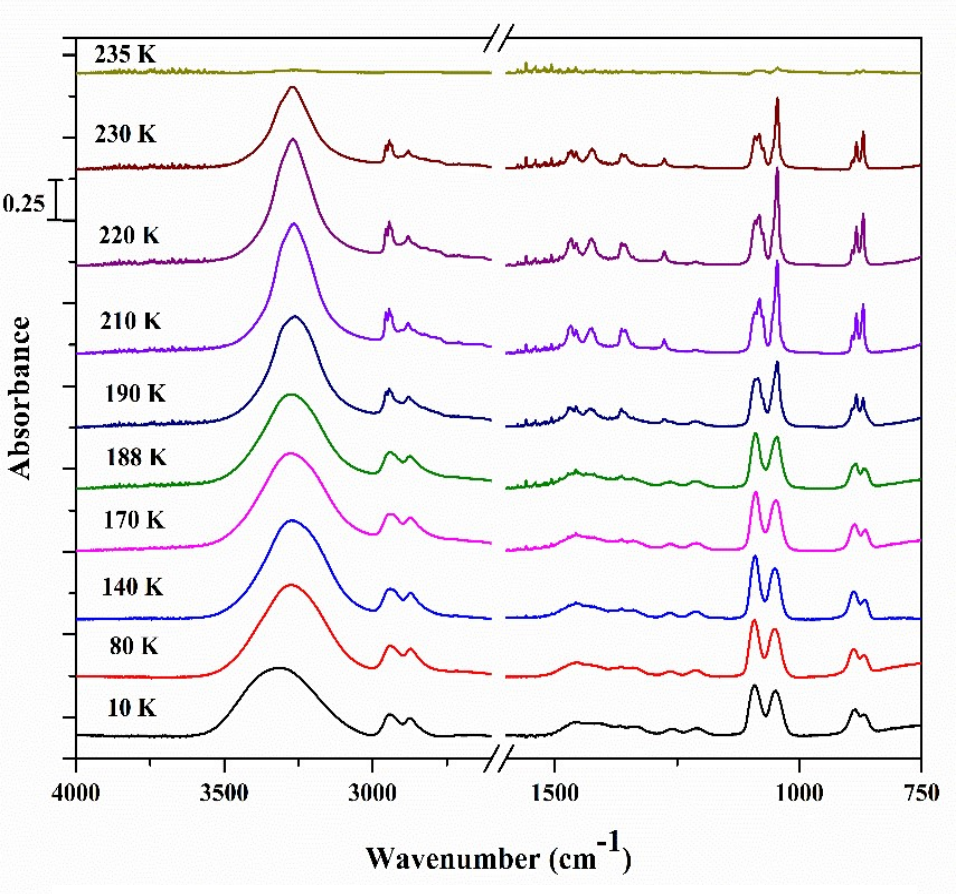

Figure 4.6 Mid-IR spectra of pure EG deposited at 10 K and then warmed to higher temperatures. Spectra are stacked for clarity.

First the column density (N, in molecules cm^{-2}) has been calculated using the formula, N = (integrated band area/band strength). Once the column density is known, the band strength of other vibrational features are obtained from their respective band areas using the same formula.

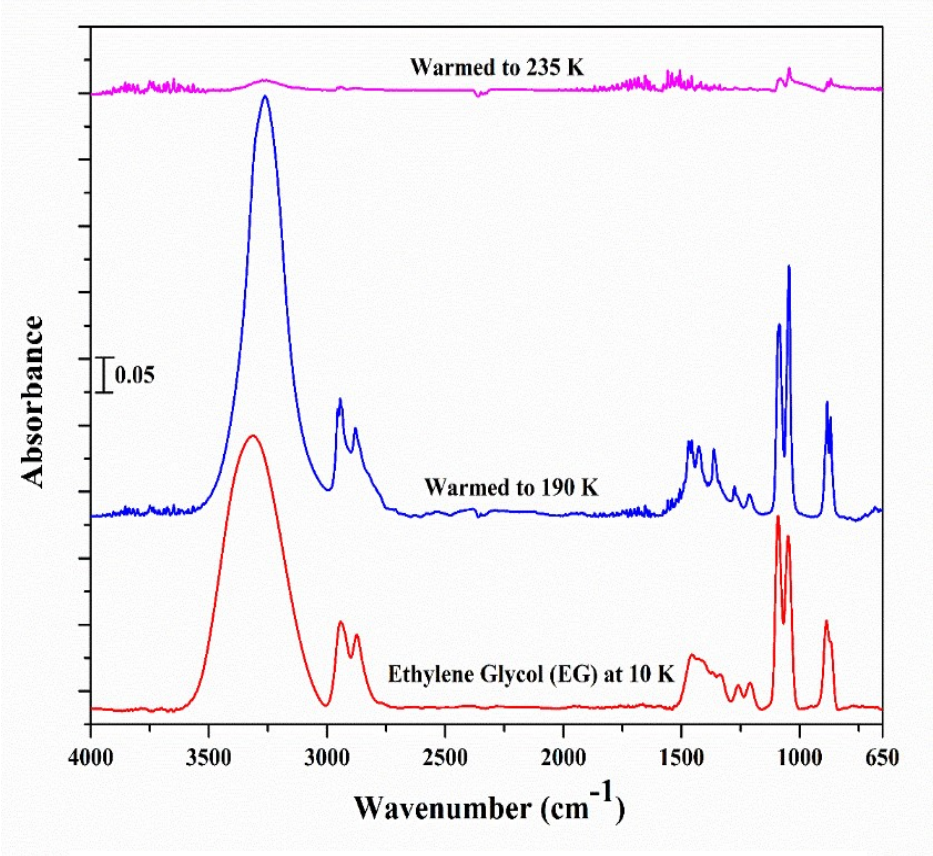

Figure 4.7 Mid-IR spectra of amorphous EG at 10 K (Red), crystalline at 190 K (Blue) and at the sublimation temperature, 235 K (Magenta). Spectra are stacked for clarity.

EG ice after deposition at 10 K shows an amorphous nature. When we heat the ice gradually to 190 K, at the rate of 5 K min^{-1}, spectral splitting of the bands was observed which is an indication of morphological phase transition from amorphous to crystalline phase. Specifically, the peak corresponding to C-H stretching band splits into to three peaks at 2937 cm^{-1}, 2944 cm^{-1} and 2956 cm^{-1}, while C-C stretching band splits to one central peak and two shoulders at 1084 cm^{-1}, 1090 cm^{-}

[1] and 1074 cm^{-1}, respectively. In addition, the C-H rocking mode also exhibited splitting at 883 cm^{-1} and 892 cm^{-1}. Therefore, the phase change for the EG ice is observed at 190 K. When the ice was further heated to higher temperature, the ice starts to sublime and ~ 235 K, the ice gets fully sublimated (Figure 4.7).

Table 4.2 Band assignments of the IR spectrum of amorphous and crystalline EG (frequencies in cm^{-1}).

♠ - (Buckley and Giguère, 1967)

Band positions ♠ ***(in cm^{-1})***	**After deposition at 10 K [Amorphous ice, 10 K]** ***(in cm^{-1})***	**Warmed to 190 K [Crystalline ice, 190 K]** ***(in cm^{-1})***	**Assignments**	**Band strength** ***(cm molecule^{-1})†***
3178	3310	3262	OH stretching	2.6×10^{-17}
2930 2878	2943 2875	2955,2944, 2937 2880	CH stretching	3.1×10^{-18}
1473 1462	1466 1453	1472 1457	CH_2 scissoring	-
1360 1313	1364 1332	1363 1340	CH_2 wagging	-

1279 1215	1262 1210	1277 1212	CH_2 twisting	4.4×10^{-19}
1094 1050	1092 1048	1090, 1084,1074 1045	CO stretching and CC stretching	3.9×10^{-18}
885 871	886 868	891,883 869	CH_2 rocking	1.2×10^{-18}

†Infrared band strengths (A) are derived using the known value from (Hudson et al., 2005) for the CO and CC stretching.

As explained earlier, the use of D_2O in our experiments is solely intended to avoid the spectral overlap in the OH stretching region. Similar to the previous experiment with EG, D_2O molecules were deposited on to the substrate at 10 K and gradually warmed to higher temperatures until the complete sublimation of molecular ice. The temperature-dependent spectral evolution of D_2O is shown in Figure 4.8.

The D_2O molecular ice formed at 10 K after the deposition is amorphous. The mid-IR spectral features are also consistent with those reported in the literature (Engquist et al., 1997). The absorption feature appearing at 1214 cm^{-1} corresponds to the O-D bending mode, while the O-D stretching band appears at 2475 cm^{-1}. A peak around O-H stretching region at 3313 cm-1 is also present, which can be attributed to trace amounts of HDO in the sample (Engquist and Liedberg, 1996).

In addition, small features are seen at 2731 cm^{-1} and 2749 cm^{-1}. These arise from the dangling bonds which are characteristic of a highly porous amorphous ice structure.

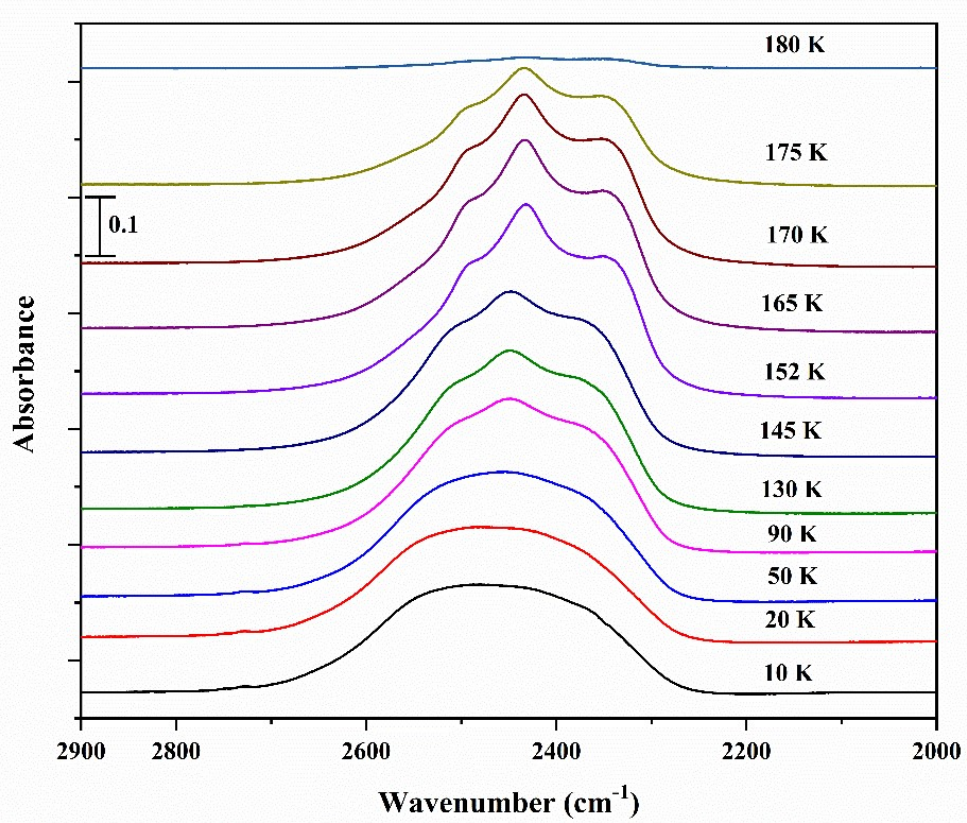

Figure 4.8 Mid- IR spectra of OD stretching band of D_2O deposited at 10 K and then warmed to higher temperatures. Spectra are stacked for clarity.

In Figure 4.9, we show the different spectra corresponding to amorphous, crystalline ice, and sublimation. The ice, upon warming from 10 K to higher temperature at the rate of 5 K min^{-1}, at 152 K, changed its morphology from amorphous to crystalline, which is evident from the splitting of the O-D stretching band into two peaks at 2343 cm^{-1} and 2357 cm^{-1} and a shoulder at around 2500 cm^{-1}. This transformation of the spectral features at higher temperature is also in good agreement with a previous work (Engquist et al., 1997) . On further heating the ice sublime around 180 K.

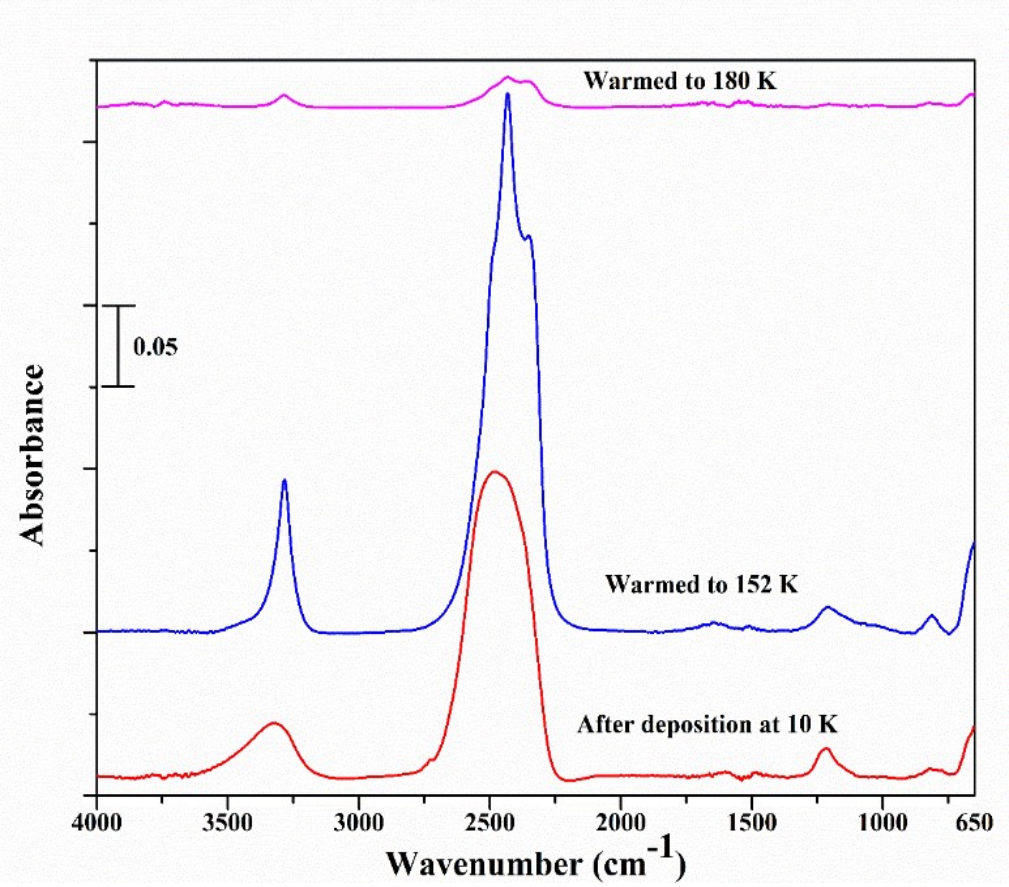

Figure 4.9 Mid-IR Spectra of amorphous D_2O at 10 K (Red), crystalline at 152 K (Blue) and at the sublimation temperature, 180 K (Magenta). Spectra are stacked for clarity.

4.3.2 Layered ices:

4.3.2.1 D_2O on top of EG

Following the analysis of pure EG and D_2O ices, further experiments were carried out to investigate the interaction between EG and D_2O under the astrochemical conditions. In these configurations, layered ices were prepared by sequentially depositing one molecular species over the other on the cold substrate.

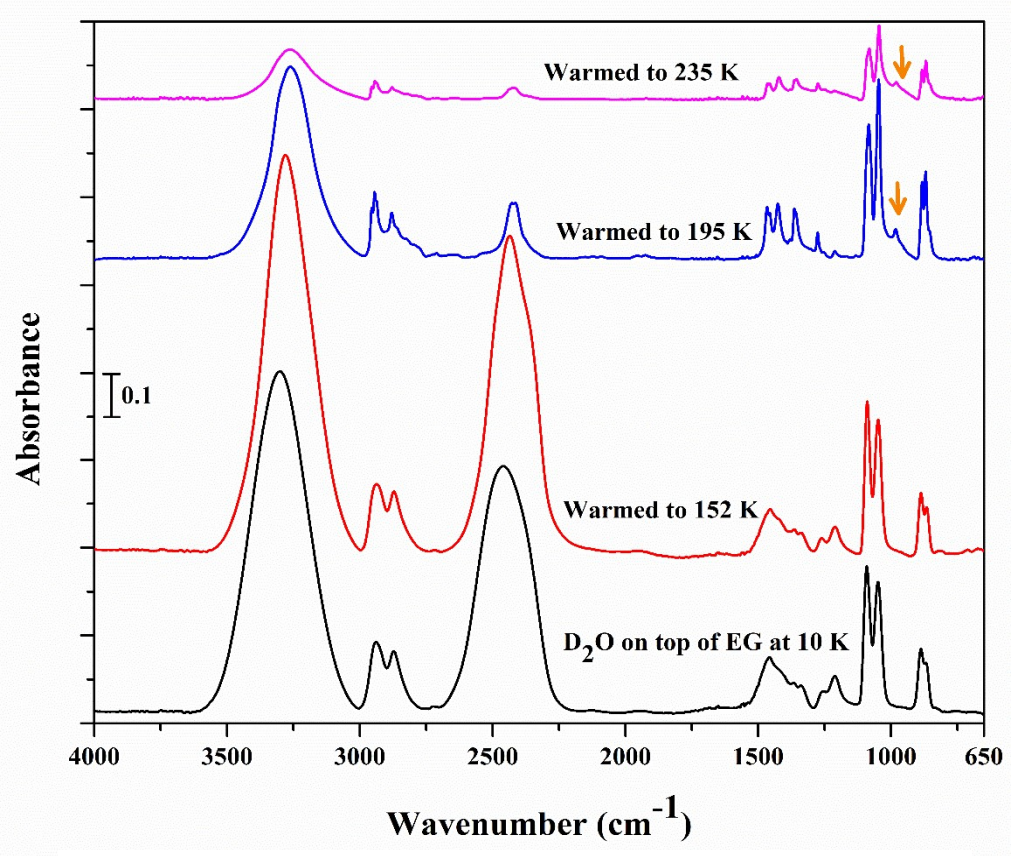

Figure 4.10 Mid-IR spectra of D_2O on top of EG deposited at 10 K and warmed to higher temperatures until sublimation. Bands marked by an arrow points to the new peak arising from the interaction between EG and D_2O. Spectra are stacked for clarity.

For these experiments, a ZnSe substrate was cooled and maintained at 10 K, onto which EG was first deposited. Subsequently, D_2O was deposited over the EG ice layer, forming a layered ice Figure 4.1. Mid-IR spectra were recorded to monitor the vibrational features of both components after deposition. Figure 4.10 represents the temperature dependent spectra of the layered ice. The spectrum obtained after deposition at 10 K clearly shows the characteristic absorption bands of both EG and D_2O, confirming coexistence of both the molecules in the layered ice. At this low temperature, both ices were amorphous, as expected under such astrochemical conditions. Upon warming of the layered ice system, to of 152 K, corresponding to the known phase transition temperature of pure D_2O ice we observed the O–D stretching band did not exhibit the expected splitting which typically suggests

crystallization of the D_2O ice. This indicates that the D_2O ice present has not turned crystalline like the pure D_2O. This means that the phase transition of D_2O have been affected due to its interaction with the underlying EG layer.

As the temperature was further increased above 180 K, a significant amount of D_2O sublimated. However, the most prominent OD stretching feature remained visible in the IR spectrum even at 195 K suggesting that D_2O is not fully sublimated. At this temperature, the EG spectrum began to exhibit signs of structural transformation, indicative of a phase change, from an amorphous to a crystalline state. Concurrently, a new absorption band appeared at 987 cm^{-1}, as marked in Figure 4.10. This band is not a characteristic feature of D_2O or EG. We propose that this new band is from the hydrogen bonding interaction between EG and D_2O. The absence of the 987 cm^{-1} band immediately after deposition does not imply a complete lack of interaction between the two molecules. Rather, it is likely that the number of interacting molecules was below the detection limit of the IR spectrometer, which is approximately 10^{12} molecules cm^{-2}. The appearance of the interaction band is then evidence of more interactions occurring as the higher temperatures induces molecular diffusion. When the substrate temperature was increased further to 235 K, near the known sublimation temperature of EG, the OD stretching feature was still present in the spectrum. This persistence implies that some D_2O molecules remained bound to EG via hydrogen bonds, resisting immediate sublimation. Only upon reaching 240 K the complete sublimation of the layered ice occurred which is evident from the disappearance of all spectral features related to both EG and D_2O.

4.3.2.2 EG on top of D_2O:

In this case, the other layer configuration was studied. That is ZnSe substrate was cooled down to 10 K. First D_2O was deposited on to the substrate at 10 K and another layer of EG was deposited on top of it at 10 K (Figure 4.2).

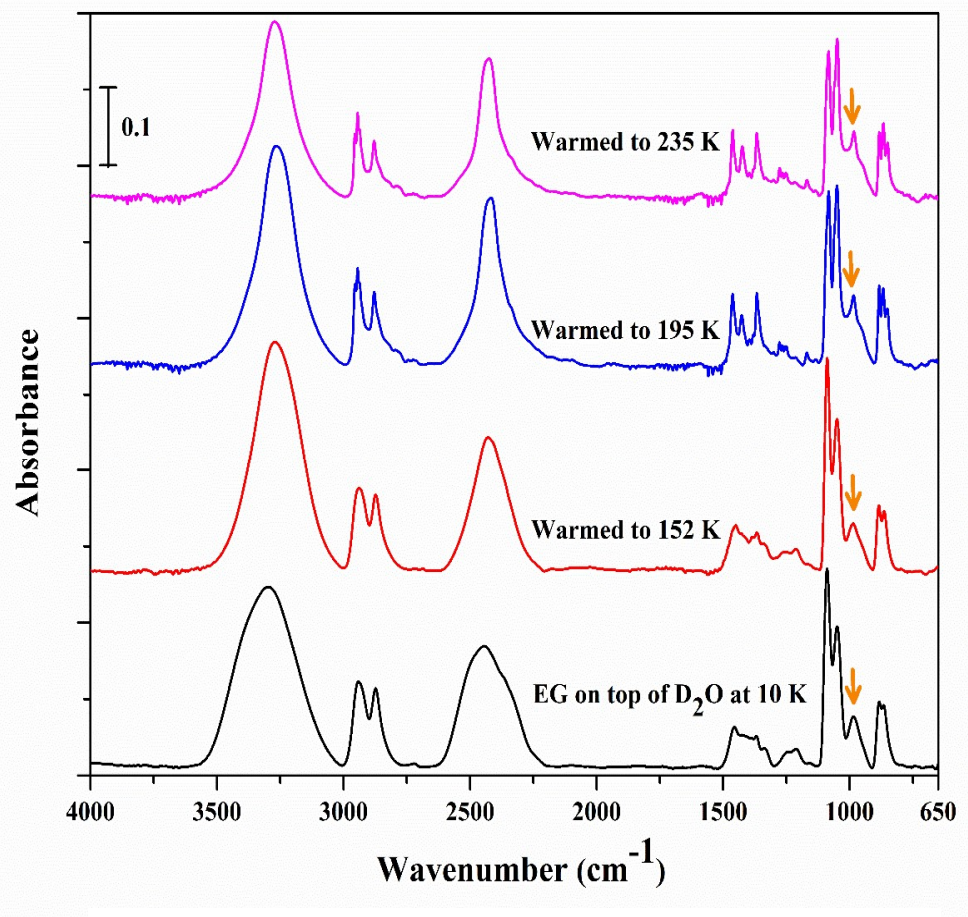

Figure 4.11 Mid-IR spectra of EG on top of D_2O ice deposited at 10 K and warmed to higher temperatures until sublimation. Bands marked by an arrow points to the new peak arising from the interaction between EG and D_2O Spectra are stacked for clarity.

The spectral evolution of the layered ice at different temperature is shown in Figure 4.11. The infrared spectra recorded immediately after deposition at 10 K confirm that both D_2O and EG exist in the amorphous phase within the layered ice system. Additionally, the appearance of an absorption band at 987 cm^{-1} indicates the presence of intermolecular interactions between EG and D_2O molecules. This

interaction may result from the porous nature of amorphous D_2O ice, which likely allow EG molecules to diffuse into the D_2O matrix, thereby facilitating molecular interactions at the interface.

As the sample was gradually heated from 10 K to 152 K, the known crystallization temperature of pure D_2O ice- no splitting of the O–D stretching band was observed. This indicates that the D_2O ice even in this case is also amorphous. However, when the temperature reached 195 K, the spectra displayed features consistent with a phase transition in the EG component. Despite this, the OD stretching band associated with D_2O remained strong and prominent, indicating that a significant portion of D_2O molecules remained bound to EG. Furthermore, a narrowing of the full width at half maximum (FWHM) of the O–D stretching band was observed, which could be attributed to D_2O molecules becoming more uniformly incorporated into the EG matrix.

At 195 K, the intensity of the 987 cm^{-1} band—assigned to EG–D_2O interactions—increased slightly, suggesting that additional molecular interactions had occurred, likely due to increased molecular mobility at elevated temperatures. Interestingly, the degree of interaction appears to be influenced by the layering sequence. When EG is deposited below D_2O, as in this case, fewer interactions are observed compared to configurations where EG is deposited on top of the D_2O layer.

Upon further heating to 235 K, the overall spectral profile remained unchanged from that at 195 K, with only a slight decrease in intensity, indicating gradual sublimation. Complete sublimation of the ice was observed at 240 K, as evidenced by the disappearance of all characteristic absorption features.

4.3.2.3 Mixture of EG and D_2O:

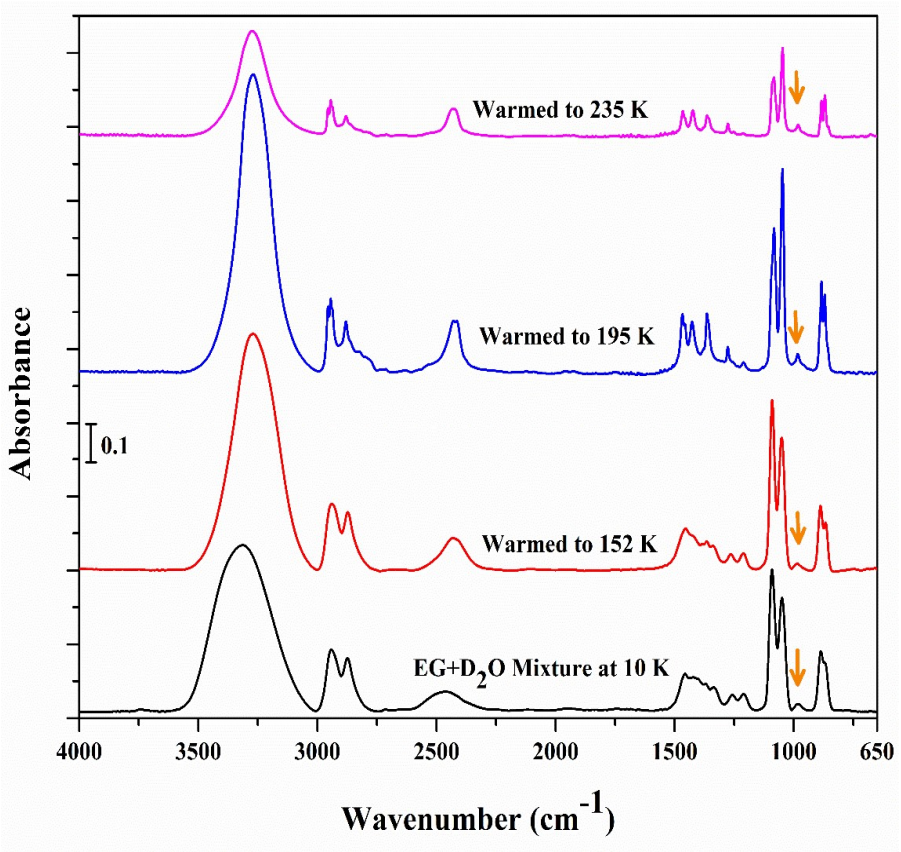

Figure 4.12 Mid-IR spectra of a mixture of EG and D_2O ice deposited at 10 K and warmed to higher temperatures until sublimation. Bands marked by an arrow points to the new peak arising from the interaction between EG and D_2O. Spectra are stacked for clarity.

A mixture of EG and D_2O was co-deposited onto a ZnSe substrate held at 10 K simulating a scenario where both molecules condense simultaneously under astrochemical conditions. Figure 4.12 presents the absorbance spectra of this EG + D_2O mixture recorded at various temperatures. The spectrum obtained immediately after deposition at 10 K exhibited a prominent interaction band at 987 cm^{-1}, along with broad absorption features associated with both EG and D_2O, indicative of their amorphous nature at this low temperature.

The sample was then gradually warmed to 152 K and subsequently to 195 K, with spectra collected at each stage. A slight increase in the intensity of the 987 cm^{-1} interaction band was observed during this temperature progression, suggesting enhanced molecular interactions within the mixture. At 195 K, spectral changes characteristic of a phase transition in EG were evident. Additionally, the presence of an amorphous O–D stretching feature confirmed that D_2O molecules remained in the mixture even at elevated temperatures, consistent with observations made in layered ice experiments.

As the temperature increased further to 235 K, a general decline in overall band intensities was observed, corresponding to ongoing sublimation of the ice mixtures. Complete sublimation of the ice mixture occurred at 240 K, as evidenced by the disappearance of all spectral features associated with both molecules.

4.4 Temperature-Dependent EG:D_2O Ratio and Its Implications:

Figure 4.13 presents the variation in the EG to D_2O ratio as a function of temperature. This ratio was calculated using the calculated band area of a band and the corresponding known band strengths for both EG and D_2O, with values taken from Hudson et al., 2005 for EG and Bennett et al., 2014 for D_2O. In the configuration where D_2O was deposited on top a pre-existing EG ice layer, the initial ratio was approximately 5:1 (EG:D_2O), indicating about five EG molecules for every D_2O molecule. As the temperature increased, this ratio remained relatively stable up to the D_2O crystallization temperature (~152 K). Beyond this point, the ratio increased sharply, reaching around 25:1 near the sublimation temperature of pure D_2O (~180 K). Continued warming led to further sublimation of D_2O from the

top layer, causing the ratio to rise dramatically, peaking at approximately 150:1 just before complete sublimation of the ice at 240 K.

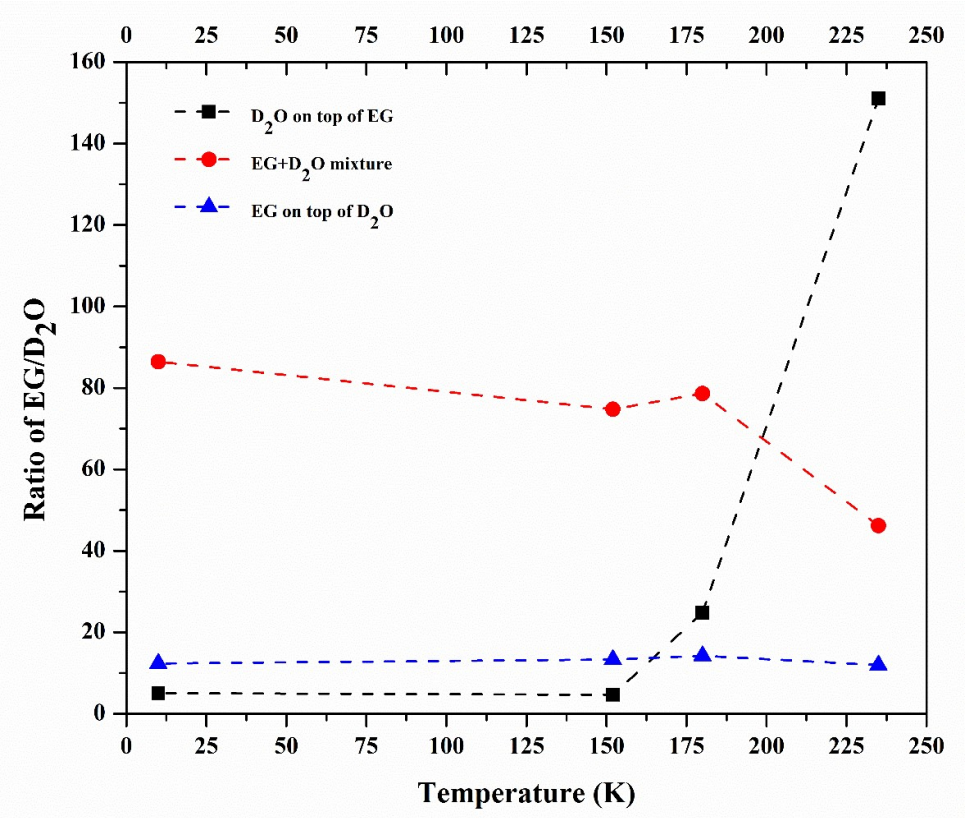

Figure 4.13 Ratio of ethylene glycol and water vs temperature.

Conversely, in the reverse configuration—where EG was deposited on top of D_2O—the EG:D_2O ratio remained consistently around 12:1 from the initial deposition at 10 K up to the point of ice sublimation. This observation strongly suggests that an EG layer overlaying D_2O can effectively trap D_2O molecules through hydrogen bonding interactions. This configuration not only inhibits the sublimation of D_2O but may also suppress its crystalline phase transition.

In the case of a co-deposited mixture of EG and D_2O, the initial ratio at 10 K was approximately 85:1. As the temperature approached the known phase transition regions of both EG and D_2O, the ratio decreased slightly to about 75:1. Upon further

heating towards the sublimation temperature, the ratio dropped even further to around 45:1. These results indicate strong hydrogen bonding between EG and D_2O molecules in the amorphous phase, which appears to inhibit molecular segregation. This bonding likely prevents D_2O from undergoing its typical phase transition behaviour, effectively stabilizing it within the EG matrix.

These findings have significant implications for environments where EG and water are known to coexist, such as on cometary nuclei (see Table 1). Under such conditions, water molecules bound to EG may survive at temperatures considerably higher than previously assumed. For instance, water in EG-rich ice matrices could remain intact and chemically active at temperatures between 200 K and 235 K—well above the typical sublimation temperature for pure water ice (~180 K). This implies that water may be available for chemical reactions in warmer regions of comets, closer to the Sun, than earlier models accounted for.

Moreover, these results highlight the necessity of extending such studies to other diol molecules, such as 1,3-propanediol and 1,4-butanediol, to better understand the role of hydrogen bonding in governing the physicochemical behaviour of water-containing ices. Such studies could further elucidate how the structure and functionality of different organic molecules influence water retention and phase behaviour in astrochemical environments.

4.4 Conclusions:

To explore the influence of ethylene glycol (EG) on the physico-chemical properties of water in the solid phase, laboratory simulations were conducted under cryogenic conditions that mimic icy astrophysical environments. These experiments revealed

a previously unreported strong interaction between EG and water molecules at low temperatures. Notably, EG was observed to effectively trap D_2O molecules through hydrogen bonding, which not only alters the morphological evolution of D_2O but also significantly raises its sublimation temperature.

The hydrogen bonding interactions between EG and water molecules—whether in layered configurations or mixed ices—play a crucial role in inhibiting the segregation and crystallization of water. Typically, water transitions from an amorphous to crystalline phase at specific temperatures; however, the presence of EG suppresses this transformation by stabilizing water in its amorphous form. Interestingly, despite the presence of trapped water, EG itself undergoes crystallization between 190 K and 195 K. This behaviour is attributed to the dominant concentration of EG molecules at temperatures exceeding the sublimation point of water. It is important to note that the retention of water within the EG matrix is primarily driven by hydrogen bonding rather than physical entrapment within EG molecular cages.

Our experimental observations provide compelling evidence to classify EG as an effective "anti-crystallizing" agent for water in the solid phase. Up to the typical sublimation temperature of water (~180 K), EG maintains water in a bound, amorphous state. Even beyond this threshold, water molecules remain hydrogen-bonded to EG, thereby persisting in the ice matrix at temperatures as high as 230 K. This extended thermal stability has significant implications, as it enables water molecules to participate in surface or bulk chemical reactions at temperatures nearly 50 K higher than the sublimation temperature of pure water ice.

The detection of water molecules at temperatures approaching 230 K is of considerable astrochemical importance. It suggests that hydrogen-bonded water may be present on icy grains and cometary surfaces closer to stellar heat sources than previously assumed. Consequently, astrochemical models of interstellar and planetary ice mantles must account for the extended presence of water in environments where hydrogen-bonding agents such as EG are present. This insight opens new avenues for understanding molecular evolution and the role of water in chemical processes occurring in warm ice-rich regions of space.

.

Chapter 5 Water ice formation above its sublimation temperature in astrochemical conditions

Chapter overview:

Building on the findings of the previous chapter, where ethylene glycol was shown to significantly affect the physical behaviour of ices like the phase and sublimation of water. In this chapter, we have explored the effect of diols (utilizing ethylene glycol and 1,3-propanediol) on the condensation and stability of water at temperatures above the sublimation temperature of pure water (~180 K). We have explored the possibility of the formation of water ice onto the dust grains at a temperature of 200 K, beyond water's sublimation temperature. For that, water vapor was deposited directly onto a bare ZnSe substrate held at 200 K, and as expected, no stable water ice formation was observed. However, when a thin layer of either EG or 1,3-PD was first deposited onto the substrate, and water was subsequently deposited onto this diol ice, a stable water ice layer was observed to form at 200 K because of the strong hydrogen bonding between diols and water. The stability of the formed water ice was studied at elevated temperatures.

5.1 Introduction:

Water ice is known to be the most abundant form of ice in the solar system, as well as in the interstellar medium (ISM) (Ehrenfreund et al., 2000). In the ISM, water ice not only serves as a reservoir for oxygen (Van Dishoeck et al., 2013) but also acts as a crucial site for grain surface chemistry in the molecular clouds, leading to

the formation of more complex molecules. In general, water ice formation in the ISM happens through the hydrogenation of atomic and molecular oxygen species (O, O_2, and O_3) on the cold grain surface (~10 K) (Tielens and Hagen, 1982). Recently, laboratory studies have shown that water ice can form at higher temperatures up to 85 K on polycyclic aromatic hydrocarbon-like carbonaceous dust surfaces (acting as a catalytic surface) (Grieco et al., 2024) . Hence, the surface plays an important role in the formation of water molecules in the ISM. In the case of a protoplanetary disk, water is known to freeze out onto the dust grains from gaseous vapor to the solid phase beyond the cold outer region of the disk. This region is known to be beyond the water snowline, which is usually at a temperature less than 150 K (van't Hoff and Bergner, 2024). The formation and presence of ice in such environments are also important to understand grain coagulation, which takes part in the formation of planetesimals (Öberg et al., 2011). Laboratory experiments (Fraser et al., 2001, Khan et al., 2025) mimicking the low temperature, low pressure astrochemical conditions, have shown that the sublimation temperature of pure water ice is 180 K making it unlikely to condense at higher temperature under the astrochemical conditions.

On the other hand, a large number of molecules have been detected in the ISM and protoplanetary disk along with water. Ethylene glycol $(CH_2OH)_2$ is one of the complex molecules to be found in the ISM (Hollis et al., 2002) and in several comets (Biver et al., 2022) , also in the hot core of orion (Brouillet et al., 2015), in NGC 1333-IRAS2A (Maury et al., 2014), towards the intermediate-mass protostar NGC 7129 FIRS 2 (Fuente et al., 2014) and in the core of NGC63341(McGuire et al., 2017) . EG is also present in meteorites (Cooper et al., 2001) . While EG has not been detected yet in the protoplanetary disk, it is known to be formed upon the

energetic processing of methanol (CH_3OH) and water(Hudson and Moore, 2000) , and both CH_3OH (Walsh et al., 2016) and water (Hogerheijde et al., 2011) are known to be present in the protoplanetary disk. So, including EG, many more complex organic molecules might be present in the protoplanetary disk and await their discovery. In the coexistence scenario, the molecular ices are known to interact with each other and affect their physico-chemical behaviour. In Chapter 4, we showed the effect of EG on the morphology and sublimation temperature of water in astrochemical conditions. In this chapter, we explored the effect of diols, mainly ethylene glycol and 1,3-propanediol, on the condensation temperature of water in such extreme conditions.

5.2 Experimental Methodology:

All experiments were conducted using the Simulator for Astromolecules at Low Temperatures (SALT) experimental facility at the Physical Research Laboratory, Ahmedabad. The setup is explained in Chapter 3. In this study, we have used three different molecules, 1,3-propanediol (1,3 PD) (>99% purity, Merck), EG (>99% purity, Merck) and deutarated water (D_2O) (>99% purity, Fisher scientific). The experiments dealt with investigating the effect of these diols (diols are the molecules with two hydroxyl groups) on the condensation and thermal stability of water (represented as D_2O here) in the astrochemical conditions beyond the known sublimation temperature of water (~180 K).

We conducted two different sets of experiments:

- **Deposition of D_2O on 1,3 PD at 200 K**: 1,3 PD was deposited onto the substrate held at 200 K followed by the deposition of D_2O vapor at a base pressure 10^{-9} mbar.
- **Deposition of D_2O on EG at 200 K**: The same procedure was repeated with EG as a replacement of 1,3 PD.

The visual representation of the experiments is given in Figure 5.1.

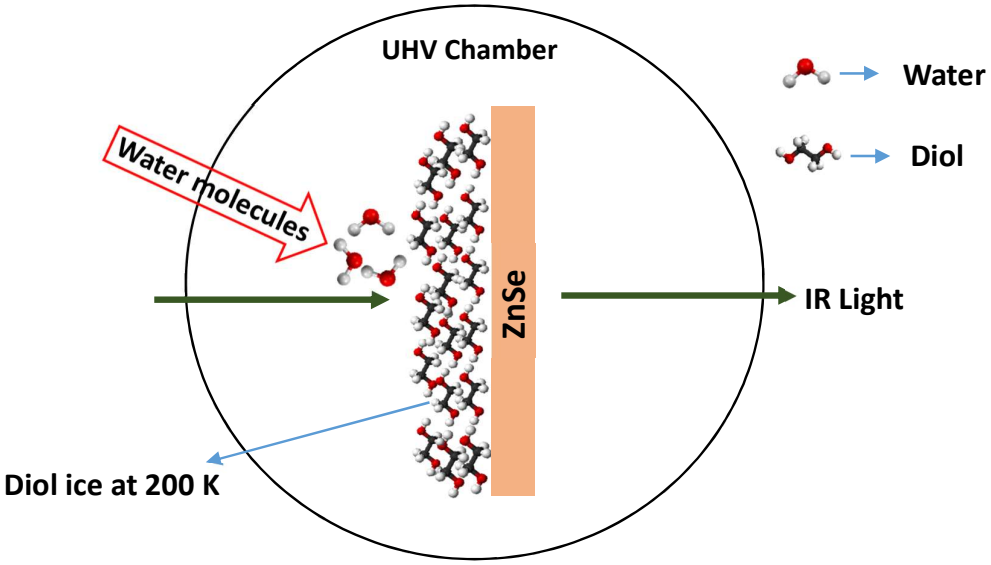

Figure 5.1 Diol ice is deposited at 200 K, on top of that, water molecules are deposited at 200 K.

After the deposition, the ice was heated at a ramp rate 5 $Kmin^{-1}$ up to the sublimation temperature of the ice combinations. The ices were probed *in-situ* using FTIR spectroscopy in the range 4000-650 cm^{-1}. Each final spectrum was obtained by averaging 32 scans recorded with a resolution of 4 cm^{-1}.

5.3 Results and Discussion:

The ices are prepared and analysed using mid-IR spectroscopy. Initially the diol molecules and water are studied individually first to check their spectral characteristics and the sublimation temperature. Since the –OH stretching band of both diols and H_2O significantly overlap in the IR spectrum, in this study we have used deutarated water (D_2O) to distinguish the diols and water separately in the IR spectrum. In the previous chapter, we reported the detailed temperature dependent behaviour of ethylene glycol and D_2O ice in astrochemical conditions. When deposited at low temperature, D_2O molecules form an amorphous ice which is evident from the broad profile of the OD stretching band centred at around 2475 cm^{-1}. When the ice is heated to higher temperatures, the ice reorients and forms a crystalline structure at around 152 K evident from the splitting of the OD stretching band two peaks at around 2343 cm^{-1}, 2357 cm^{-1} along with one shoulder at around 2500 cm^{-1}. Further heating results in the sublimation of D_2O with complete sublimation occurring at around 180 K (Figure 4.9). So the probability that it will form a stable ice onto the substrate at a temperature >180 K is nearly zero. Nevertheless, in this current study, we have tried to deposit D_2O on to the ZnSe substrate at 200 K at a base pressure 10^{-9} mbar. The deposition was carried out for 56 minutes; however, no spectral features corresponding to the most intense OD stretching band of D_2O is observed in the spectrum as shown in Figure 5.2. Although during deposition of D_2O, the chamber pressure increased up to 10^{-6} mbar indicating a large number of molecules entering the chamber but at a temperature above its sublimation, the sticking coefficient becomes nearly zero, reducing the probability of molecular adsorption on to the substrate. As a result, no D_2O molecular ice layer is formed.

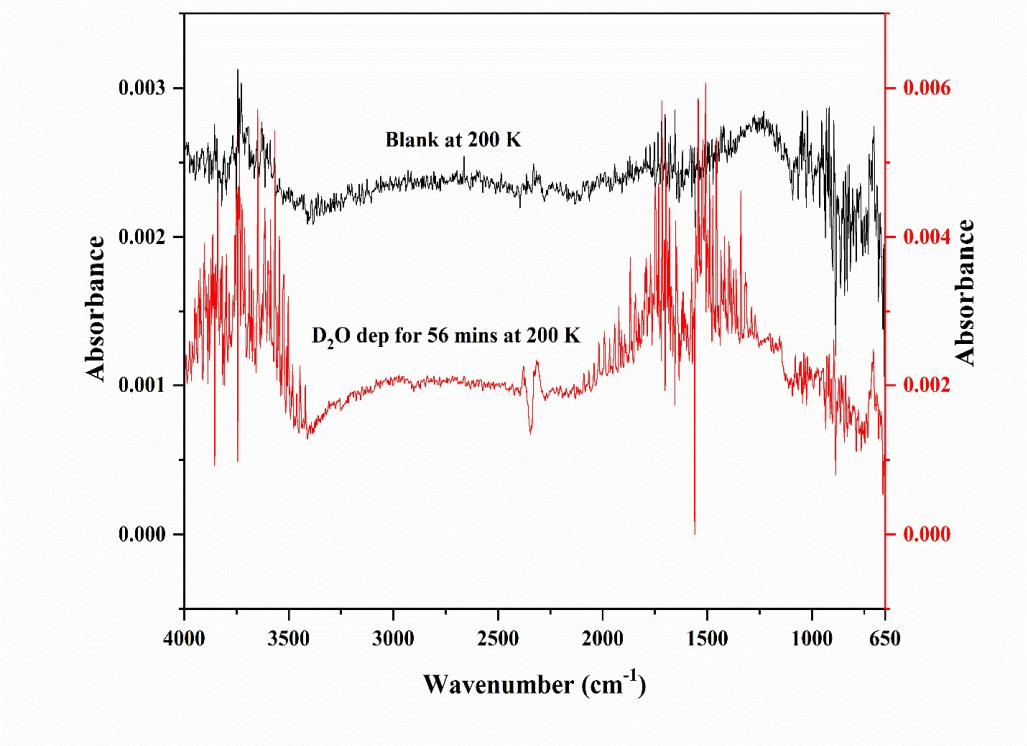

Figure 5.2 Mid-IR spectra during pure D_2O deposition Blank at 200 K (black) and after deposition of D_2O (red).

The molecules are then evacuated from the chamber using the connected pumps. On the other hand, the sublimation temperature of pure EG is 235-240 K (Khan et al., 2025) and also from the current experiments, 1,3 PD showed a sublimation temperature in the range 255-260 K which is well above 200 K. Both the molecules remain stable on to the substrate at 200 K. Hence they are suitable to study the interaction with D_2O.

5.3 1 D_2O on top of 1,3 PD at 200 K:

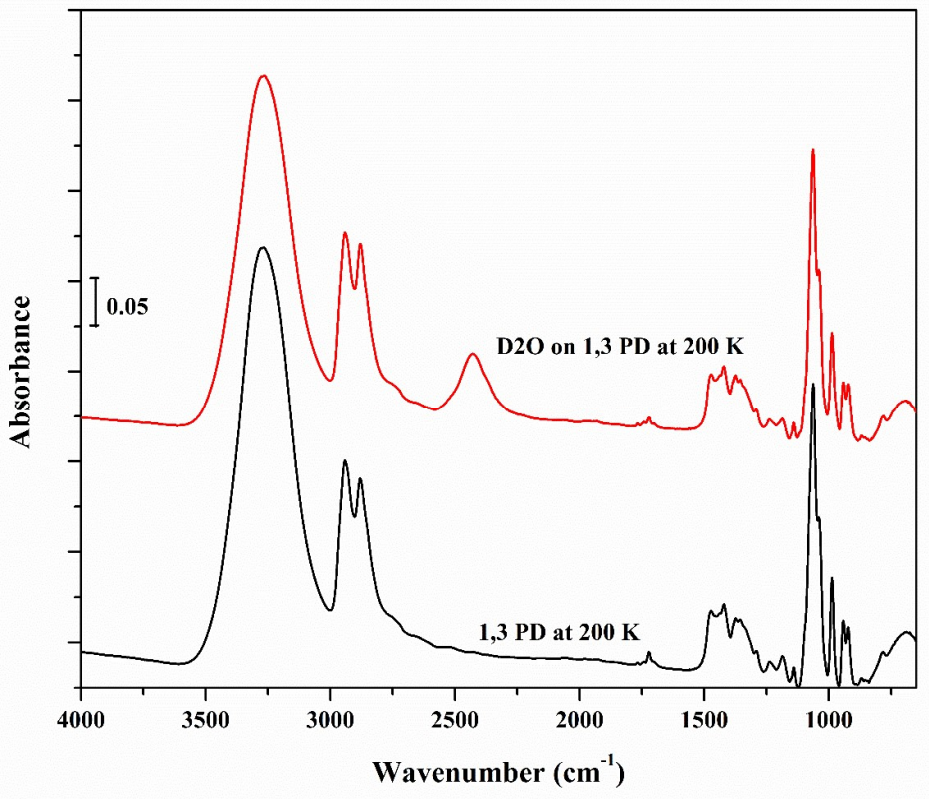

Figure 5.3 Mid-IR spectra during pure 1,3 propanediol at 200 K (black) and after deposition of D_2O on top of 1,3 propanediol at 200 K (red). Spectra are stacked for clarity.

The IR spectrum of pure 1,3 PD recorded at 200 K is shown in Figure 5.3 (black spectrum). The characteristic absorption features are evident including the O-H stretching band at around 3500-3000 cm^{-1}, while C-H stretching band around 3000-2750 cm^{-1}, C-C and C-O stretching band appear in the range around 1100-1000 cm^{-1}. Following the formation of 1,3 PD ice onto the substrate, we deposited D_2O on top of it at 200 K at a base pressure ~ 10^{-9} mbar. The resulting spectrum in Figure 5.3 (red spectrum) reveals the appearance of O-D stretching band around 2600-2250 cm^{-1} region indicating successful formation of D_2O ice on top of 1,3 PD ice surface. It should be noted that 200 K is higher than the known sublimation temperature (~180 K) of Pure D_2O ice. We attribute this behaviour of D_2O to the strong

hydrogen bonding interactions between the hydroxyl groups of the 1,3 PD molecules and the incoming D_2O molecules which might increase the binding energy of the D_2O molecules with the surface making it possible to form at this elevated temperature.

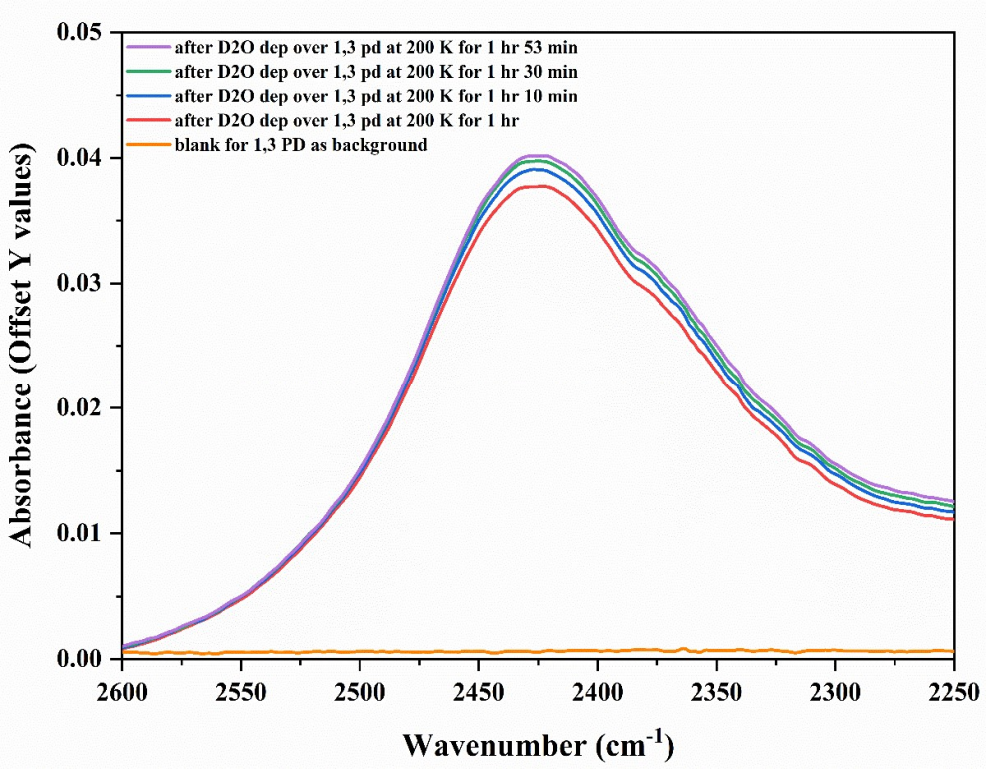

Figure 5.4 Mid-IR spectra of OD stretching peak after D_2O deposition. PD was deposited onto ZnSe substrate at 200 K, it was set to background at 200 K and (a) Blank (orange) , D_2O deposition on top of 1,3 PD at 200 K for (b) 1 hr (red) , (c) for 1 hr 10 mins (blue), (d) for 1 hr 30 mins (green), (e) for 1 hr 53 mins (violet).

To better understand the reason for the formation of D_2O ice we have studied the growth of O-D stretching band intensity as a function of the time of deposition. Figure 5.4 shows the growth of the O-D stretching feature during deposition of D_2O onto the previously present 1,3 PD molecular ice. Although the OD stretching region is featureless in the IR spectrum of 1,3 PD, here we have kept the molecular ice feature of 1,3 PD at 200 K as a background to isolate the O-D stretching peak

feature in the spectra. In the beginning of the deposition of D_2O onto the pre-existing 1,3 PD ice, the peak intensity (/area under the O-D stretching region) rises very rapidly while it slows down over the time of deposition.

This behaviour can be explained as follows, in the beginning the number of available 1,3 PD molecules capable of forming hydrogen bonding with the incoming D_2O molecules is maximum, so there is a large number of free hydroxyl groups on the 1,3 PD surface which makes hydrogen bonding with the incoming D_2O molecules. As a result, the peak intensity grows rapidly. Also at 200 K, the mobility of the D_2O molecules is high, and as a result they can diffuse inside the 1,3 PD ice to find the available hydrogen bonding sites. Over the time, as more D_2O molecules bind to the available diol sites, the number of hydroxyl groups free to make hydrogen bonding with the incoming D_2O molecule decreases, which is evident from the reduced rate of growth of the intensity of the O-D stretching peak. Once almost all the binding sites are filled, and the maximum number of hydrogen bonding are completed, a layer of D_2O forms onto the 1,3 PD surface. Consequently, the next incoming D_2O molecules interact primarily with the already formed layer of D_2O ice instead of the 1,3 PD. As the interaction between D_2O molecules is weaker than the stronger hydrogen bonding with the 1,3 PD molecules, the additional incoming molecules are very less effectively deposited as a result the growth of the O-D stretching peak nearly saturates over the time. Hence as a result of hydrogen bonding between 1,3 PD and D_2O, the binding energy of water increases which gives rise to its formation at this elevated temperature.

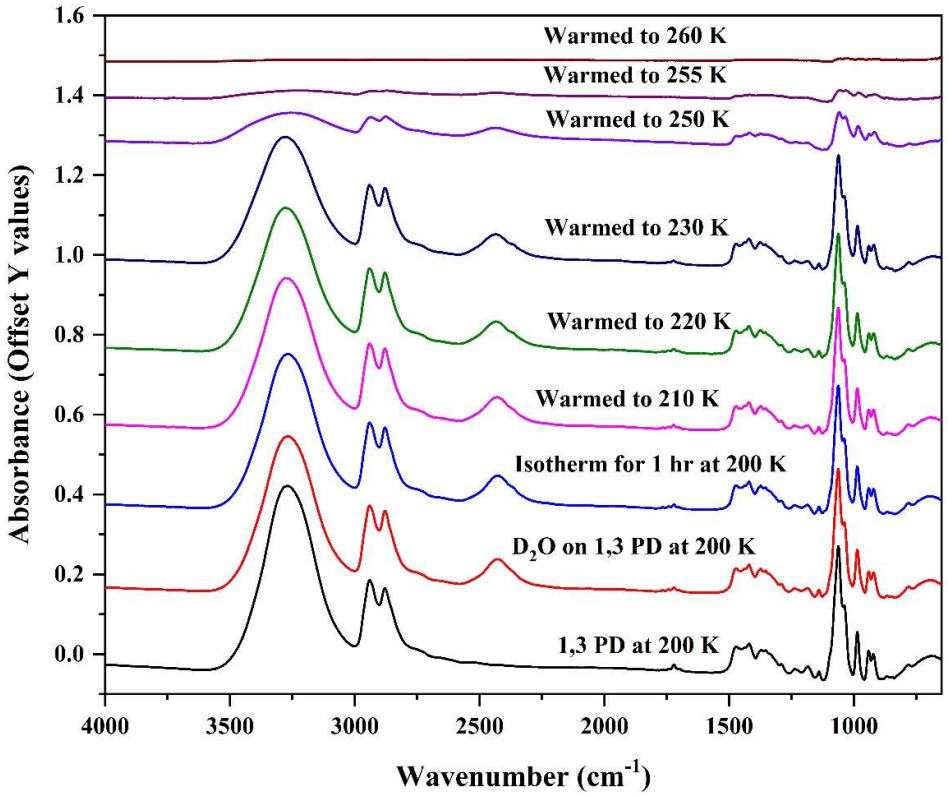

Figure 5.5 Mid-IR spectra of D_2O deposited on top of pure 1,3 propanediol at 200 K isotherm for 1 hour and heated to higher temperature until sublimation Spectra are stacked for clarity.

So in the ISM, the condensation of the molecules will not only depend on the temperature of the dust surface, but it will also depend on the composition of the surface onto which it is colliding.

To investigate the stability of this the formed D_2O molecule on the surface of 1,3 PD, we kept the formed ice in an isotherm at 200 K for 1 hour. After the isotherm, we did not see any change in the intensity of the OD stretching peak. This indicates that once the D_2O ice is formed because of the hydrogen bonding onto 1,3 PD ice, it remains stable. Also the morphology of the formed D_2O ice appears to be amorphous as evident from the broad profile of the OD stretching band. We further heated the sample to a higher temperature at a ramp rate of 5 $Kmin^{-1}$, and in Figure

5.5, as we observe the OD stretching peak intensity reduces significantly only around 250 K. Hence, the formed ice is strongly bound with the 1,3 PD molecules and remains stable up to the sublimation temperature of the 1,3 PD molecules. Complete sublimation of both D_2O and 1,3 PD occurred near 260 K.

5.3.2 D_2O on top of EG at 200 K:

Due to the structural similarity between 1,3 PD and EG, The whole set of experiments are repeated with D_2O and EG. In this case, EG was deposited onto the ZnSe substrate maintained at 200 K, D_2O was deposited on top of it at 200 K at a pressure ~ 10^{-9} mbar.

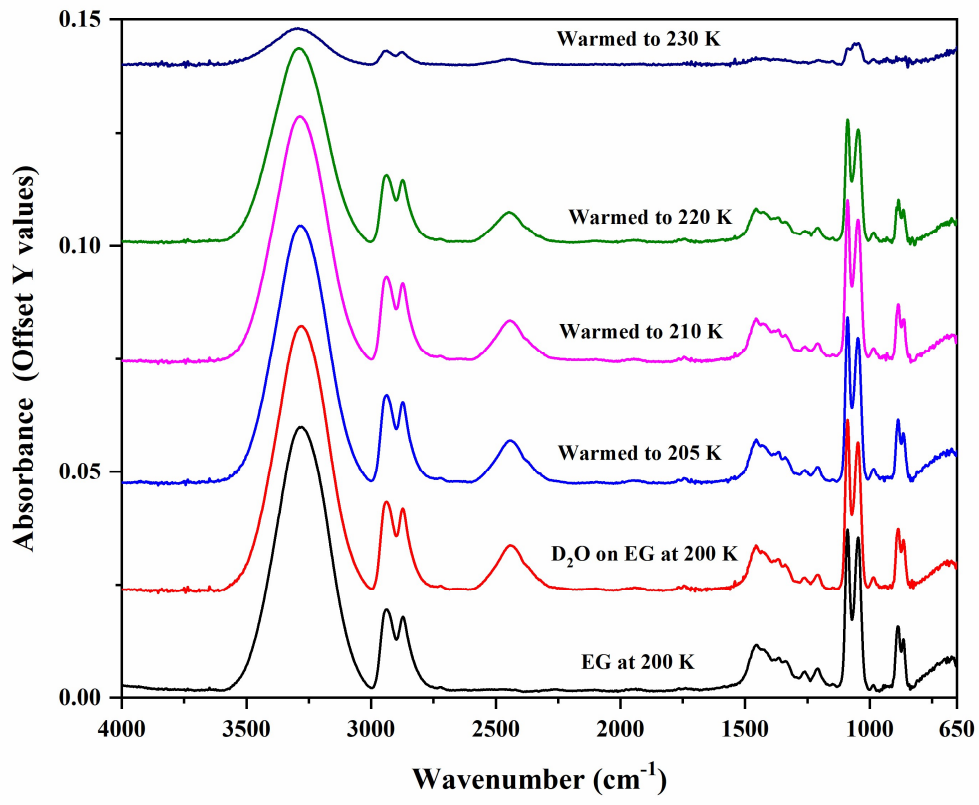

Figure 5.6 Mid- IR spectra of D_2O deposited on top of pure ethylene glycol at 200 K and heated to higher temperature until sublimation. Spectra are stacked for clarity.

The spectral features of the formed EG ice at 200 K can be observed in the black spectrum of Figure 5.6. The characteristic features are similar to the 1,3 PD ice because of the similar kind of vibrations. All the band positions, along with their assignments and the corresponding band strength is documented in Table 4.2. The D_2O molecule is deposited onto the previously formed EG ice at 200 K as evident from the red spectrum in Figure 5.6. The broad band corresponding to the O-D stretching signifies it to be amorphous in nature. Here we have heated the ice system to higher temperature and we observe there is a change in the O-D stretching band only after 220 K. This is similar to the behaviour of pure EG, which starts to sublime at a temperature above 225 K. The hydrogen bonding between EG and D_2O is strong, such that both molecules are subliming together. The complete sublimation occurs after 235 K. Surprisingly, both EG and D_2O were amorphous during the whole experiment until their sublimation.

To explore the effect of surface morphology of the diol ice onto the formed D_2O molecule at 200 K, we at first deposited a layer of EG ice at 10 K, the ice was heated to higher temperature at a ramp rate 5 $Kmin^{-1}$. As already reported in the literature, the phase change from amorphous to crystalline occurs at a temperature 190 K. On top of the crystalline EG, D_2O was deposited at the similar way as explained earlier.

The OD stretching band for the deposited D_2O ice onto two different EG ice, one if crystalline and another is amorphous is shown. The typical feature of OD stretching band of crystalline D_2O is the splitting of it into two different peaks and one shoulder. But in this case, we see that when D_2O is formed on top of crystalline EG above its sublimation temperature, the resulting OD stretching band is sharper compared to the broad one which is on top of amorphous EG. Besides, a shoulder

appears at the lower wavenumber. This indicates that when D_2O is formed on top of crystalline diols ice, it undergoes some degree of structural reorientation that means the ice became compacted although it is not fully crystalline. So the morphology of the underlying diols ice plays a major role on the morphology of the formed water ice.

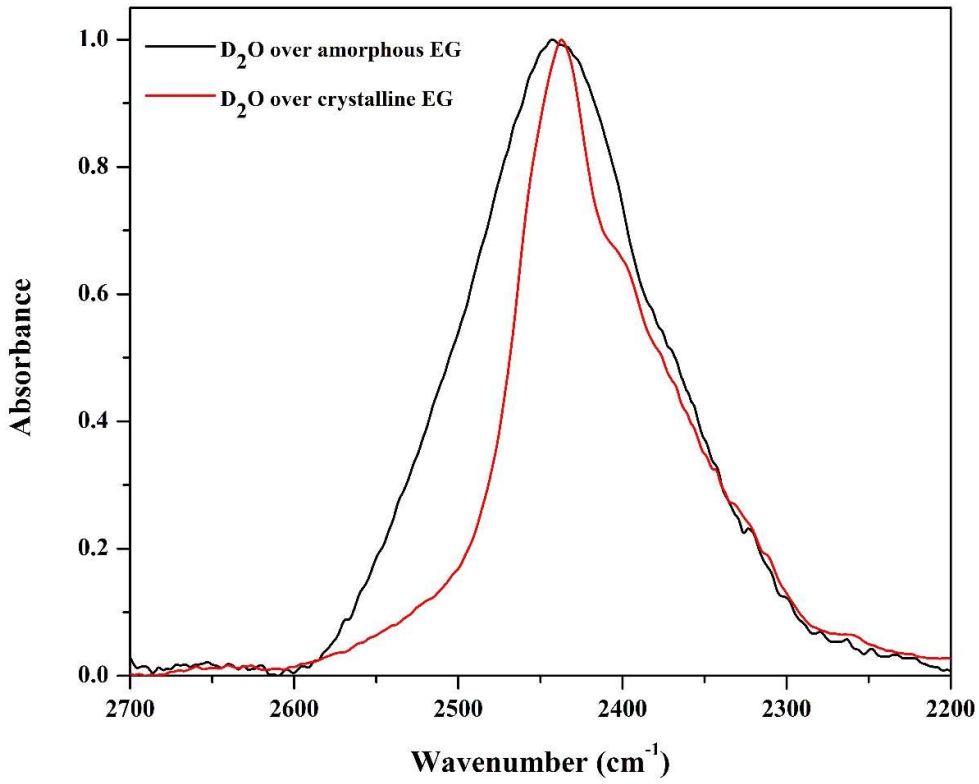

Figure 5.7 Mid-IR spectra (normalized from 0 to 1) of D_2O deposited on top of amorphous (black) and crystalline (red) ethylene glycol at 200 K

5.4. Conclusions:

Here we have investigated the effect of diol ice on the formation and stability of water ice in the astrochemical conditions. We have taken two different diols- 1,2 ethanediol/ethylene glycol (EG) and 1,3-propanediol (1,3 PD) and D_2O. Our experimental results demonstrate that water ice which typically sublimes at a

temperature around 180 K in the ISM cold dust conditions (low temperature and ultrahigh vacuum) conditions, can stably form on the diol surfaces at a temperature 200 K which is much higher than its sublimation temperature. The water ice not only forms on to the diol ice at these conditions, but also remain stable up to the stability of the underlying diol ice. The stability arises from the strong hydrogen bonding between water and the diols, which significantly increases the binding energy of the water ice compared to water interacting with the typical ISM dust grains. This interaction signifies that water in the protoplanetary disk can condense onto the dust grains at a temperature higher than previously known; in other words, water can condense and persist onto the dust grain at smaller radial distances from the central star than previously known. So the presence of diol ice which is well stable at temperatures higher than the sublimation temperature of water can effectively bring the snowline inward, closer to the star. On the other hand, the morphology of the ice forming onto the diol ice will also depend on the morphology of the underlying diol ice. The stability and morphology of water ice plays a major role in case of comets as well. The presence of water ice (amorphous) at elevated temperature can enable it to participate in the chemical reactions on the astrochemical conditions more effectively and may lead to the formation of many complex molecules.

Chapter 6 Irradiation of condensed CO reveals a new pathway for the formation of aromatic molecules in astrochemical ices

Chapter overview:

Given the ubiquitous presence of Polycyclic Aromatic Hydrocarbons (PAHs) in the interstellar medium, and in the solar system bodies like asteroids, comets etc, it has become essential to look for their formation pathways at the low temperature. The known pathways start from acetylene which is not much abundant, on the other hand there are some drawbacks in the known mechanism. In this chapter, we proved carbon monoxide (CO), the second most abundant molecule in the ISM to be an effective precursor for PAHs formation. We have energetically processed CO ice by irradiating it with 2 keV electrons for 10 hours and probed the ice in the vacuum ultraviolet / ultraviolet (VUV/UV) spectroscopy techniques. The *in-situ* VUV/UV spectral analysis of irradiated products provided compelling evidence (peak at ~ 240 nm) for the presence of a refractory residue made of carbon atoms. The ex-situ analysis carried out using high resolution transmission electron microscopy (HR-TEM) revealed the presence of ordered carbon atoms viz-a-viz graphene, graphitic carbon and quantum dots. The direct ring closure from carbon atoms released from CO reveals a new pathway to be considered in the bottom-up formation of polycyclic aromatic hydrocarbon (PAH) molecules, on cold dust in the ISM, via the hydrogenation of graphene / graphitic carbon.

6. 1 Introduction

Carbon Monoxide (CO) is the second most abundant molecule in the solid phase after water ice in the in the interstellar medium (Caro et al., 2016). Due to its high abundance, this molecule is considered to be a key precursor for low-temperature chemical synthesis of other molecules under astrochemical conditions. There are many studies dedicated to understand the chemical complexity originating from the processing of CO ice. CO has been studied under various kinds of energetic processing, starting from photons, to electrons, and ion irradiation. The understanding on the effect of irradiation on condensed CO started long back when Haring et al., 1983 irradiated CO with 3 keV Ar+ ion to understand the sputtering of the CO ice during ion irradiation. The newly formed molecules were sputtered and detected using the mass spectrometry. The products were mainly carbon dioxide (CO_2), C_2,O_2, C+, O+ ions etc. Later the same group studied the sputtering of CO with 6 keV H_2+, 3 keV He+ ions at 15-20 K and found similar products with a higher yield. When the irradiated ice was heated to room temperature, it resulted in the formation of a fine powdered like residue which was supposedly carbon rich. Previously irradiation on CO gas with MeV protons and alpha particle also resulted in the formation of such residue which was found to contain carbon suboxides (Baird, 1972). After that Schou et al., 1985 irradiated solid CO with 2 keV electrons and reported the formation of an involatile residue stable up to room temperature. This time the processing also resulted into the formation of molecules like C_2O along with the previously reported products. The irradiation by higher energetic 30 keV Kr+ ion also resulted in the formation of a residue from the irradiated CO molecule along with the sputtered molecules like the previous ones (Chrisey et al., 1986). The nature of the residue is important to fully understand the effect of energetic irradiation

on CO. Later Chrisey et al., 1990 while explaining the processing of condensed CO with 34 keV Ar+ and 53 keV He+ came up with an explanation of the formed residue to be made up of carbon suboxides like C_3O. Apart from these there exist other studies by (Palumbo and Strazzulla, 1993) where they irradiated CO 3 keV He+ ions, but did not report any residue, although similar products including carbon suboxides were reported to be formed. Even Gerakines et al., 1996 did not report the residue formation when CO was irradiated using 10.2 eV photons reporting the fomation of the known products with carbon chains like C_3. There exists a vast literature for the irradiation of condensed CO and the formed products due to the processing. The different type of irradiation on pure CO at low temperature (~10 K) and the results are tabulated in Table-6.1.

Table 6.1 Energetic processing of pure CO in condensed phase

Type of irradiation	Energy of irradiation	Products formed	Residue reported	Reference
Ion	3 keV Ar+	C_2, O_2, CO_2	-	(Haring et al., 1983)
Ion	6 keV H_2+, 3 keV He+	C_2, O_2, CO_2	Yes	(Haring et al., 1984)
Electron	2 keV	-	Yes	(Schou et al., 1985)
Ion	30 keV Kr+	C_2, O_2, CO_2, $(CO)_2$	Yes	(Chrisey et al., 1986)

Ion	34 keV Ar+ 53 keV He+	O_2, CO_2, C_2O_3	Yes	(Chrisey et al., 1990)
Ion	3 keV He+	C_2O_2,O_2, CO_2, polymerized carbon suboxides	-	(Palumbo and Strazzulla, 1993)
UV	10.2 eV	CO_2, C_2O, C_3O, C_3, C_3O_2	-	(Gerakines et al., 1996)
Ion	60 keV Ar++	CO_2, C_3O_2, C_3O, C_2O, carbon suboxides	Yes	(Strazzulla et al., 1997)
Ion	1.5 keV H+, 1.5 keV N+, 3 keV He+, 30 keV Ar+	Carbon suboxides	-	(Brucato et al., 1997)
Ion	9 keV H+	-	Yes	(Schou and Pedrys, 2001)
Ion & UV	0.8 MeV H+ & 5-11 eV	CO_2, C_2O, C_3O, C_4O, C_3O_2	Yes	(Gerakines and Moore, 2001)
UV	7.41 eV	-	-	(Cottin et al., 2003)
Ion	2 MeV	CO_2, C_2O,C_4O, C_3O_2, C_5O_2, C_7O_2, O_3 and C_6	-	(Trottier and Brooks, 2004)

Ion & UV	200 keV H+ & 10.2 eV	CO_2, C_2O , C_3O_2, C_5O_2, C_7O_2	-	(Loeffler et al., 2005)
Electron	5 keV	CO_2, C_2O,C_3O, C_4O, C_5O, C_6O, C_7O C_3O_2, C_4O_2, C_5O_2, C_3 & C_6	-	(Jamieson et al., 2006)
Ion	200 keV H+	CO_2, C_2O,C_3O, C_4O, C_3O_2, C_5O_2, C_7O_2 & O_3	-	(Palumbo et al., 2008)
Electron	5 keV	CO_2, C_2O & C_3O_2	-	(Bennett et al., 2009)
Ion	50 MeV Ni^{13+} and 537 MeV Ni^{24+}	CO_2, C_2O,C_3O, C_4O, C_5O, C_6O, C_7O C_3O_2, C_4O_2, C_5O_2, C_3 & C_6 & O_3	-	(Duarte et al., 2010)
Ion	46 MeV Ni^{11+} and 537 MeV Ni^{24+}	CO_2, C_2O, C_5O, C_3O_2, C_4O_2, C_5O_2, C_3,C_4 & O_3	-	(Domaracka et al., 2010)
Ion	28 keV O^{6+}	CO_2, C_2O, C_5O, C_3O_2, C_5O_2, C_3 & O_3	-	(De Barros et al., 2011)
Soft X-ray	0.3keV	CO_2,C_2O, C_3O_2,C_3,C_4O, & CO_3/C_5	-	(Ciaravella et al., 2012)

Soft X-ray	1.2 keV	CO_2, C_2O,C_3O, C_5O, C_6O, C_7O C_3O_2, C_5O_2, C_7O_2, C chains up to C11	Yes	(Ciaravella et al., 2016)
Electron	150-1000 eV	C_n (n = 3, 5, 6, 8, 9, 10, 11, 12) C_nO (n=2, 3, 4, 5, 6, 7), & C_nO_2 (n=1, 3, 4, 5, 7)	-	(Huang et al., 2020)
Ion	95.2 MeV Xe^{23+}	CO, CO_2, C_3 , O_3 , C_2O, C_3O, C_3O_2 & C_5O	-	(Pilling et al., 2024)

Table-6.1 helps us to understand the molecular complexity originating from the irradiation on condensed CO. The CO can be dissociated and give rise to the formation of linear chains of molecules up to C_{12}, also it can lead to the formation of different carbon suboxides like C_3O_2, C_5O_2, C_7O_2 and others. Although the products formed were identified by spectroscopy, the nature of the residue obtained from the irradiation was never clearly understood. It was mostly regarded as carbon suboxides. However, there exist other studies (Table 6.1) where carbon suboxides are reported, but no residue was reported to be formed upon irradiation and heating it to room temperature. So the nature of the residue remained still not clearly understood. In the past it has been observed that when SO_2 was irradiated with MeV F+ or H+ and He+ (Melcher et al., 1982, Moore, 1984), a yellowish residue was observed which was expected to be sulfur rich but surprisingly the residue was rich in oxygen. Therefore, the residue has to be examined very carefully.

Generally, the residue obtained after irradiated astrochemical ices were heated to room temperature has been known to provide various new results. Recently Sivaraman et al., 2023 reported the formation of N-graphene which was synthesized by irradiating benzonitrile ice and heating it to room temperature. Also the morphology of the interstellar dust has been explained by studying the residue formed after the irradiation of benzene ice in the astrochemical conditions (Rahul et al., 2020). The residue of the irradiated ices has even been crucial to understand different interstellar spectral features (Moore and Donn, 1982). So the analysis of the residue is an important part of the irradiation experiments in the astrochemical conditions.

On the other hand, Polycyclic aromatic hydrocarbons (PAHs), molecules with fused aromatic rings are known to be ubiquitous in the interstellar medium (ISM). They are known to contain nearly 20% of the carbon atoms in the ISM and Milky Way (Tielens, 2013, Allamandola et al., 1987) and other galaxies (Smith et al., 2007). PAHs have been found in carbonaceous chondrites in the Stardust mission (Sabbah et al., 2017, Lecasble et al., 2022), the samples returned from comet 81P/Wild 2 also show the presence of PAHs (Clemett et al., 2010). The recent discovery of PAHs in asteroid Ryugu samples has provided new clues about their formation processes. Carbon-13 isotope analysis revealed that most of the 2 and 4-ring PAHs, like naphthalene, pyrene, and fluoranthene, appear to have formed in the low-temperature environment, like a molecular cloud. In contrast other PAHs including 3-ring PAHs like anthracene, phenanthrene are likely to be synthesized or reprocessed at high temperature environment like the circumstellar environment (Zeichner et al., 2023). The first detection of ring containing molecule, Benzonitrile, in the Taurus Molecular Cloud (TMC-1) was in 2018 (McGuire et al., 2018). After

that, the search for the other ring containing molecules were intensified and there was and subsequent detection of other PAHs starting from cyclopentadiene (Cernicharo et al., 2021c) , o-Benzene (Cernicharo et al., 2021b), indene (Burkhardt et al., 2021, Cernicharo et al., 2021a) 2-cyano-1,3 cyclopentadiene (Lee et al., 2021) , 1 cyanonapthalene and 2-cyanonapthalene (McGuire et al., 2021) phenylacetylene in TMC-1 (Loru et al., 2023) , 1-cyanopyrene (Wenzel et al., 2024a), up to 2-cyanopyrene and 4-cyanopyrene (Wenzel et al., 2024b) at low temperatures. The presence of the PAHs in these different extraterrestrial bodies and in the ISM makes it important to look for their formation pathways in the low temperature. There are two main pathways discussed in the literature-

- **Top-down approach**

  This theory suggests that large carbon cluster like graphite or graphene gets dissociated due to the ultraviolet (UV) irradiation from the star and can give smaller specis. These species when hydrogenated can give rise to the formation of PAHs (Merino et al., 2014).

- **Bottom up approach**

  This theory suggests that small molecules react together to form larger molecules which can give rise to the formation of aromatic molecules. The precursors that are considered in the literature includes the acetylene, vinylacetylene, and propargyl radicals etc are the precursors of the PAHs (Reizer et al., 2022, Kaiser and Hansen, 2021).

The bottom up formation considered different precursors range from simple to complex molecules, acetylene being the simplest one. However, their abundance is not as good as CO. Also very recently, Kocheril et al., 2025 showed that the

known bottom up formation pathway from acetylene terminates at $C_6H_5^+$, making it difficult to contribute to the formation of aromatic molecules/ PAHs in the astrochemical conditions. The connection between CO and aromatic molecules in the low temperature astrochemical conditions are yet to be established in spite of its abundance in the ISM.

6.2 Experimental Methodology:

We have carried out irradiation of CO ice at 10 K with 2 keV electrons and probed the resultant ice *in-situ* by VUV/UV spectroscopy. The experiments were carried out at the UV beamline – ASTRID2, Aarhus University, Denmark. The experimental set-up is similar to the one described earlier, consisting of a copper cold finger placed inside an ultrahigh vacuum (UHV) chamber (base pressure 10^{-9} mbar) and connected to a cryostat. The cold finger contains a Vacuum Ultraviolet (VUV) transparent Lithium Fluoride (LiF) substrate which acts as an analog of the dust in the ISM. So the combination of the cryostat, UHV chamber and substrate replicates the interstellar cold dust conditions. After the substrate reaches 10 K, we deposit the CO molecules from the gas phase onto the substrate resulting in an ice at a base pressure of 10^{-9} mbar. For our experiments, CO was deposited at a pressure of ~10^{-6} mbar for 100 seconds (nearly 100 monolayers) onto the substrate. The ice was purposefully made thick since the aim was to synthesize a good amount of residue after the irradiation. The ice prepared was then irradiated with 2 keV electrons for 10 hours. After the irradiation, the ice was heated to higher temperatures at a ramp rate 5 K min^{-1}. The temperature was maintained using a Lakeshore temperature controller. VUV spectrum in a range 120 nm - 320 nm was recorded in an interval of 1 nm. The method of recording the VUV spectrum is

explained in (Ramachandran et al., 2024a). The detailed experimental set up can be found in (Ramachandran et al., 2023).

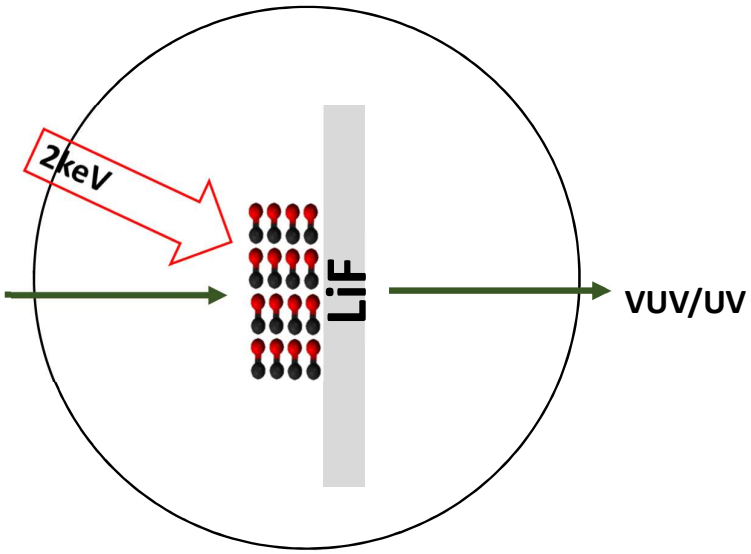

Figure 6.1 Visual representation of the experiment, CO ice under irradiation

After the sublimation of the ice, the substrate was taken out of the chamber. The morphology of the residue obtained on the substrate was further analysed using the High Resolution-Transmission Electron Microscopic (HR-TEM) imaging at the Indian Institute of Science (IISc) Bangalore. The sample for HR-TEM analysis was prepared by carefully transferring the residue onto a Quantifoil grid using a restricted airflow table to minimize contamination. Subsequently, the grid was cleaned with $Ar+O_2$ plasma to remove any dust particles. During the sample analysis the operating voltage was 300 keV. The analysis of a blank substrate was done first without any residue on it and there was no particle feature in the corresponding TEM image. The interplanar spacing was calculated using the Image J software (Abràmoff et al., 2004).

6.3 Results

6.3.1 VUV spectrum of pure CO:

First we have studied the VUV spectrum of pure CO at low temperature (~10 K), characterized the peak positions.

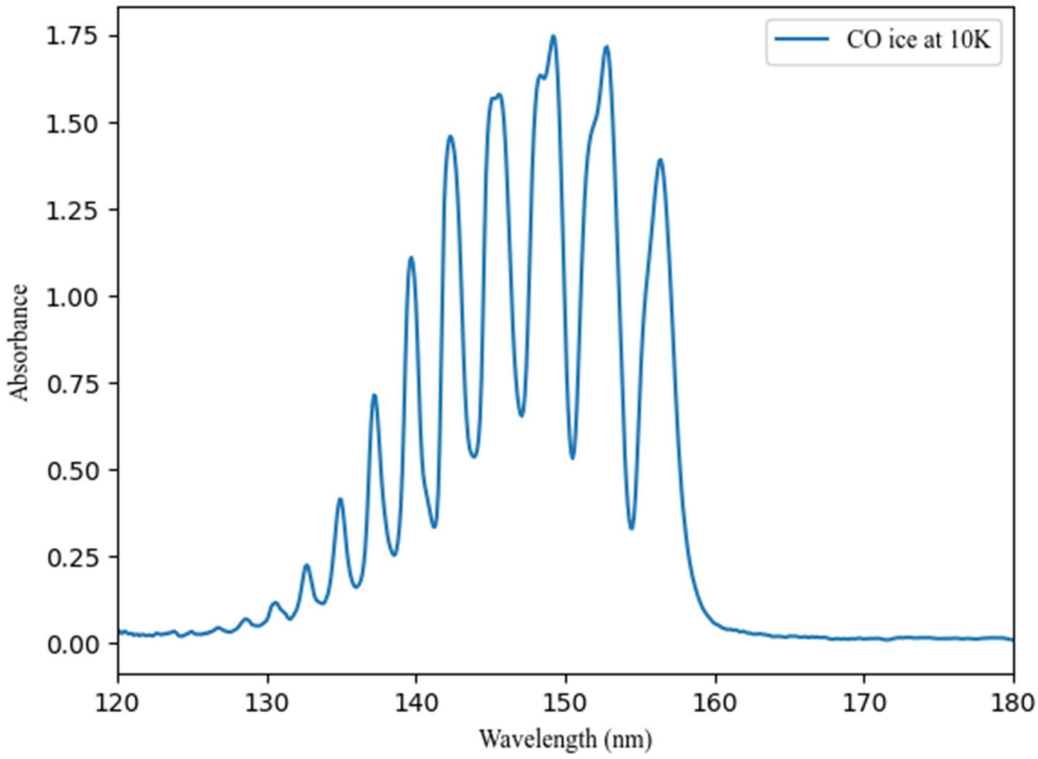

Figure 6.2 VUV spectrum of pure CO at 10 K.

The VUV spectrum of pure CO is shown in Figure 6.2. The wavelength region in the spectra is known as the fourth positive band system which is for the electronic transition $X^1\sum^+ \rightarrow A^1\prod$. This transition is associated with a number of vibronic transitions for the different vibrational states (v', v") governed by the Frank Condon principle. We can identify twelve bands from (0,0) to (0,11). The transitions from (0,11) vibronic state appear to be around 126.78 nm, (0,10) transition around 128.6 nm and so on for the other transitions. The spectral features match well with the existing literature (Mason et al., 2006, Cruz-Diaz et al., 2014). The band positions are tabulated in Table 6.2.

Table 6.2 Band positions of pure CO ice at 10 K

Main peak (nm)	Shoulder(nm)
156.41	155.43
152.70	151.78
149.24	148.30
145.61	145.06
142.29	
139.67	
137.27	
134.96	
132.78	
130.56	
128.63	
126.78	

The ice when heated to higher temperature sublimated at a temperature around 30 K.

6.3.2 VUV / UV spectroscopy of CO before and after irradiation:

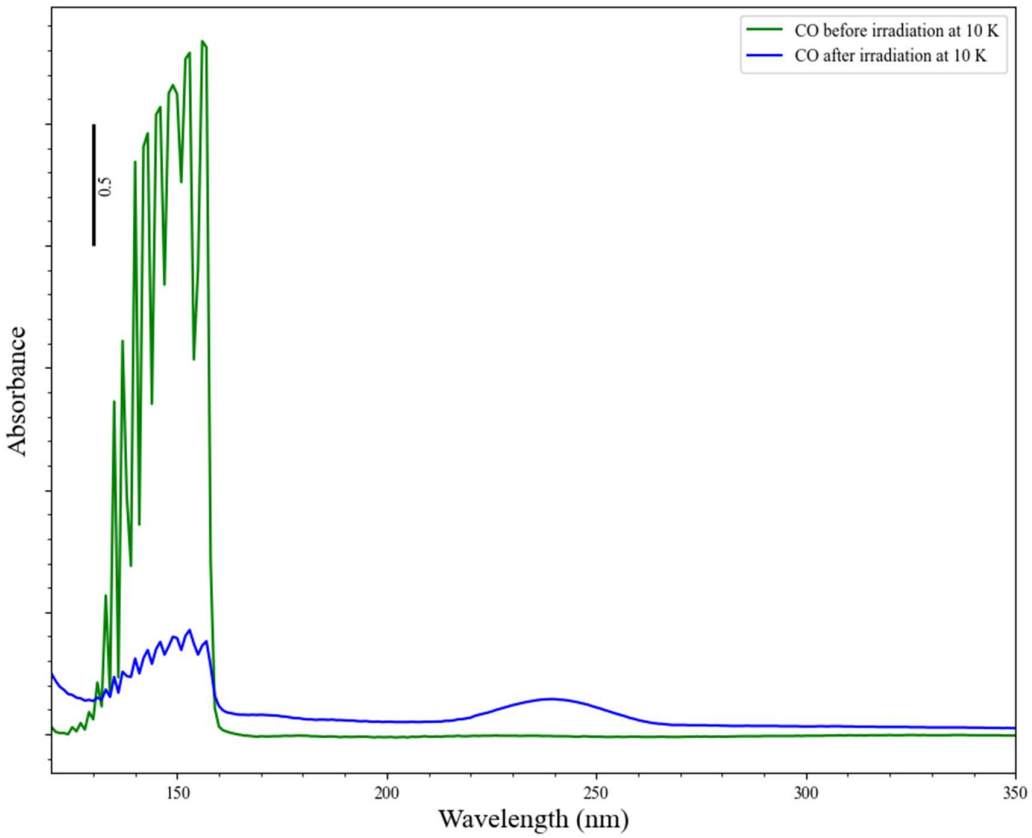

Figure 6.3 VUV spectra of pure CO at 10 K before (green) and after (blue) irradiation.

The VUV/UV spectrum of pure CO before and after irradiation is shown in Figure 6.3. The spectrum before irradiation shows the presence of vibrational progression, although the peaks appearing here are seemed to be saturated because of large amount of CO molecule deposition on to the substrate. Because the main motivation of this trial was to produce a significant amount of residue after the irradiation.

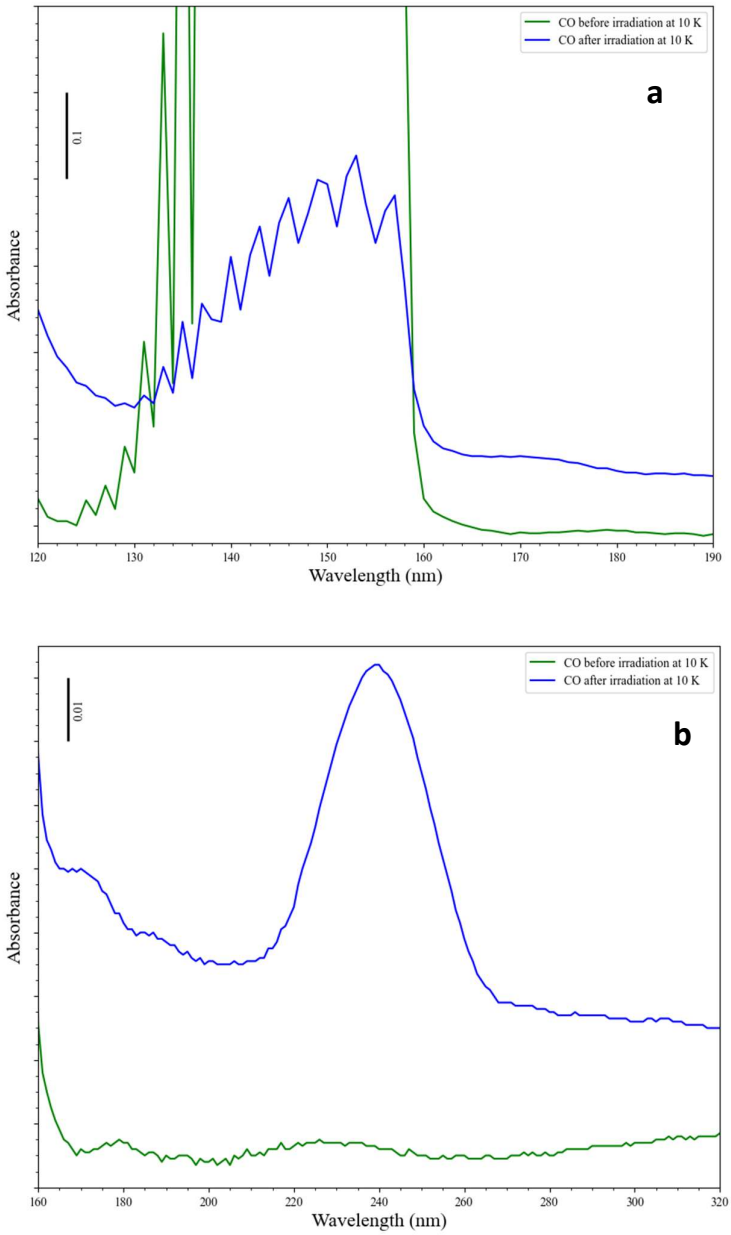

Figure 6.4 Different wavelengths of the VUV spectra of pure CO at 10 K before (green) and after (blue) irradiation. (a) From 120-190 nm (b) from 190-320 nm

The spectrum of CO ice before and after electron irradiation with 2 keV electrons at 0.1 mA current for 10 hours is shown in Figure 6.3 & 6.4. Figure 6.4(a) highlights the fourth positive band system of the CO ice before and after irradiation. Here we observe a significant change in the intensity of the peaks after the irradiation at 10

K. This can be due to the formation of other products from CO upon irradiation thereby reducing the number of CO molecules and consequently intensity of CO bands. Also we see the formation of a broad peak near 174 nm, this is well known peak of O_2. The presence of O_2 is an indication that carbon atoms are available in the irradiated ice for reaction from the dissociation of CO to C + O and adding another O to make O_2 molecule. Therefore, for every O_2 molecule 2 carbon atoms are available for reaction. So the lower wavelength region of the spectrum is consisting the combined features of different molecules such as CO and O_2.The higher wavelength region, 190-320 nm as known was featureless before the irradiation. The spectrum after irradiation consists of a new peak appearing at around 240 nm at 10 K.

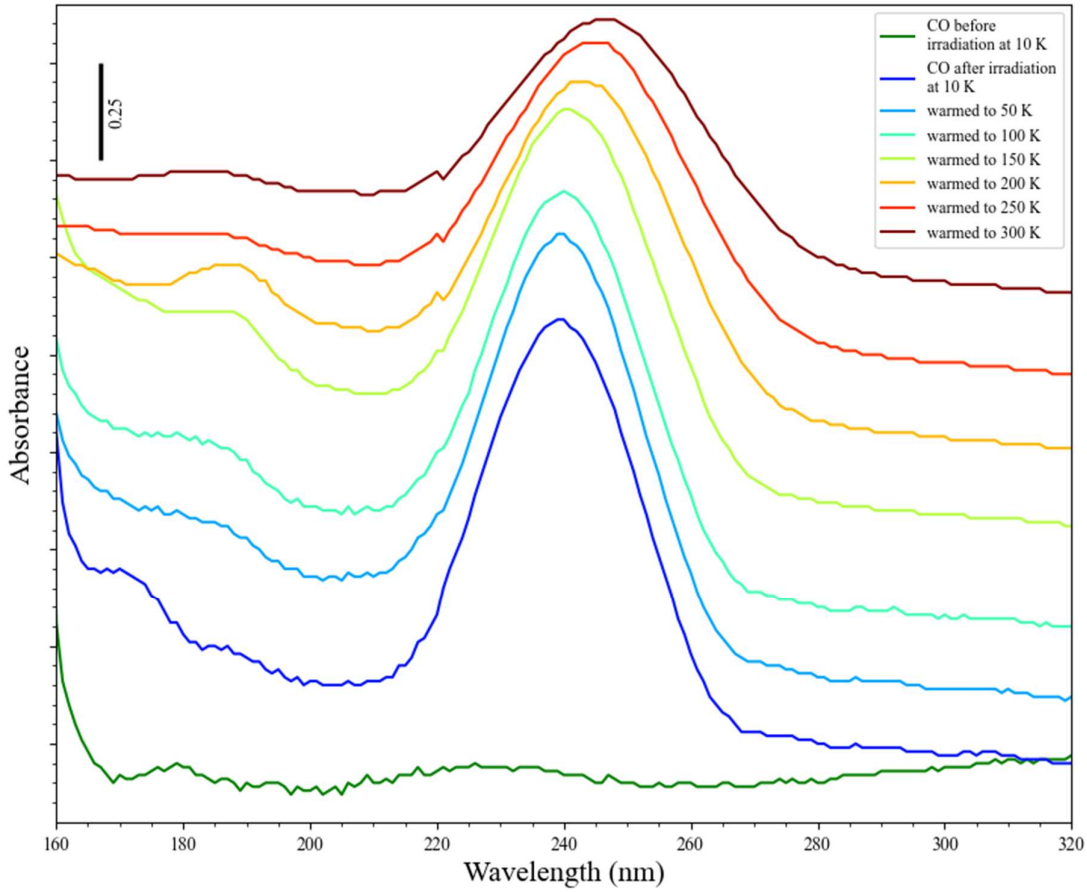

Figure 6.5 VUV spectra of CO - before irradiation and after irradiation at 10 K, and warmed to higher temperatures. Spectra are stacked for clarity.

The ice after the irradiation at 10 K was heated to higher temperature at a ramp rate 5 K min^{-1}. The spectra at higher temperatures are shown in Figure 6.5. Since the spectral changes were observed mainly at higher wavelengths, the spectra are plotted from 160-320 nm. While heating we observe the presence of another new peak around 187 nm along with the 240 nm peak.

Heating the irradiated ice, we observed the peak corresponding to molecular oxygen disappearing because of its sublimation while the other peaks are still present. While heating the substrate further to a higher temperature, 300 K, we observe that the peaks at around 187 nm and 240 nm are still present (Figure 6.5). From Table-6.1, listing the previously carried out irradiation on condensed CO, we can clearly see that a variety of products are synthesized which are probed using IR spectroscopy. However, due to the limitations in the UV spectroscopy we are left with a few bands to known at the irradiated ice. The spectral shift of the peak appearing around 240 nm after irradiation is shifted up to 246 nm as we warm from 10 K to room temperature (300 K) could be due to effect of temperature.

The UV extinction peak at 217 nm is known to be caused by the $\pi \rightarrow \pi^*$ transition of sp^2 hybridized carbon. The UV extinction peak was initially referred to graphite-like structures (Stecher and Donn, 1965). While Mennella et al., 1996 proposed hydrogenated amorphous carbon (HAC), which is a disordered material that contains a mixture of aliphatic and aromatic structure to be a carrier of the UV bump. Laboratory studies (Duley and Hu, 2012, Steglich et al., 2010, Gavilan et al., 2017) also suggested that polycyclic molecules are the reasons for the 217 nm UV extinction peak. On the other hand for hydrogen deficient stars like R Coronae Borealis (RCB), the peak near 217 nm is absent, instead a broad peak at 240 nm along with another peak around 180 nm is present (Jeffery, 1995). Also, Mennella

et al., 1997 showed that amorphous carbon has a characteristic feature around 240 nm in the UV range. Hence the spectral feature observed in the UV spectrum, ~ 240 nm, is an indication of carbon residue, the product formed after the irradiation of CO ice (without hydrogen).

6.3.3 HR-TEM imaging

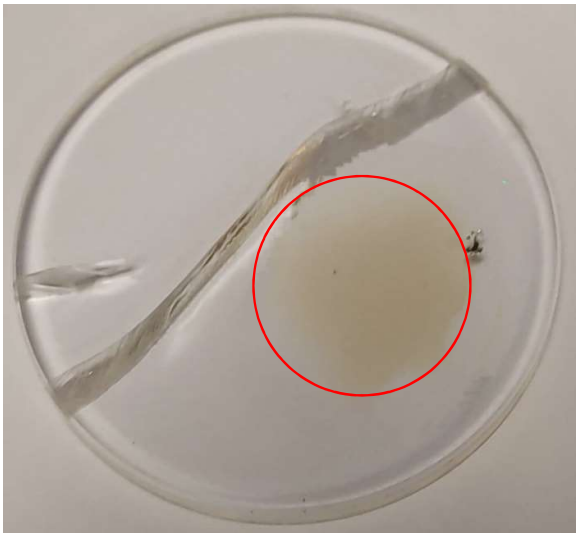

Figure 6.6 LiF substrate for ex-situ analysis at room temperature, the dark brownish residue is marked. The black dot next to the red circle is made using a marker for reference.

The product formed was stable at room temperature, therefore, an *ex-situ* analysis of the refractory residue can be carried out. After removing the LiF substrate, we observed the presence of the residue on the substrate (Figure 6.6). Such a residue was not observed when CO ice was formed at 10 K and heated without any irradiation. Although in previous studies involving the irradiation of CO using high energy ions or electrons it was evident that a residue forms that remains on the substrate up to room temperature (Table-1). Haring et al., 1984 irradiated CO with 3 keV He+/Ar+ ions and showed the formation of a non-volatile material which

was considered as carbon rich and thought to contain polymerized carbon suboxides. The residue was formed even when CO was irradiated using 2 keV electrons (Schou et al., 1985) . Besides Chrisey et al., 1986 and Chrisey et al., 1990 processed CO with energetic irradiation and explained the formation of residue due to the fragmentation of molecules and production of C, O, O_2 and CO_2. The excess amount of available carbon is expected to react with other carbon forming a long chain of carbon atoms. Even graphitic carbon was suggested to be a component of the residue synthesized from irradiation, and the experimental proof for the presence of graphite was still open. Strazzulla et al., 1997 irradiated the CO with 60 keV Ar++ and concluded the residue to be formed by the carbon suboxides. The formation of residue has also been mentioned by Schou and Pedrys, 2001, Gerakines and Moore, 2001 and Ciaravella et al., 2016. However no residue formation is mentioned in the studies by Jamieson et al., 2006 , Bennett and Kaiser, 2005 [irradiation of 5keV electrons on CO], and Huang et al., 2020 [irradiation of 200-1000 eV electrons on CO]. Although carbon suboxides are formed in all these works.

Clearly there is a need for a dedicated study to understand the nature of the residue. In this work we took the substrate out of the chamber and analysed the residue using HR-TEM imaging technique.

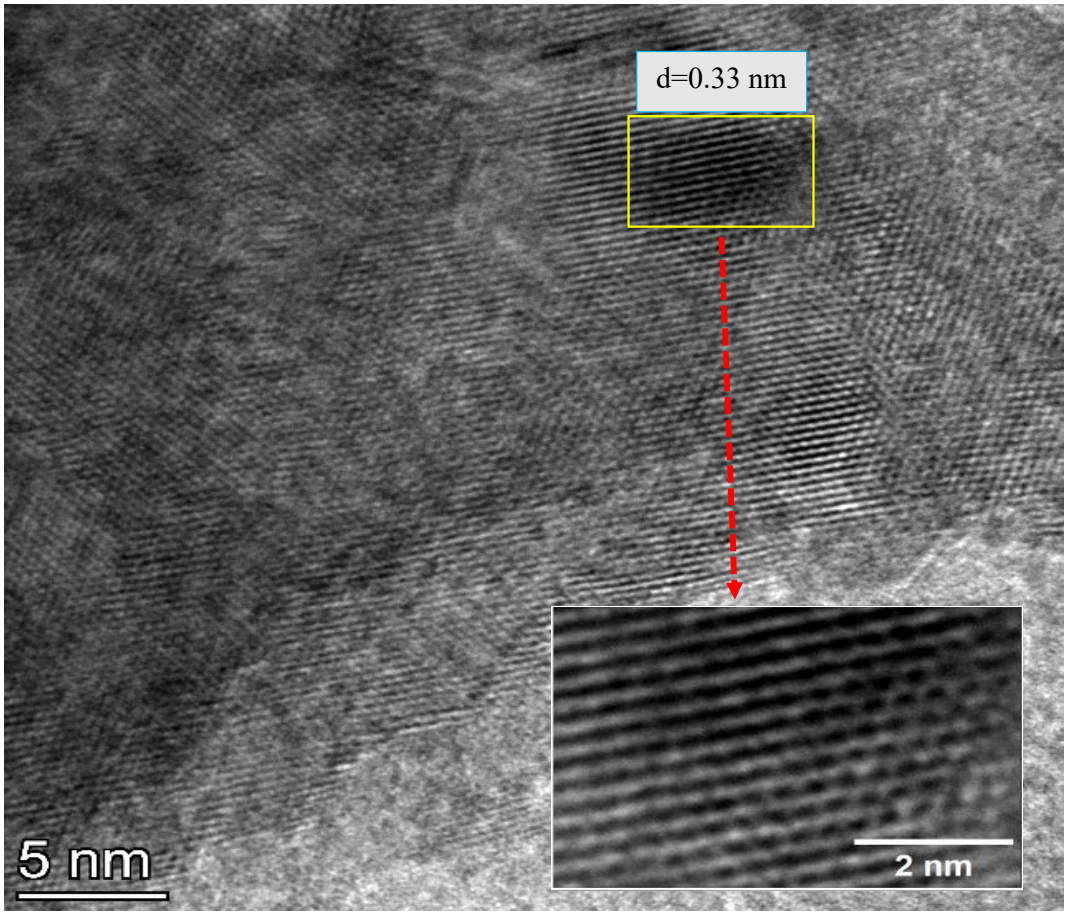

Figure 6.7 Graphitic features of the residue observed using HR-TEM: (002) plane of graphite.

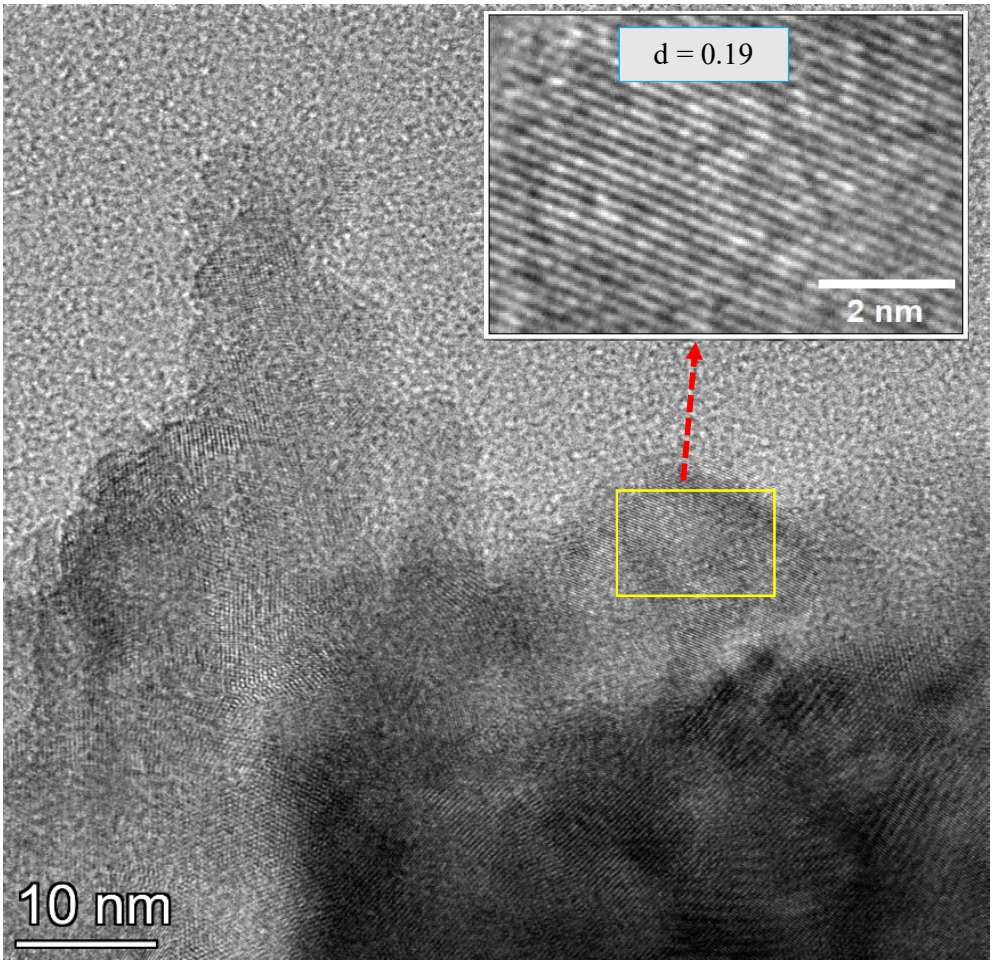

Figure 6.8 Graphitic features of the residue observed using HR-TEM: (101) plane of graphite.

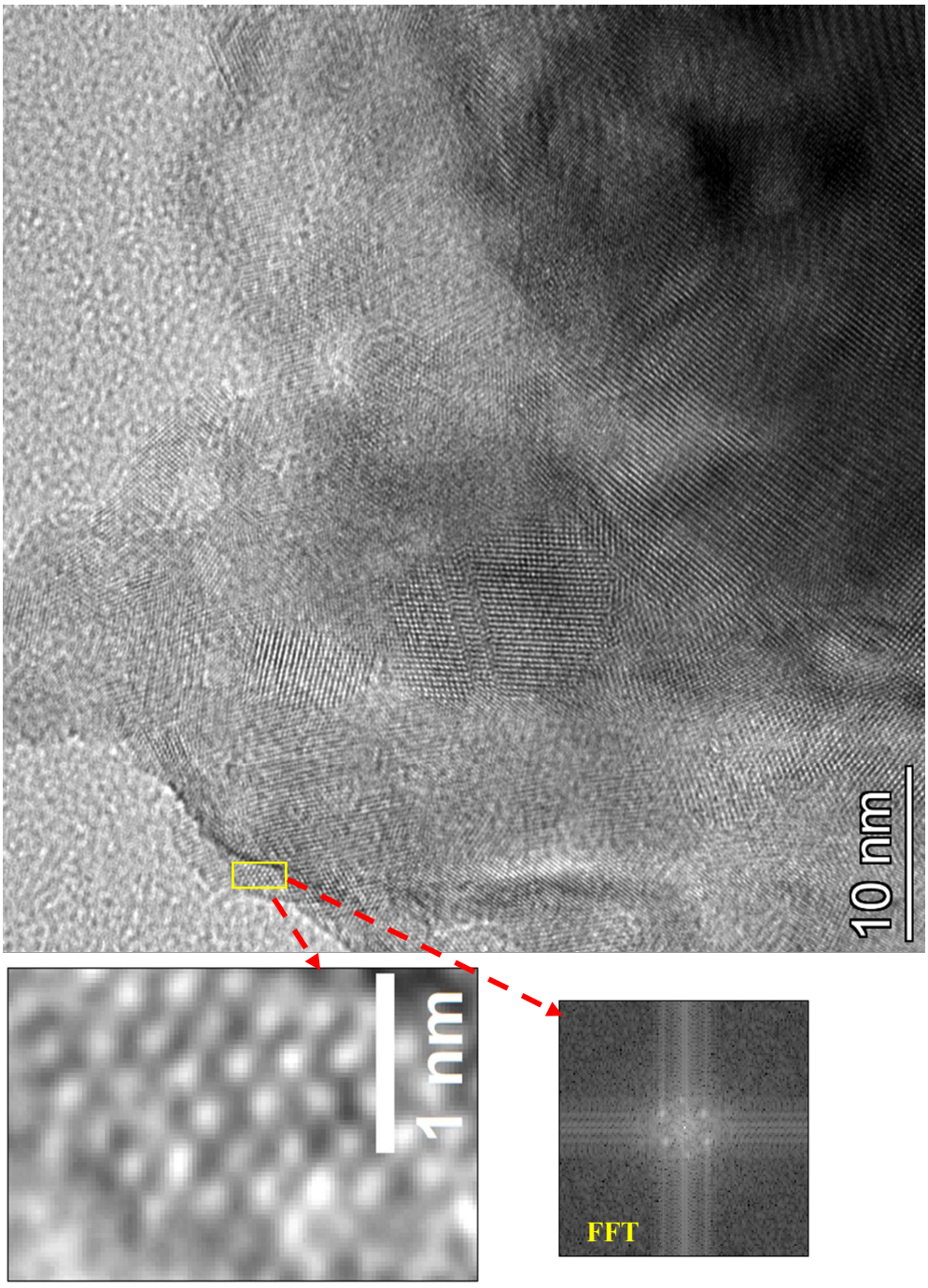

Figure 6.9 HR-TEM image of graphene in the residue.

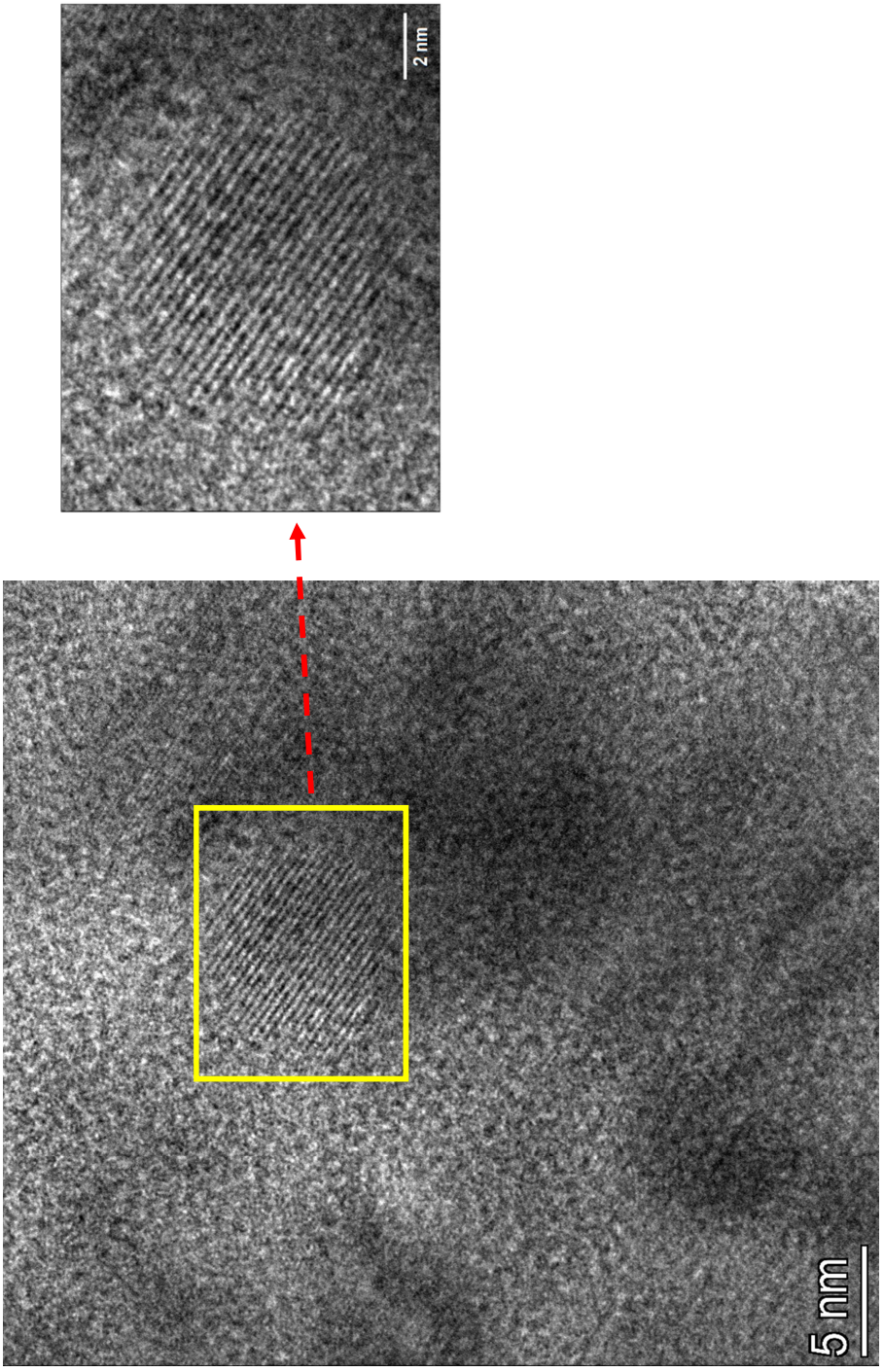

Figure 6.10 Presence of quantum dot in the residue.

The residue as observed using HR-TEM imaging is shown in Figure 6.7 to Figure 6.10. The observed features indicate a high degree of atomic order throughout the sample. The interplanar spacing in Figure 6.7 between the arrays are of the order of 0.34 nm, which is similar to the known interplanar spacing of the (002) plane of graphite (Kim et al., 2016). The ring structures are evident from the zoomed in image. Also in Figure 6.8 the interplanar spacing is of the order of 0.195 nm, which is the known d spacing for the graphite (101) plane (Howe et al., 2003) . This gives a clear picture of (six membered) carbon rings to be present in the residue. Nevertheless, graphite is a stacked layer of graphene, so we even see the presence of graphene. In Figure 6.9, we see the presence of a sheet like structure in the zoomed part of the full image. The fast Fourier transform (FFT) of the region of interest also shows the pattern of hexagonal symmetry and the calculated lattice parameter is 0.25 nm which is close to the known value 0.246 nm (Yan et al., 2013) of lattice constant of graphene. In Figure 6.10, we see the presence of graphene quantum dots, of size approximately 8 nm, sp^2 hybridized carbon atoms with an interplanar spacing of 0.33 nm.

6.4 Discussion

A clear idea of the PAH formation pathway in a low temperature condition is scarce in the literature. The first step towards the formation of an aromatic molecule is the formation of a benzene ring. Many previous studies have examined the formation of benzene rings in different low and high temperature conditions summarized in (Reizer et al., 2022) . In the molecular could conditions, where temperatures are extremely low, benzene formation can proceed under single-collision conditions. Jones et al. (2011) demonstrated that the gas-phase reaction between the ethynyl

radical and 1,3-butadiene efficiently produces benzene without an activation barrier, making it feasible under interstellar conditions. Related experiments using crossed molecular beam techniques have revealed additional barrierless and exoergic pathways to aromatic species. For example, phenyl radicals can be formed from reactions of dicarbon with 1,3-butadiene (Zhang et al., 2010), while reactions between ethynyl and vinylacetylene yield ortho-benzene (Zhang et al., 2011). Other studies have shown the formation of toluene from ethynyl reacting with 2-methyl-1,3-butadiene (Dangi et al., 2013), and benzyl radical from dicarbon reacting with 2-methyl-1,3-butadiene (Dangi et al., 2014). Collectively, these findings highlight several mechanistic routes for producing monocyclic aromatic species in the cold environments of molecular clouds.

Once an aromatic ring is formed, its growth into larger PAHs can proceed through a number of well-characterized mechanisms. These include hydrogen abstraction–acetylene addition (HACA), hydrogen abstraction–vinylacetylene addition (HAVA), phenyl addition–dehydrocyclization (PAC), radical–radical reactions (RRR), and methylidyne addition–cyclization–aromatization (MACA) (Reizer et al., 2022; Kaiser and Hansen, 2021). Each mechanism provides a different sequence for adding carbon units and expanding aromatic frameworks under astrophysical conditions. Importantly, Zhao et al., 2019 demonstrated that the HAVA mechanism can efficiently drive the low-temperature formation of higher PAHs, such as anthracene and phenanthrene, via reactions of 1-/2-naphthyl radicals with vinylacetylene.

Contrary to previously known pathways, our results show compelling evidence for ring closure from the C atoms (Pathway 1) available from the dissociation of CO. The ring closure is one step closer towards the formation of

PAH's. The graphitic carbon and graphene observed in the residue can lead to PAH formation upon hydrogenation in an irradiation environment (Merino et al., 2014) . Hence, with the abundant CO and H_2 in the ISM the PAH formation pathway could be much shorter (Pathways 1 & 2) than previously thought.

$$\mathbf{CO_{(ice)} \xrightarrow{Irradiation} Graphene_{(residue)} / Graphite_{(residue)}} \qquad \mathbf{(1)}$$

$$\mathbf{Graphene_{(residue)} / Graphite_{(residue)} \xrightarrow{+ H / H_2} PAH_{(solid/gas)}} \qquad \mathbf{(2)}$$

Once the graphite is synthesized, it can even lead to the formation of fullerenes upon energetic processing (Bunshah et al., 1992, Kroto et al., 1985). Also the formation of fullerene from graphene is observed under the energetic irradiation in a TEM study which involves the paths like the loss of carbon from the edge, forming the pentagons to curving the graphene sheet and forming the fullerenes (Chuvilin et al., 2010) . A similar pathway from graphene to fullerene is explained in Berné and Tielens, 2012. Hence our experimental results are important in the interstellar carbon chemistry that directly starts from the second most abundant molecule in the ISM.

6.6 Conclusions:

Condensed CO was irradiated using 2 keV electrons for 10 hours and the ice was further heated to higher temperatures until room temperature. Spectra recorded at various temperature intervals clearly showed the presence of refractory

residue. The substrate containing the residue was analysed *ex-situ*. HR-TEM analysis showed the presence of carbon chains in ring forms (graphene and graphitic carbon). The irradiation of 2 keV electrons on CO dissociates the molecule releasing a large amount of carbon, these carbons react with each other forming other carbon containing species including allotropes of carbon, graphene and graphite. Hence CO, dissociation provides a new pathway for ring closure and such a pathway must be considered in the ISM for efficient PAH formation, as hydrogenation of graphene/graphite can synthesize a variety of PAHs. Our results not just support the bottom up process for the formation of PAHs in the ISM but also suggests an efficient pathway which directly emerges from the second most abundant molecule in the ISM.

Chapter 7 Revisiting Ammonia ice: Resolving the phase debate using mid-IR spectroscopy

Chapter overview:

Ammonia (NH_3) plays a vital role in interstellar and planetary chemistry serving as a key reservoir of nitrogen and a precursor to complex organic molecules in astrochemical conditions. Since the morphological phase of molecular ices influence their reactivity it is an essential requirement to have an idea on the morphological phase of the abundant molecules in the astrochemical conditions. NH_3 is one such molecules whole morphological phase has been a topic of interest to the scientific community for the last 7 decades, still the phase of NH_3 is not clear at different temperatures. Here in this chapter, we have carried out extensive systematic experimental investigation to understand the phase of NH_3 from as low as 10 K to its sublimation temperature. The evolution of key spectral features across different temperatures were analysed to identify the phase transitions. Our results were then compared with the existing literature to understand the consistencies discrepancies.

7. 1 Introduction:

Nitrogen is the fifth most abundant element in the universe and the most crucial element towards the creation of life (Hily-Blant et al., 2010). Nitrogen- and oxygen-bearing complex organic molecules (COMs) in the ISM are of substantial significance as they are considered the precursors to biomolecules such as amino acids and proteins (Ramachandran et al., 2024c). One of the abundant nitrogen

containing molecular ice in the ISM and in comets is NH_3 with varying abundances from approximately 1% - 10% with respect to water ice, depending on it is in comets or background stars, or it is in the low-mass young stellar objects or it is in massive young stellar objects (Cuppen et al., 2024). The study of ammonia in terms of astrophysical applications started with the discovery of ammonia in the interstellar medium using the microwave radiation (Cheung et al., 1968). The presence of ammonia has been confirmed in the planetary atmospheres of Jupiter and Saturn (Lebofsky and Fegley Jr, 1976, Slobodkin et al., 1978). The computational models and observations confirms the presence of ammonia in gaseous planets like Uranus (Horedt and Hubbard, 1983, Hofstadter and Muhleman, 1989) and Neptune (Lindal, 1992). Ammonia ices were detected in icy bodies like Charon (Krasnopolsky, 2001) Miranda (Bauer et al., 2002) Enceladus (Emery et al., 2005) and others. Ammonia was also detected in other astrophysical bodies like protostars (Lacy et al., 1998), comets (Meier et al., 1994, Kawakita and Watanabe, 2002) etc. It is believed to be the major carrier of nitrogen in cometary nuclei (Kawakita and Mumma, 2011). In regard of extragalactic astronomy, ammonia has been detected in other galaxies like Seyfert 2 (Ao et al., 2011), NGC 4418 (González-Alfonso et al., 2012), etc. Laboratory studies of ammonia are very important to detect and to predict the evolution of ammonia in astrochemical conditions. Over the years, It has been well studied with different probing methods like Microwave (Bellotti et al., 2016), VUV (Dressler and Schnepp, 1960, Dawes et al., 2007), IR (Reding and Hornig, 1951), Raman (Reding and Hornig, 1954) etc at low temperature. Infrared spectroscopy allows us to study the vibrational modes of a molecule and plays a vital role in determining the phase transition in ice phase (Sivaraman et al., 2013). The first IR spectra of crystalline ammonia in ice phase were reported at 83 K temperature long

in 1951 (Reding and Hornig, 1951). Over the past seven decades, many studies have been carried out to fully understand the morphological phase of NH_3, still there exists a debate on the phases of ammonia in the ice state. The debate on the phases of ammonia began with the X-Ray study by Mauer (not available/unpublished), which was followed by a study of ammonia ice in the IR region reported by Staats et al., 1959. The spectra reported by Staats et al showed two metastable phases at 77 K(MS-II) and 112 K (MS-I) and a crystalline phase when deposited at 77 K and heated to 150 K. Subsequent attempts by various groups (Anderson and Walmsley, 1965, Bromberg et al., 1977, Wolff et al., 1971, Ferraro et al., 1980) to reproduce these findings largely resulted in spectra similar to those of Reding & Hornig , 1951, suggesting discrepancies in earlier phase assignments.

Further research studies by Pipes et al., 1978, Ferraro et al., 1980 found that the metastable phase-II reported by Staats et al was observed due to the presence of water in ammonia. They concluded that the metastable phase (MS-I) at 112 K may also correspond to a crystalline phase which matches well with the spectrum of reported by Reding and Hornig, 1951. They also quoted that many other irreproducible results of ammonia available in literature may corresponds to the impurities present in ammonia when the experiments were carried out. The problem of the metastable phase reported by Staats et al was partly solved whereas Pipes et al., 1978 reported a metastable phase spectrum of ammonia when deposited at 20 K and warmed to 100 K and recooled to 20 K. Also another metastable phase when deposited at 80 K, and an amorphous spectrum at 20 K deposition. Due to the experimental difficulties they have not observed a perfect cubic phase spectra of ammonia above 140 K. Ferraro et al., 1980 and Sill et al., 1980 further showed a transition of ammonia from a metastable phase to a cubic crystalline phase between

88 K to 119 K whereas they have not reported other low temperature phase of ammonia. Since the already available literature were not sufficient to address the debate on metastable phase, after two decades, Holt et al., 2004 performed the trials on solid ammonia and reported the three phases for ammonia which depend upon the temperature of deposition. They also concluded that there is a possibility that an exciton feature or different molecular orientations of ammonia may correspond to this metastable behaviour. Further studies disproved the presence of a metastable phase of ammonia and reported only one phase transition at 57 K corresponding to the crystalline phase, which persists up to the sublimation temperature of ammonia, 110 K (Zheng and Kaiser, 2007). The conclusion derived by Zheng & Kaiser cannot be considered as a complete explanation for the disagreement of the metastable phase of ammonia since the study of Zheng and Kaiser was carried out in one particular low temperature deposition at 10 K. Similarly, the sublimation temperature of ammonia was reported at 110 K which further caused a debate on the spectra which are already available in the literature above 110 K. Similarly, they also claimed that the spectra have a dependence over the thickness of ice deposited which needs to be further investigated for the reproducibility of the spectra. In the contemporary timeline of ammonia research Dawes et al., 2007 reported a metastable phase between 50 K and 65 K. They derived a conclusion that the metastable phase was due to the formation of crystallites between those temperatures. Without the X-ray diffraction studies, we can hypothesis our results whereas we cannot conclude about the shape and size of a solid from the IR and VUV Spectra only. Over a decade this study of Zheng and Kaiser, 2007 & Dawes et al., 2007 were considered to be latest reports available in literature of solid ammonia till date. These kinds of contrary results of ammonia in literature on a

particular year one after the other made the debate to be still open. Meanwhile there were many works like deriving the optical constants, band intensities and other calculations were reported on the ice phase of ammonia which did not consider the metastable phase of ammonia at those particular temperatures taken for calculations (Robertson et al., 1975, Zanchet et al., 2013, Hudson et al., 2022a). The phases of ammonia play a vital role in the evolution of further molecules in space. It is necessary to revisit the phases of ammonia since it prevails in the ice phase in many of the astrophysical bodies. It also has a wide range of implications in the formation of Nitrogen substituted compounds (Zheng et al., 2008) which may further lead to the formation of life bearing molecules in Space. The advancements of technology and instruments were increased over the past few decades, so we tried to revisit the phases of ammonia in a very detailed perspective in all the above mentioned temperature regimes. This study will try to address the seven-decade debate on ammonia ice in a more qualitative manner.

7.2 Experimental Methodology:

Ammonia (>99% purity, Vadilal), available as a compressed gas, was used in these experiments. The experiments were carried out using the SALT facility explained in Chapter 3. The chamber pressure and temperature was 10^{-9} mbar and 10 K before deposition. The gas was introduced to the chamber through the all metal leak valve and deposited onto the ZnSe substrate. After the deposition, the ice was heated at a ramp rate 2 $Kmin^{-1}$ and the *in situ* FTIR spectra in a range 4000-650 cm^{-1} were recorded as a function of temperature at regular interval until sublimation. For our experiments, we have deposited NH_3 at various temperatures from 10 K to

100 K and the similar procedure was followed for all the different sets of experiments.

7.3 Results and Discussion:

7.3.1 NH_3 deposited at 10 K:

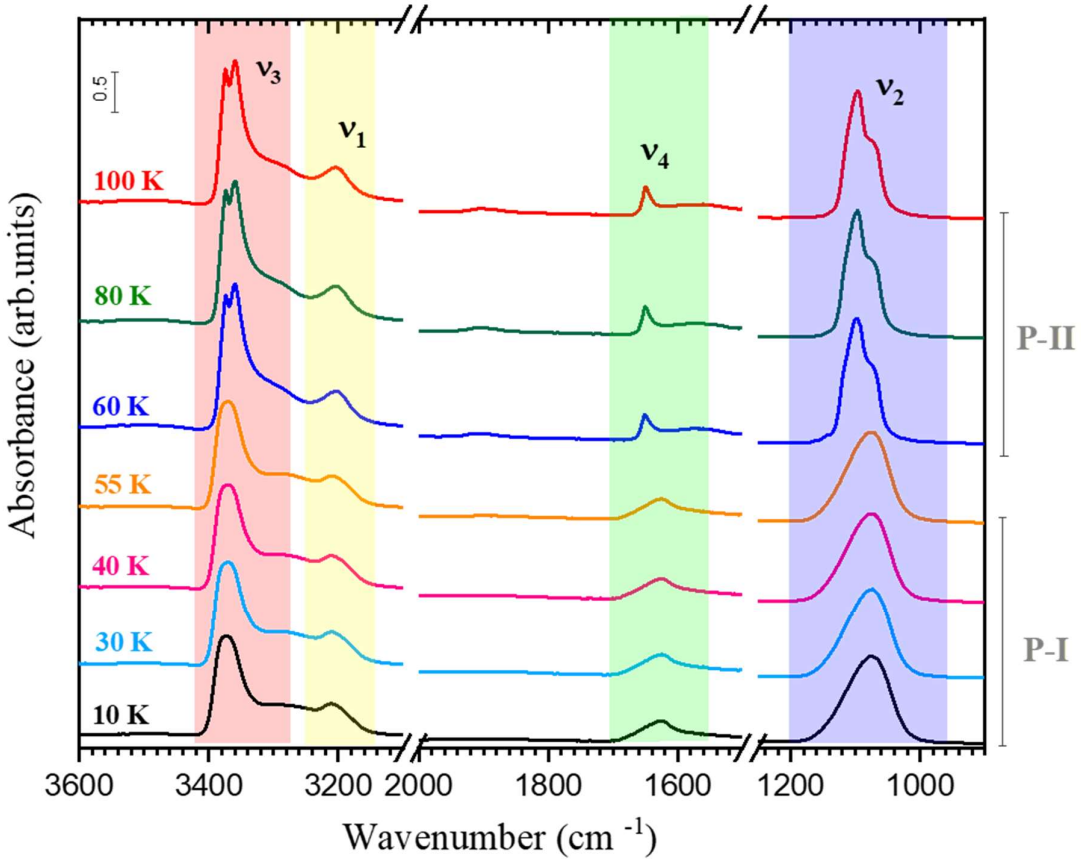

Figure 7.1 Mid-IR spectra of Ammonia deposited at 10 K and warmed to higher temperatures. The spectra are stacked for clarity

The mid-IR spectra of ammonia deposited at 10 K and warmed to higher temperatures are presented in Fig.7.1. The bands corresponding to different modes of vibrations of ammonia and their assignments are listed in Table 7.1. At 10 K, upon deposition, ammonia is in the amorphous phase (P-I). While warming the ice to higher temperatures, the beginning of a phase change is observed at 57 K, evident

with the splitting of the peaks of ν_3 and ν_2 bands (we will denote this phase as P-II hereafter). The splitting and shift of the ν_4 band are also observed.

Table 7.1 Infrared absorption features of solid NH_3

Tentative assignments	Deposited at 10 K	Type of vibration
ν_1	3211.24	N-H symmetric stretch
ν_2	1077	N-H symmetric deformation
ν_3	3372	N-H degenerated stretching
ν_4	1625 1562 1471 1361	H-N-H scissoring

An additional feature at 1912 cm^{-1} and 2119 cm^{-1} was observed during the phase change, and its band assignment is still unclear (Dawes et al., 2007). These phase change features are similar to previous works available in the literature. As reported earlier by (Zheng and Kaiser, 2007), when deposited at 10 K, we also report only one phase transition (PT-I) at 57 K until sublimation. The complete sublimation of NH_3 ices takes place at 120 K for 10 K deposition.

7.3.2 NH_3 deposited at higher temperatures:

In previous studies of ammonia ices, it has been reported that the phases of ammonia depend on the temperature of deposition (Holt et al., 2004, Dawes et al., 2007) . To verify this, we conducted experiments at deposition temperatures higher than 10 K, i.e., 20 K, 30 K, 40 K, 50 K, 55 K, 60 K, 65 K, 80 K, 100 K, and warmed to higher temperatures as usual.

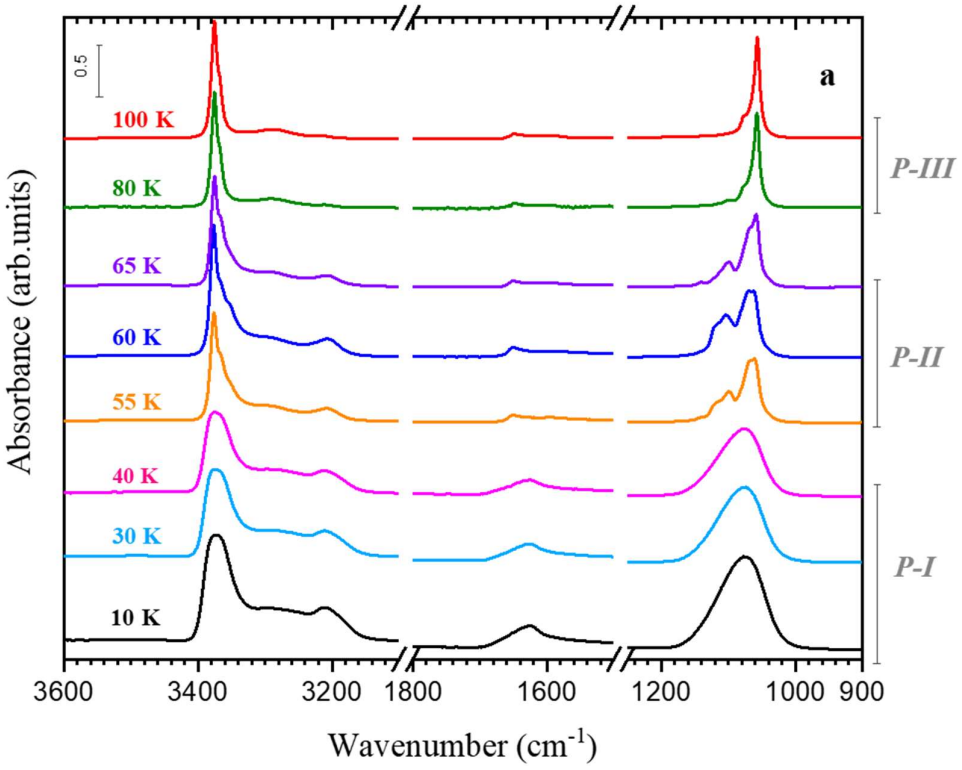

Figure 7.2 Comparison of Mid-IR spectra of Ammonia deposited at various temperatures. The spectra are stacked for clarity

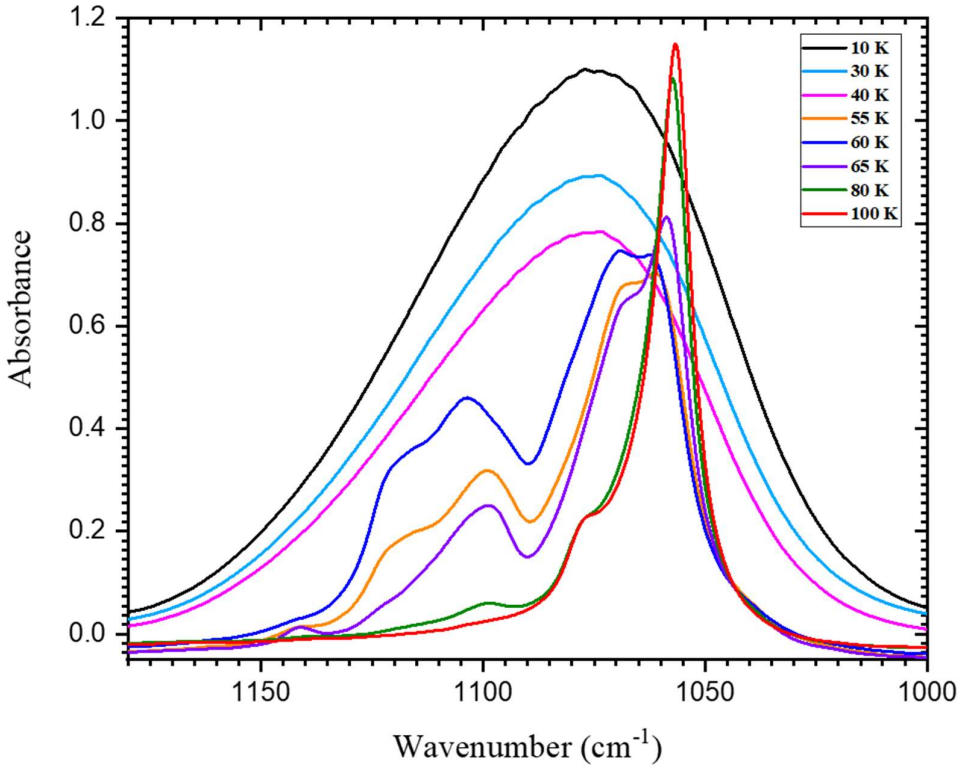

Figure 7.3 Spectral features of ν_2 band of Ammonia deposited at various temperatures

Figure. 7.2 presents the mid-IR spectra at a few deposition temperatures. We observe three distinct spectral variations, which can be seen in the ν_2 band (Figure 7.3):

For deposition temperatures below 45 K- ν_2 exhibits a single broad band with its peak centred at 1077 cm^{-1} (FWHM = 78.06 ± 2 cm^{-1}), corresponding to the amorphous phase (P-I). This amorphous spectral feature is similar to those reported in previous studies (Zheng and Kaiser, 2007, Dawes et al., 2007, Holt et al., 2004)

For deposition temperatures between 45 K and 80 K- the spectral features are similar to those of P-II. Many shoulder bands of ν_2 are observed in this temperature regime.

For deposition temperatures above 80 K- a drastic shift of the ν_2 band from 1096 cm^{-1} to 1057 cm^{-1} is observed, which appears very sharp and intense (we denote this phase as P-III). This sharp peak at 1057 cm^{-1} (FWHM = 11.16 ± 1 cm^{-1}) is accompanied by a shoulder band at 1077 cm^{-1}.

These observations indicate that ammonia ice has three distinct phases. While it is clear that P-I is amorphous, to understand P-II and P-III better, we compare direct deposition and warmed spectra at two different temperatures (60 K and 100 K)

7.3.3 60 K spectra comparison

NH_3 was deposited directly at 60 K (just above PT-I) and compared with spectra warmed from lower temperature depositions.

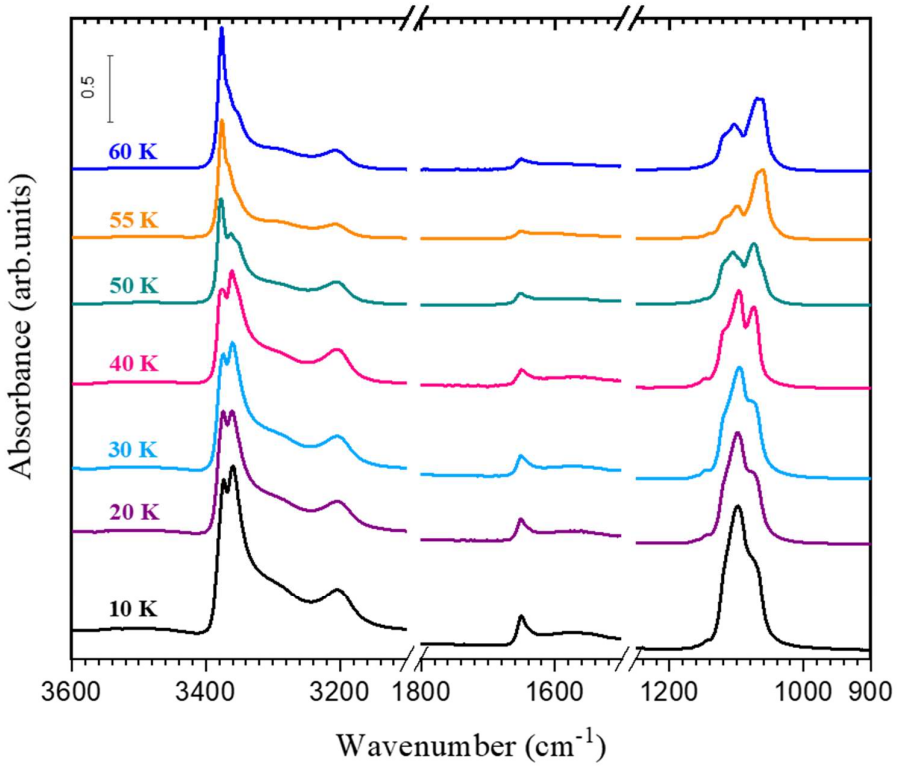

Figure 7.4 Mid -IR spectra of ammonia deposited at 60 K with ammonia deposited various temperatures and warmed to 60 K. The spectra are stacked for clarity

Figure 7.4 represents the MIR spectra of ammonia deposited at 60 K compared with ammonia deposited at various temperatures and warmed to 60 K. It can be observed that the spectral bands of direct deposition at 60 K are different from the ones warmed to 60 K. Especially, Fig 7.5 which shows only the ν_2 band of the previous comparison, we can clearly observe that ammonia deposited at temperatures lower than 45 K and warmed to 60 K exhibits a different phase at 60 K with three bands (1145, 1070, and 1096 cm^{-1}), whereas deposition between 45 K and 60 K shows many shoulder bands which looks like neither amorphous nor crystalline. Similar variations were observed in the ν_3 band also. It is also observed that there is a switch in intensities of the bands (1070 and 1096 cm^{-1}) i.e., the intensity of 1070 cm^{-1} is higher than 1096 cm^{-1} when deposited directly at 60 K whereas 1096 cm^{-1} is higher when warmed to 60 K from the lower temperature depositions.

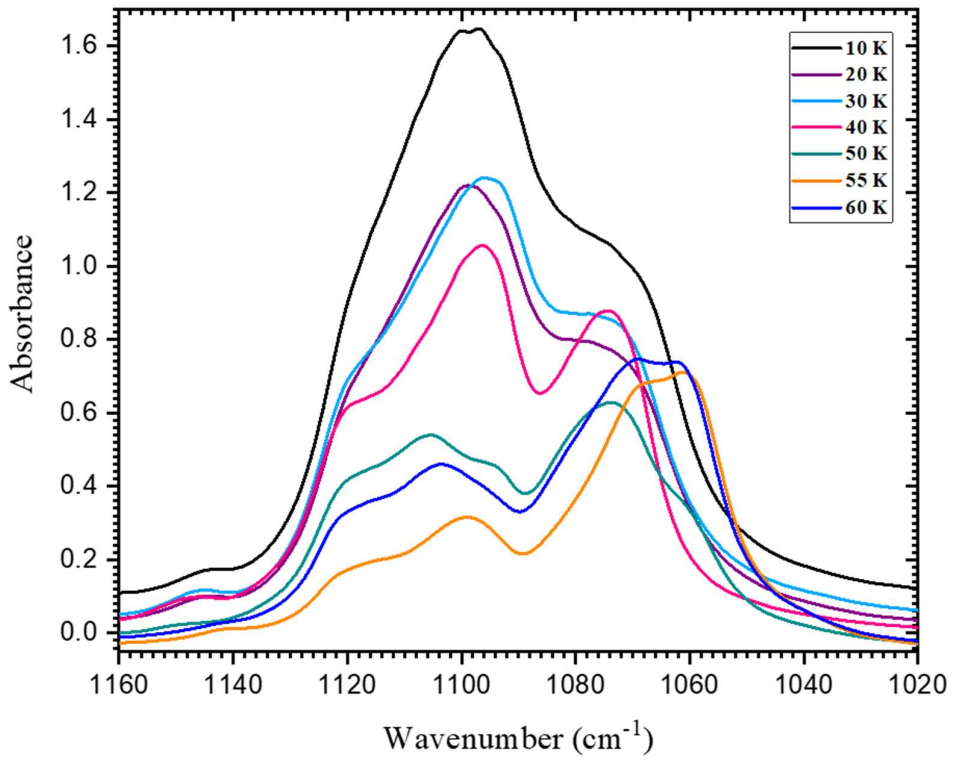

Figure 7.5 Spectral features of ν_2 band of ammonia deposited at 60 K with ammonia deposited at various temperatures and warmed to 60 K

This switching of intensities for a particular temperature could be due to different molecular orientations which are dependent on the temperature of deposition. These observations also indicate that P-II is indeed a metastable phase. It is worth noting that while the P-II spectral feature (specifically the ratio of the intensities of individual peaks in each shoulder) may vary depending on the parameters the general pattern of the spectra remains the same.

7.3.4 100 K spectra comparison

For depositions above 75 K, we observe that the spectra of the ice so formed (P-III) are different from that of both the amorphous (P-I) and metastable (P-II) phases.

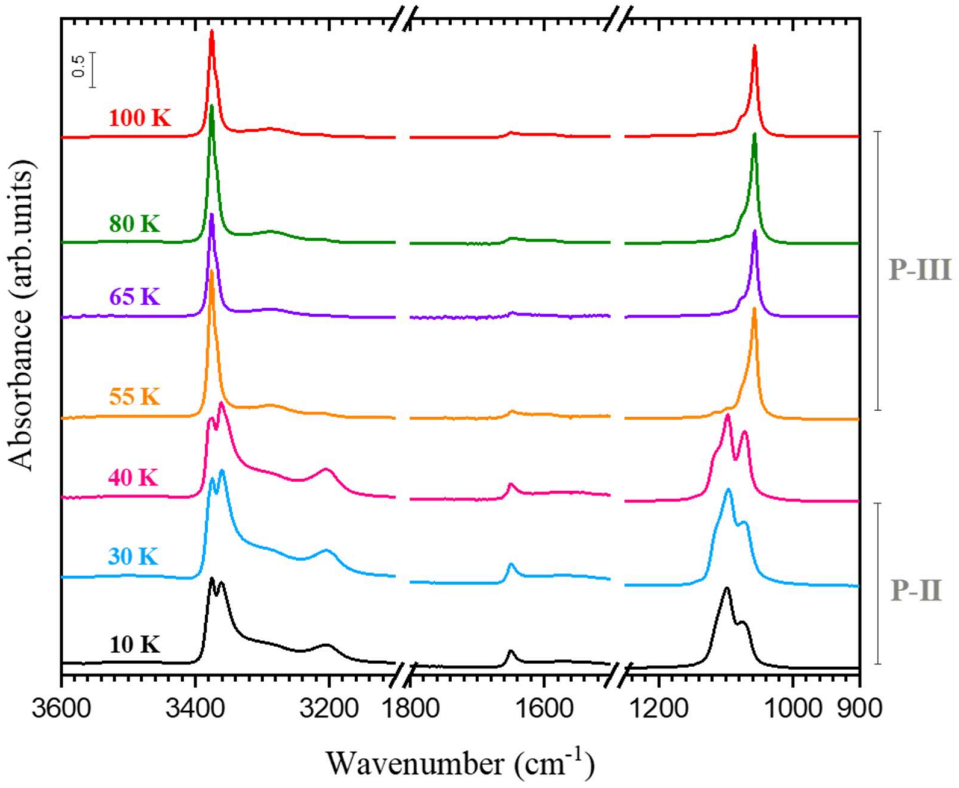

Figure 7.6 Mid-IR spectra of ammonia deposited at 100 K with ammonia deposited various temperatures and warmed to 100 K. The spectra are stacked for clarity

To investigate the behaviour of (P-III), the spectrum of NH_3 deposited directly at 100 K (above PT-II) was compared with the 100 K spectra that were warmed from other lower temperature depositions (Figure 7.6). For deposition temperatures below 55 K, we observe that the 100 K spectra follow the pattern of that of the (P-II). This can be distinctly seen in Figure 7.7 which shows only the variations of the ν_2 band. Beyond 55 K deposition, the spectra of warmed to 100 K and direct 100 K deposition have very similar spectral features without much difference. This shows the stability of (P-III). This observation combined with the fact that earlier X-ray studies which reported ammonia to possess a perfect cubic crystalline phase at high temperatures and similarity of (P-III) spectral feature (especially ν_2 and ν_3) with that of (Sill et al., 1980) we claim with a certain degree of certainty that (P-III) corresponds to a (perfect) cubic phase and PT-II is the metastable to cubic phase transition.

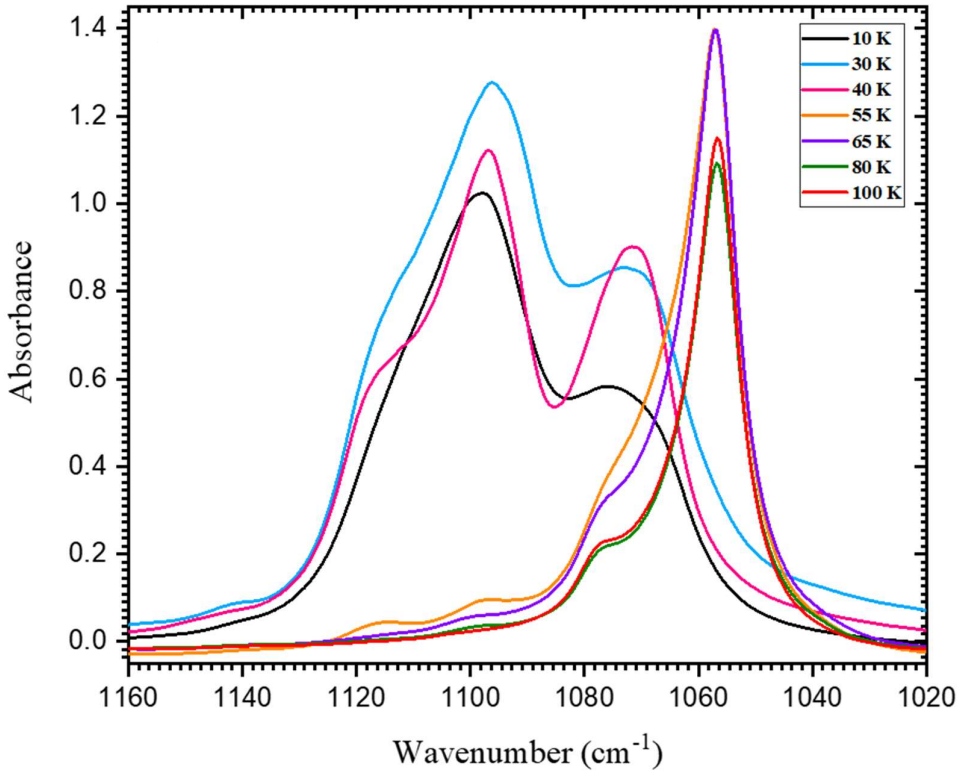

Figure 7.7 Spectral features of ν_2 band of ammonia deposited at 100 K with ammonia deposited at various temperatures and warmed to 100 K

So, the phase transition reported earlier by (Zheng and Kaiser, 2007) at 57 K cannot correspond to a perfect crystalline phase transition but it might be a stable phase transition for that particular lower temperature deposition, which existed till sublimation. Similar trends were reported in previous study (Holt et al., 2004) as well.

With regards to the phases of ammonia ice, we agree with the results of Holt et al. (2004), and in disagreement with the report of Zheng and Kaiser (Zheng and Kaiser, 2007). From our above-mentioned observations, we also agree with Holt et al (Holt et al., 2004) that the metastable phase can be formed in two ways—direct deposition between 55 K and 80 K or deposited at low temperature and warmed to temperatures above 55 K. We disagree with the statement of Holt et al., 2004 that the metastable spectra are not comparable because from our experiments and fig 7.5, we clearly see comparability. From our results and comparison, we infer that the intensity ratios of the different peaks of the ν_2 band in the metastable phase are deposition temperature dependent and hold well with Dawes et al (Dawes et al., 2007). However, our 10 K deposition shows only one phase transition at 57 K, consistent with Zheng and Kaiser (Zheng and Kaiser, 2007). In comparison with Dawes et al., 2007, our spectral trends show major differences with respect to their temperatures. For example, for deposition temperatures below 50 K we observe a complete phase transition (PT-I) at 57 K and no further changes until sublimation, whereas Dawes et al (Dawes et al., 2007) observed drastic changes above 65 K and the complete transformation was observed till 75 K. We suspect these differences are because Dawes et al. 2007's were annealed spectra whereas our spectra correspond to the exact temperature of warming. The triple peak feature during phase transition at 57 K reported by Zheng and Kaiser, 2007 could not be

reproduced even with different ice thicknesses. Hence, the only possible reason for that could be the saturation of the spectra and not necessarily a real peak. Similarly, the spectra of ice deposited above 80 K and warmed to higher temperature match well with the cubic phase spectra of Dawes et al., 2007. Our results are in agreement with Sill et al., 1980 regarding metastable to cubic phase transition for ice deposited at 88 K and annealed to 119 K, with slight differences in phase transition temperature (PT-II). This is due to the differences in the experimental methodology. The sublimation temperature is consistent with most of the previous experiments (Dawes et al., 2007, Zheng and Kaiser, 2007) . For the formation of crystallites at higher temperatures as discussed by Dawes et al., 2007, it is difficult to characterize the existence/formation/size of the crystallites only from the IR spectroscopy. To confirm the presence of crystallites, X-ray studies or imaging techniques would be necessary, which, to the best of our knowledge, are not known. So only from the IR studies we will not be able to comment on the formation of crystallites. But, if we are to consider the hypothesis of Dawes et al., 2007 that the metastable phase is contours of crystals in an amorphous system, the IR spectrum of the metastable phase should have been a combination of amorphous and crystalline spectra in some ratio. But from our results, we find the P-II spectra are not so at all. Hence we can safely say that the model proposed (fig. 9 of (Dawes et al., 2007)) is a hypothesis at best.

7.4 Conclusion:

In this study we present the experimental work to clear certain confusions concerning the spectroscopy of ammonia, especially in the ice phase and its photochemistry under interstellar conditions. The major conclusions of this work are highlighted below-

- We have tried our best to review major discussions and conclusions of ammonia ice spectroscopic studies over the past seven decades
- In this study, we presented temperature-dependent mid-IR spectra of pure ammonia ice under astrochemical conditions for different deposition temperatures. The IR spectral features outlined in this paper can be valuable for its future identification of ammonia in the interstellar ice and other cold regions of planetary and cometary bodies
- Between 10 K and 55 K, the pure ammonia ice is in amorphous phase, and above 55 K, it is in metastable phase. For deposition temperatures below 55 K, the ice remains in metastable phase until its sublimation, whereas for deposition temperatures above 55 K, it turns crystalline around 80 K. For deposition temperatures above 80 K, the ice is in (cubic) crystalline phase upon deposition itself.

Chapter 8 Summary and Future work

Chapter overview:

This chapter offers a comprehensive summary of the entire thesis, emphasizing its significant aspects and findings. It also includes future research directions inspired by the results presented throughout the work.

The aim of this thesis is to understand the morphology and stability of ices both in their pure form and under the influence of intermolecular interaction with other molecules. Additionally this thesis aimed to explore alternative low temperature formation pathway for polycyclic aromatic hydrocarbons (PAHs). To attain the aim, we have simulated the astrochemical conditions in the laboratory using a closed cycle He cryostat and investigated the stability of pure and mixture of ices at different temperatures and energetic processing of pure molecules. The ices were probed using the infrared (IR) and visible ultraviolet (UV/VUV) spectroscopy. We have addressed several key questions regarding the phase, stability and formation mechanism of molecular ices. The ices selected are known to be present in the interstellar medium (ISM) and comets, thereby giving an overall idea on the effect of thermal processing, intermolecular interaction and energetic processing on different astrochemical regions.

A summary from the chapters 4,5,6,7 is given below.

8.1 Summary of the work:

8.1.1 Effect of EG on water in comets and ISM

In chapter 4, we have explored the effect of the intermolecular hydrogen bonding between ethylene glycol (EG) and water. To investigate that, we have simulated the astrochemical conditions in the laboratory and studied the temperature dependent behaviour of these two ices in pure state as well as in the mixture and layered configurations and probed the ices using IR spectroscopy. Due to the presence of –OH groups in both EG and water, we have used D_2O instead of H_2O in our experiments to spectroscopically differentiate between these two. The results are summarized below-

- Pure D_2O when deposited at 10 K on to a ZnSe substrate forms an amorphous ice, when heated to 152 K transforms to crystalline ice (evident from the splitting of –OD stretching band) and when further heated it sublimes at 180 K.
- When D_2O ice is with EG in both layered or mixture configurations, there is no phase transitions for D_2O ice at any temperature, while the sublimation temperature of D_2O becomes ~240 K.
- In the IR spectrum of the layered or mixture ices a new band having a peak around 987 cm^{-1} appeared due to the interaction between EG and D_2O.
- These findings EG acts as an anticrystallizer for water in the astrochemical conditions.
- The stability of D_2O ice up to 240 K indicates that in comets, water ice can be found at closer distances than previously known.

- Also the hydrogen bonding enables water to be stable for chemical reactions at a temperature > 50 K than its known sublimation temperature.

8.1.2 Effect of diols on the condensation and stability of water

Building on the EG- D_2O interaction studies, this chapter investigated the condensation of water at temperatures beyond the water sublimation temperature (~180 K) in the presence of diols (EG and 1,3 propanediol (1,3 PD). The experiments are similar to the previous chapter. The results are summarized-

- When water vapors were deposited on a bare ZnSe substrate at 200 K, no stable D_2O ice formed.
- In contrast when deposited on to a preexisting diol layer (EG/1,3 PD) at 200 K, D_2O ice formed and remained stable up to a temperature equal to the sublimation temperature of the respective diols.
- The findings indicate that in a cometary surface or in the protoplanetary disk water ice can form at a temperature beyond its known sublimation temperature because of the strong hydrogen bonding with the underlying diol ice layer.
- Water can be in the reaction matrix at higher temperature than taken into account previously.

8.1.3 Low temperature formation pathway of PAHs from CO

The pathway for the formation of PAHs have been explored from the energetic processing of CO. CO ice was formed on to the LiF substrate at 10 K and irradiated

using electrons of energy 2 keV for 10 hours. The ice was heated after the irradiation. The ice before and after was probed in situ using VUV/UV spectroscopy. The substrate was taken out of the chamber at room temperature and was studied ex situ using High Resolution Transmission Electron Microscopy (HRTEM). The insterplaner spacing of the crystalline structure obtained from the residue was calculated using imageJ software. The results of the experiments are summarized:

- CO ice deposited on LiF at 10 K showed characteristic vibronic bands of the fourth positive band system.
- The ice after 10 hours of irradiation with 2 keV electrons gave rise to the formation of a strong new peak near 240 nm.
- A broad shoulder around 174 nm, an indicative of O2 is evident.
- While heating up to room temperature, two peaks remained in the spectrum, one nearly around 240 nm and another nearly 180 nm.
- Ex-situ HR-TEM analysis revealed graphitic structures (graphene, graphite, carbon quantum dots), from the interplanar spacing calculation.
- These results suggest CO can serve as a precursor to ring-based carbon structures, supporting a bottom-up pathway for PAH formation under cold astrophysical conditions, possibly via hydrogenation of graphitic carbon.

8.1.4 Revisiting Ammonia ice: Resolving the Phase Debate Using Mid-IR Spectroscopy

This chapter address the long standing debate on the morphological phase of NH_3 ice under low temperature astrochemical conditions. Here we have formed NH_3 ice

at different temperature starting from 10 K to 100 K and heated the ice until its sublimation. The results are summarized:

- NH_3 after deposition at low temperature at 10 K forms an amorphous ice structure, evident from broad features corresponding to different characteristic vibration.
- The phase of NH_3 depends on the temperature of deposition.
- When NH_3 is deposited at a temperature < 50 K, it forms an amorphous phase.
- When deposited 50 K-80 K, it forms a metastable phase
- When NH_3 is deposited at a temperature >80 K, it forms a crystalline structure.
- When NH_3 is deposited at a temperature below 40 K, a transition from amorphous to metastable phase occurred around 57 K.
- When NH_3 is deposited at a temperature above 50 K, a transition from metastable to crystalline phase was observed at ~100 K.

8.2 Future work

The effect of hydrogen bonding between diols and water has opened up a new stable temperature range of water up to ~230 K. So far in the literature water ice has been considered in the reaction matrix below 170 K. This chemical behaviour or water ice in this temperature range will be explored in pure state as well as in a mixture of water and other C, N containing stable molecules at that temperature.

Also the energetic processing of mixture of water included ices at this temperature can be crucial because of the higher rate of reaction at this high temperature.

Since Graphite/ graphene has already been synthesized from CO, it can be further hydrogenated to form PAHs (Merino et al., 2014) to understand the efficiency of different PAHs.

Besides, it has been observed that fullerenes (C_{60}/C_{70}) can be formed from the energetic processing of graphite (Bunshah et al., 1992, Kroto et al., 1985) and graphene (Chuvilin et al., 2010, Berné and Tielens, 2012). The formation of fullerenes from CO can also be explored.

References:

ABRÀMOFF, M. D., MAGALHÃES, P. J. & RAM, S. J. 2004. Image processing with ImageJ. *Biophotonics international,* 11**,** 36-42.

ALLAMANDOLA, L., SANDFORD, S. & WOPENKA, B. 1987. Interstellar polycyclic aromatic hydrocarbons and carbon in interplanetary dust particles and meteorites. *Science,* 237**,** 56-59.

ALTENHOFF, W., BATRLA, W., HUCHTMEIER, W., SCHMIDT, J., STUMPFF, P. & WALMSLEY, M. 1983. Radio observations of comet 1983 D. *Astronomy and Astrophysics (ISSN 0004-6361), vol. 125, no. 2, Sept. 1983, p. L19-L22.,* 125**,** L19-L22.

ALTWEGG, K., BALSIGER, H., BERTHELIER, J.-J., BIELER, A., CALMONTE, U., DE KEYSER, J., FIETHE, B., FUSELIER, S., GASC, S. & GOMBOSI, T. I. 2017. D2O and HDS in the coma of 67P/Churyumov–Gerasimenko. *Philosophical Transactions of the Royal Society A: Mathematical, Physical and Engineering Sciences,* 375**,** 20160253.

ANDERSON, A. & WALMSLEY, S. 1965. Far infra-red spectra of molecular crystals: IV. Ammonia, hydrogen sulphide and their fully deuterated analogues. *Molecular Physics,* 9**,** 1-8.

AO, Y., HENKEL, C., BRAATZ, J., WEIß, A., MENTEN, K. & MÜHLE, S. 2011. Ammonia (J, K)=(1, 1) to (4, 4) and (6, 6) inversion lines detected in the Seyfert 2 galaxy NGC 1068. *Astronomy & Astrophysics,* 529**,** A154.

ARUMAINAYAGAM, C. R., GARROD, R. T., BOYER, M. C., HAY, A. K., BAO, S. T., CAMPBELL, J. S., WANG, J., NOWAK, C. M., ARUMAINAYAGAM, M. R. & HODGE, P. J. 2019. Extraterrestrial prebiotic molecules: photochemistry vs. radiation chemistry of interstellar ices. *Chemical Society Reviews,* 48**,** 2293-2314.

ARUMAINAYAGAM, C. R., LEE, H.-L., NELSON, R. B., HAINES, D. R. & GUNAWARDANE, R. P. 2010. Low-energy electron-induced reactions in condensed matter. *Surface Science Reports,* 65**,** 1-44.

BAG, S., BHUIN, R. G. & PRADEEP, T. 2013. Distinguishing Amorphous and Crystalline Ice by Ultralow Energy Collisions of Reactive Ions. *The Journal of Physical Chemistry C,* 117**,** 12146-12152.

BAIRD, T. 1972. The nature of the solid products from CO radiolysis. *Carbon,* 10**,** 723-728.

BANWELL, C. N. & MCCASH, E. M. 2017. *Fundamentals of molecular spectroscopy*, Indian Edition.

BAUER, J. M., ROUSH, T. L., GEBALLE, T. R., MEECH, K. J., OWEN, T. C., VACCA, W. D., RAYNER, J. T. & JIM, K. T. 2002. The near infrared spectrum of Miranda: Evidence of crystalline water ice. *Icarus,* 158**,** 178-190.

BELLOTTI, A., STEFFES, P. G. & CHINSOMBOOM, G. 2016. Laboratory measurements of the 5–20 cm wavelength opacity of ammonia, water vapor, and methane under simulated conditions for the deep jovian atmosphere. *Icarus,* 280**,** 255-267.

BENNETT, C. J., CHEN, S.-H., SUN, B.-J., CHANG, A. H. & KAISER, R. I. 2007. Mechanistical studies on the irradiation of methanol in extraterrestrial ices. *The Astrophysical Journal,* 660**,** 1588.

BENNETT, C. J., ENNIS, C. P. & KAISER, R. I. 2014. Experimental studies on the formation of D2O and D2O2 by implantation of energetic D+ ions into oxygen ices. *The Astrophysical Journal,* 782**,** 63.

BENNETT, C. J., JAMIESON, C. S. & KAISER, R. I. 2009. Mechanistical studies on the formation of carbon dioxide in extraterrestrial carbon monoxide ice analog samples. *Physical Chemistry Chemical Physics,* 11**,** 4210-4218.

BENNETT, C. J. & KAISER, R. I. 2005. Laboratory Studies on the Formation of Ozone (O3) on Icy Satellites and on Interstellar and Cometary Ices. *The Astrophysical Journal,* 635**,** 1362.

BENNETT, C. J. & KAISER, R. I. 2007. On the formation of glycolaldehyde (HCOCH2OH) and methyl formate (HCOOCH3) in interstellar ice analogs. *The Astrophysical Journal,* 661**,** 899.

BERNÉ, O. & TIELENS, A. G. 2012. Formation of buckminsterfullerene (C60) in interstellar space. *Proceedings of the National Academy of Sciences,* 109**,** 401-406.

BISSCHOP, S., FRASER, H., ÖBERG, K., VAN DISHOECK, E. & SCHLEMMER, S. 2006. Desorption rates and sticking coefficients for CO and N2 interstellar ices. *Astronomy & Astrophysics,* 449**,** 1297-1309.

BIVER, N., BOCKELÉE-MORVAN, D., DEBOUT, V., CROVISIER, J., BOISSIER, J., LIS, D., RUSSO, N. D., MORENO, R., COLOM, P. & PAUBERT, G. 2014. Complex organic molecules in comets C/2012 F6 (Lemmon) and C/2013 R1 (Lovejoy): Detection of ethylene glycol and formamide. *Astronomy & Astrophysics,* 566**,** L5.

BIVER, N., BOCKELÉE-MORVAN, D., MORENO, R., CROVISIER, J., COLOM, P., LIS, D. C., SANDQVIST, A., BOISSIER, J., DESPOIS, D. & MILAM, S. N. 2015. Ethyl alcohol and sugar in comet C/2014 Q2 (Lovejoy). *Science Advances,* 1**,** e1500863.

BIVER, N., RUSSO, N. D., OPITOM, C. & RUBIN, M. 2022. Chemistry of comet atmospheres. *arXiv preprint arXiv:2207.04800*.

BOYER, M. C., RIVAS, N., TRAN, A. A., VERISH, C. A. & ARUMAINAYAGAM, C. R. 2016. The role of low-energy (≤ 20 eV) electrons in astrochemistry. *Surface Science,* 652**,** 26-32.

BREDEHÖFT, J. H., BÖHLER, E., SCHMIDT, F., BORRMANN, T. & SWIDEREK, P. 2017. Electron-induced synthesis of formamide in condensed mixtures of carbon monoxide and ammonia. *ACS Earth and Space Chemistry,* 1**,** 50-59.

BROMBERG, A., KIMEL, S. & RON, A. 1977. Infrared spectrum of liquid and crystalline ammonia. *Chemical Physics Letters,* 46**,** 262-266.

BROUILLET, N., DESPOIS, D., LU, X.-H., BAUDRY, A., CERNICHARO, J., BOCKELÉE-MORVAN, D., CROVISIER, J. & BIVER, N. 2015. Antifreeze in the hot core of Orion-First detection of ethylene glycol in Orion-KL. *Astronomy & Astrophysics,* 576**,** A129.

BRUCATO, J., CASTORINA, A., PALUMBO, M., SATORRE, M. & STRAZZULLA, G. 1997. Ion irradiation and extended CO emission in cometary comae. *Planetary and Space Science,* 45**,** 835-840.

BUCKLEY, P. & GIGUÈRE, P. A. 1967. Infrared studies on rotational isomerism. I. Ethylene glycol. *Canadian Journal of Chemistry,* 45**,** 397-407.

BUNSHAH, R. F., JOU, S., PRAKASH, S., DOERR, H. J., ISAACS, L., WEHRSIG, A., YERETZIAN, C., CYNN, H. & DIEDERICH, F. 1992. Fullerene formation in sputtering and electron beam evaporation processes. *The Journal of Physical Chemistry,* 96**,** 6866-6869.

BURKHARDT, A. M., LEE, K. L. K., CHANGALA, P. B., SHINGLEDECKER, C. N., COOKE, I. R., LOOMIS, R. A., WEI, H., CHARNLEY, S. B., HERBST, E. & MCCARTHY, M. C. 2021. Discovery of the pure polycyclic aromatic hydrocarbon indene (c-C9H8) with GOTHAM observations of TMC-1. *The Astrophysical Journal Letters,* 913**,** L18.

BUTNER, H., CHARNLEY, S., CECCARELLI, C., RODGERS, S., PARDO, J., PARISE, B., CERNICHARO, J. & DAVIS, G. 2007. Discovery of interstellar heavy water. *The Astrophysical Journal,* 659**,** L137.

CAMPBELL, E. K., HOLZ, M., GERLICH, D. & MAIER, J. P. 2015. Laboratory confirmation of C60+ as the carrier of two diffuse interstellar bands. *Nature,* 523**,** 322-323.

CARO, G. M., CHEN, Y.-J., APARICIO, S., JIMÉNEZ-ESCOBAR, A., ROSU-FINSEN, A., LASNE, J. & MCCOUSTRA, M. R. 2016. Photodesorption and physical

properties of CO ice as a function of temperature. *Astronomy & Astrophysics,* 589**,** A19.

CARRASCOSA, H., SATORRE, M. Á., ESCRIBANO, B., MARTÍN-DOMÉNECH, R. & MUÑOZ CARO, G. 2023. Physical properties of methanol (CH3OH) ice as a function of temperature: density, infrared band strengths, and crystallization. *Monthly Notices of the Royal Astronomical Society,* 525**,** 2690-2700.

CARTWRIGHT, R. J., HIBBITTS, C. A., HOLLER, B. J., RAUT, U., NORDHEIM, T. A., NEVEU, M., PROTOPAPA, S., GLEIN, C. R., LEONARD, E. J. & ROTH, L. 2025. JWST Reveals Spectral Tracers of Recent Surface Modification on Europa. *The Planetary Science Journal,* 6**,** 125.

CERNICHARO, J., AGÚNDEZ, M., CABEZAS, C., TERCERO, B., MARCELINO, N., PARDO, J. R. & DE VICENTE, P. 2021a. Pure hydrocarbon cycles in TMC-1: Discovery of ethynyl cyclopropenylidene, cyclopentadiene, and indene. *Astronomy & Astrophysics,* 649**,** L15.

CERNICHARO, J., AGÚNDEZ, M., KAISER, R., CABEZAS, C., TERCERO, B., MARCELINO, N., PARDO, J. & DE VICENTE, P. 2021b. Discovery of benzyne, o-C6H4, in TMC-1 with the QUIJOTE line surhydroxylated mineralsCrystallization of CO2 ice and the absence of amorphous CO2 ice in space. *Astronomy & Astrophysics,* 652**,** L9.

CERNICHARO, J., AGÚNDEZ, M., KAISER, R., CABEZAS, C., TERCERO, B., MARCELINO, N., PARDO, J. & DE VICENTE, P. 2021c. Discovery of two isomers of ethynyl cyclopentadiene in TMC-1: Abundances of CCH and CN derivatives of hydrocarbon cycles. *Astronomy & Astrophysics,* 655**,** L1.

CHEUNG, A., RANK, D. M., TOWNES, C., THORNTON, D. D. & WELCH, W. 1968. Detection of N H 3 Molecules in the Interstellar Medium by Their Microwave Emission. *Physical Review Letters,* 21**,** 1701.

CHRISEY, D., BORING, J., PHIPPS, J., JOHNSON, R. & BROWN, W. 1986. Sputtering of molecular gas solids by keV ions. *Nuclear Instruments and Methods in Physics Research Section B: Beam Interactions with Materials and Atoms,* 13**,** 360-364.

CHRISEY, D., BROWN, W. & BORING, J. 1990. Electronic excitation of condensed CO: Sputtering and chemical change. *Surface science,* 225**,** 130-142.

CHUVILIN, A., KAISER, U., BICHOUTSKAIA, E., BESLEY, N. A. & KHLOBYSTOV, A. N. 2010. Direct transformation of graphene to fullerene. *Nature chemistry,* 2**,** 450-453.

CIARAVELLA, A., CHEN, Y.-J., CECCHI-PESTELLINI, C., JIMÉNEZ-ESCOBAR, A., CARO, G. M., CHUANG, K.-J. & HUANG, C.-H. 2016. Chemical evolution of a CO ice induced by soft X-rays. *The Astrophysical Journal,* 819**,** 38.

CIARAVELLA, A., JIMÉNEZ-ESCOBAR, A., CARO, G. M., CECCHI-PESTELLINI, C., CANDIA, R., GIARRUSSO, S., BARBERA, M. & COLLURA, A. 2012. Soft X-ray irradiation of pure carbon monoxide interstellar ice analogues. *The Astrophysical Journal Letters,* 746**,** L1.

CLEMETT, S. J., SANDFORD, S. A., NAKAMURA-MESSENGER, K., HOERZ, F. & MCKAY, D. S. 2010. Complex aromatic hydrocarbons in Stardust samples collected from comet 81P/Wild 2. *Meteoritics & Planetary Science,* 45**,** 701-722.

COLLINGS, M. P., ANDERSON, M. A., CHEN, R., DEVER, J. W., VITI, S., WILLIAMS, D. A. & MCCOUSTRA, M. R. 2004. A laboratory survey of the thermal desorption of astrophysically relevant molecules. *Monthly Notices of the Royal Astronomical Society,* 354**,** 1133-1140.

COOPER, G., KIMMICH, N., BELISLE, W., SARINANA, J., BRABHAM, K. & GARREL, L. 2001. Carbonaceous meteorites as a source of sugar-related organic compounds for the early Earth. *Nature,* 414**,** 879-883.

COTTIN, H., MOORE, M. H. & BÉNILAN, Y. 2003. Photodestruction of relevant interstellar molecules in ice mixtures. *The Astrophysical Journal,* 590**,** 874.

CROVISIER, J., BOCKELÉE-MORVAN, D., BIVER, N., COLOM, P., DESPOIS, D. & LIS, D. C. 2004. Ethylene glycol in comet C/1995 O1 (Hale-Bopp). *Astronomy & Astrophysics,* 418**,** L35-L38.

CRUZ-DIAZ, G., CARO, G. M., CHEN, Y.-J. & YIH, T.-S. 2014. Vacuum-UV spectroscopy of interstellar ice analogs-I. Absorption cross-sections of polar-ice molecules. *Astronomy & Astrophysics,* 562**,** A119.

CUPPEN, H. M., LINNARTZ, H. & IOPPOLO, S. 2024. Laboratory and Computational Studies of Interstellar Ices. *Annual Review of Astronomy and Astrophysics,* 62.

DALLE ORE, C. M., PROTOPAPA, S., COOK, J., GRUNDY, W., CRUIKSHANK, D., VERBISCER, A., ENNICO, K., OLKIN, C., STERN, S. & WEAVER, H. 2018. Ices on Charon: Distribution of figure and NH3 from New Horizons LEISA observations. *Icarus,* 300**,** 21-32.

DALTON, J. 2010. Spectroscopy of icy moon surface materials. *Space science reviews,* 153**,** 219-247.

DANGI, B. B., PARKER, D. S., KAISER, R. I., JAMAL, A. & MEBEL, A. M. 2013. A combined experimental and theoretical study on the gas-phase synthesis of toluene under single collision conditions. *Angewandte Chemie International Edition,* 52.

DANGI, B. B., PARKER, D. S., YANG, T., KAISER, R. I. & MEBEL, A. M. 2014. Gas-Phase Synthesis of the Benzyl Radical (C6H5CH2). *Angewandte Chemie,* 126**,** 4696-4701.

DAWES, A., MUKERJI, R. J., DAVIS, M. P., HOLTOM, P. D., WEBB, S. M., SIVARAMAN, B., HOFFMANN, S. V., SHAW, D. A. & MASON, N. J. 2007. Morphological study into the temperature dependence of solid ammonia under astrochemical conditions using vacuum ultraviolet and Fourier-transform infrared spectroscopy. *The Journal of chemical physics,* 126.

DE BARROS, A., DUARTE, E. S., FARENZENA, L., DA SILVEIRA, E., DOMARACKA, A., ROTHARD, H. & BODUCH, P. 2011. Destruction of CO ice and formation of new molecules by irradiation with 28 keV O6+ ions. *Nuclear Instruments and Methods in Physics Research Section B: Beam Interactions with Materials and Atoms,* 269**,** 852-855.

DE NINNO, A., DEL GIUDICE, E., GAMBERALE, L. & CASTELLANO, A. C. 2013. The structure of liquid water emerging from the vibrational spectroscopy: Interpretation with QED theory. *arXiv preprint arXiv:1310.0635*.

DELITSKY, M. L., PAIGE, D. A., SIEGLER, M., HARJU, E., SCHRIVER, D., JOHNSON, R. & TRAVNICEK, P. 2017. Ices on Mercury: Chemistry of volatiles in permanently cold areas of Mercury's north polar region. *Icarus,* 281**,** 19-31.

DOMARACKA, A., DUARTE, E. S., BODUCH, P., ROTHARD, H., RAMILLON, J.-M., DARTOIS, E., PILLING, S., FARENZENA, L. & DA SILVEIRA, E. F. 2010. Infrared study of astrophysical ice analogues irradiated by swift nickel ions. *Nuclear Instruments and Methods in Physics Research Section B: Beam Interactions with Materials and Atoms,* 268**,** 2960-2963.

DRESSLER, K. & SCHNEPP, O. 1960. Absorption spectra of solid methane, ammonia, and ice in the vacuum ultraviolet. *The Journal of Chemical Physics,* 33**,** 270-274.

DUARTE, E. S., DOMARACKA, A., BODUCH, P., ROTHARD, H., DARTOIS, E. & DA SILVEIRA, E. 2010. Laboratory simulation of heavy-ion cosmic-ray interaction with condensed CO. *Astronomy & Astrophysics,* 512**,** A71.

DULEY, W. & HU, A. 2012. The 217.5 nm band, infrared absorption, and infrared emission features in hydrogenated amorphous carbon nanoparticles. *The Astrophysical Journal,* 761**,** 115.

DUNHAM JR, T. 1937. Interstellar neutral potassium and neutral calcium. *Publications of the Astronomical Society of the Pacific, Vol. 49, No. 287, p. 26-28,* 49**,** 26-28.

EDDINGTON, A. S. 1988. *The internal constitution of the stars*, Cambridge University Press.

EHRENFREUND, P. The Diffuse Interstellar Bands as evidence for polyatomic molecules in the diffuse interstellar medium. American Astronomical Society Meeting Abstracts# 194, 1999. 41.01.

EHRENFREUND, P., BOOGERT, A., GERAKINES, P., JANSEN, D., SCHUTTE, W., TIELENS, A. & VAN DISHOECK, E. 1996. A laboratory database of solid CO and CO_2_ for ISO. *Astronomy and Astrophysics, v. 315, p. L341-L344,* 315**,** L341-L344.

EHRENFREUND, P., SCHUTTE, W., MINH, Y. & VAN DISHOEK, E. Astrochemistry: From molecular clouds to planetary systems. IAU Symp, 2000. 135-46.

ELOWITZ, M., SIVARAMAN, B., HENDRIX, A., LO, J.-I., CHOU, S.-L., CHENG, B.-M., SEKHAR, B. R. & MASON, N. J. 2021. Possible detection of hydrazine on Saturn's moon Rhea. *Science Advances,* 7**,** eaba5749.

EMERY, J., BURR, D., CRUIKSHANK, D., BROWN, R. & DALTON, J. 2005. Near-infrared (0.8–4.0 m) spectroscopy of Mimas, Enceladus, Tethys, and Rhea. *Astronomy & Astrophysics,* 435**,** 353-362.

ENGQUIST, I. & LIEDBERG, B. 1996. D2O Ice on Controlled Wettability Self-Assembled Alkanethiolate Monolayers: Cluster Formation and Substrate– Adsorbate Interaction. *The Journal of Physical Chemistry,* 100**,** 20089-20096.

ENGQUIST, I., LUNDSTRÖM, I., LIEDBERG, B., PARIKH, A. N. & ALLARA, D. L. 1997. Infrared characterization of amorphous and polycrystalline D2O ice on controlled wettability self-assembled alkanethiolate monolayers. *The Journal of chemical physics,* 106**,** 3038-3048.

ESCRIBANO, R. M., MUNOZ CARO, G. M., CRUZ-DIAZ, G. A., RODRÍGUEZ-LAZCANO, Y. & MATÉ, B. 2013. Crystallization of CO2 ice and the absence of amorphous CO2 ice in space. *Proceedings of the National Academy of Sciences,* 110**,** 12899-12904.

FAMÁ, M., LOEFFLER, M., RAUT, U. & BARAGIOLA, R. 2010. Radiation-induced amorphization of crystalline ice. *Icarus,* 207**,** 314-319.

FEDOSEEV, G., CUPPEN, H. M., IOPPOLO, S., LAMBERTS, T. & LINNARTZ, H. 2015. Experimental evidence for glycolaldehyde and ethylene glycol formation by surface hydrogenation of CO molecules under dense molecular cloud conditions. *Monthly Notices of the Royal Astronomical Society,* 448**,** 1288-1297.

FELDMAN, P. Carbon monoxide in cometary ice. Asteroids, Comets, Meteors II, 1986. 263-267.

FELDMAN, P. & BRUNE, W. 1976. Carbon production in comet West 1975n. *Astrophysical Journal, vol. 209, Oct. 1, 1976, pt. 2, p. L45-L48.,* 209**,** L45-L48.

FERRARO, J., SILL, G. & FINK, U. 1980. INFRARED INTENSITY MEASUREMENTS OF CRYODEPOSITED THIN FILMS OF NH3, MH4HS, H2S, AND ASSIGNMENTS OF ABSORPTION BANDS.

FRASER, H. J., COLLINGS, M. P., MCCOUSTRA, M. R. & WILLIAMS, D. A. 2001. Thermal desorption of water ice in the interstellar medium. *Monthly Notices of the Royal Astronomical Society,* 327**,** 1165-1172.

FUENTE, A., CERNICHARO, J., CASELLI, P., MCCOEY, C., JOHNSTONE, D., FICH, M., VAN KEMPEN, T., PALAU, A., YıLDıZ, U. & TERCERO, B. 2014. The hot core towards the intermediate-mass protostar NGC 7129 FIRS 2-Chemical similarities with Orion KL. *Astronomy & Astrophysics,* 568**,** A65.

GAVILAN, L., LE, K. C., PINO, T., ALATA, I., GIULIANI, A. & DARTOIS, E. 2017. Polyaromatic disordered carbon grains as carriers of the UV bump: FUV to mid-infrared spectroscopy of laboratory analogs. *arXiv preprint arXiv:1711.06175*.

GERAKINES, P. & MOORE, M. 2001. Carbon suboxide in astrophysical ice analogs. *Icarus,* 154**,** 372-380.

GERAKINES, P., MOORE, M. & HUDSON, R. 2004. Ultraviolet photolysis and proton irradiation of astrophysical ice analogs containing hydrogen cyanide. *Icarus,* 170**,** 202-213.

GERAKINES, P., SCHUTTE, W. & EHRENFREUND, P. 1996. Ultraviolet processing of interstellar ice analogs. I. Pure ices. *Astronomy and Astrophysics, v. 312, p. 289-305,* 312**,** 289-305.

GERAKINES, P. A., MATERESE, C. K. & HUDSON, R. L. 2023. Carbon monoxide ices–a semicentennial review and update for crystalline CO along with the first IR spectrum and band strength for amorphous CO. *Monthly Notices of the Royal Astronomical Society,* 522**,** 3145-3162.

GONZÁLEZ-ALFONSO, E., FISCHER, J., GRACIÁ-CARPIO, J., STURM, E., HAILEY-DUNSHEATH, S., LUTZ, D., POGLITSCH, A., CONTURSI, A., FEUCHTGRUBER, H. & VEILLEUX, S. 2012. Herschel/PACS spectroscopy of NGC 4418 and Arp 220: H2O, H218O, OH, 18OH, O I, HCN, and NH3. *Astronomy & Astrophysics,* 541**,** A4.

GRIECO, F., DULIEU, F., DE LOOZE, I. & BAOUCHE, S. 2024. Experimental H2O formation on carbonaceous dust grains at temperatures up to 85 K. *Monthly Notices of the Royal Astronomical Society,* 527**,** 10604-10614.

GRIEVES, G. A. & ORLANDO, T. M. 2005. The importance of pores in the electron stimulated production of D2 and O2 in low temperature ice. *Surface science,* 593**,** 180-186.

HAMA, T., ISHIZUKA, S., YAMAZAKI, T., KIMURA, Y., KOUCHI, A., WATANABE, N., SUGIMOTO, T. & PIRRONELLO, V. 2017. Fast crystalline ice formation at extremely low temperature through water/neon matrix sublimation. *Physical Chemistry Chemical Physics,* 19**,** 17677-17684.

HARING, R., HARING, A., KLEIN, F., KUMMEL, A. & DE VRIES, A. 1983. Reactive sputtering of simple condensed gases by keV heavy ion bombardment. *Nuclear Instruments and Methods in Physics Research,* 211**,** 529-533.

HARING, R., PEDRYS, R., OOSTRA, D., HARING, A. & DE VRIES, A. 1984. Reactive sputtering of simple condensed gases by keV ions II: Mass spectra. *Nuclear Instruments and Methods in Physics Research Section B: Beam Interactions with Materials and Atoms,* 5**,** 476-482.

HE, J., TORIELLO, F.E., EMTIAZ, S.M., HENNING, T. & VIDALI, G.2021. Phase traorganinsition of interstellar CO ice. The Astrophysical Journal Letters, 915, L23.

HEGER, M. L. 1922. The spectra of certain class B stars in the regions 5630A-6680A and 3280A-3380A. *Lick Observatory Bulletin,* 10**,** 146-147.

HERBIG, G. H. 1995. The diffuse interstellar bands. *Annual Review of Astronomy and Astrophysics,* 33**,** 19-73.

HILY-BLANT, P., MARET, S., BACMANN, A., BOTTINELLI, S., PARISE, B., CAUX, E., FAURE, A., BERGIN, E., BLAKE, G. & CASTETS, A. 2010. Nitrogen hydrides in the cold envelope of IRAS 16293-2422. *Astronomy & Astrophysics,* 521**,** L52.

HOFMANN, F., ASANOVA, N., URSO, R. G. & ELSAESSER, A. 2025. Exploring the formation and alteration of organics in ice: experimental insights for astrochemistry and space missions. *Earth, Planets and Space,* 77**,** 1-13.

HOFSTADTER, M. D. & MUHLEMAN, D. O. 1989. Latitudinal variations of ammonia in the atmosphere of Uranus: An analysis of microwave observations. *Icarus,* 81**,** 396-412.

HOGERHEIJDE, M. R., BERGIN, E. A., BRINCH, C., CLEEVES, L. I., FOGEL, J. K., BLAKE, G. A., DOMINIK, C., LIS, D. C., MELNICK, G. & NEUFELD, D. 2011. Detection of the water reservoir in a forming planetary system. *Science,* 334**,** 338-340.

HOLLIS, J. M., LOVAS, F. J. & JEWELL, P. R. 2000. Interstellar glycolaldehyde: The first sugar. *The Astrophysical Journal,* 540**,** L107.

HOLLIS, J. M., LOVAS, F. J., JEWELL, P. R. & COUDERT, L. 2002. Interstellar antifreeze: ethylene glycol. *The Astrophysical Journal,* 571**,** L59.

HOLT, J. S., SADOSKAS, D. & PURSELL, C. J. 2004. Infrared spectroscopy of the solid phases of ammonia. *The Journal of chemical physics,* 120**,** 7153-7157.

HOREDT, G. & HUBBARD, W. 1983. Two-and three-layer models of Uranus. *The moon and the planets,* 29**,** 229-236.

HOWE, J. Y., RAWN, C. J., JONES, L. & OW, H. 2003. Improved crystallographic data for graphite. *Powder diffraction,* 18**,** 150-154.

HUANG, C.-H., CIARAVELLA, A., CECCHI-PESTELLINI, C., JIMÉNEZ-ESCOBAR, A., HSIAO, L.-C., HUANG, C.-C., CHEN, P.-C., SIE, N.-E. & CHEN, Y.-J. 2020. Effects of 150–1000 eV electron impacts on pure carbon monoxide ices using the interstellar energetic-process system (IEPS). *The Astrophysical Journal,* 889**,** 57.

HUDSON, R. L., GERAKINES, P. A. & FERRANTE, R. F. 2018. IR spectra and properties of solid acetone, an interstellar and cometary molecule. *Spectrochimica Acta Part A: Molecular and Biomolecular Spectroscopy,* 193**,** 33-39.

HUDSON, R. L., GERAKINES, P. A. & YARNALL, Y. Y. 2022a. Ammonia ices revisited: New IR intensities and optical constants for solid NH3. *The Astrophysical Journal,* 925**,** 156.

HUDSON, R. L. & MOORE, M. H. 2000. IR spectra of irradiated cometary ice analogues containing methanol: a new assignment, a reassignment, and a nonassignment. *Icarus,* 145**,** 661-663.

HUDSON, R. L., MOORE, M. H. & COOK, A. M. 2005. IR characterization and radiation chemistry of glycolaldehyde and ethylene glycol ices. *Advances in Space Research,* 36**,** 184-189.

HUDSON, R. L. & YARNALL, Y. Y. 2022. Infrared spectra and optical constants of astronomical ices: IV. Benzene and pyridine. *Icarus,* 377**,** 114899.

HUDSON, R. L., YARNALL, Y. Y. & GERAKINES, P. A. 2022b. Infrared spectral intensities of amine ices, precursors to amino acids. *Astrobiology,* 22**,** 452-461.

IOPPOLO, S., CUPPEN, H., VAN DISHOECK, E. & LINNARTZ, H. 2011. Surface formation of HCOOH at low temperature. *Monthly Notices of the Royal Astronomical Society,* 410**,** 1089-1095.

ISLAM, F., BARATTA, G. & PALUMBO, M. 2014. Simultaneous UV-and ion processing of astrophysically relevant ices-The case of CH3OH: N2 solid mixtures. *Astronomy & Astrophysics,* 561**,** A73.

JAMIESON, C. S., MEBEL, A. M. & KAISER, R. I. 2006. Understanding the kinetics and dynamics of radiation-induced reaction pathways in carbon monoxide ice at 10 K. *The Astrophysical Journal Supplement Series,* 163**,** 184.

JEFFERY, C. 1995. The ultraviolet properties of cool material ejected by hydrogen-deficient stars. *Astronomy and Astrophysics, v. 299, p. 135,* 299**,** 135.

JONES, B. M., ZHANG, F., KAISER, R. I., JAMAL, A., MEBEL, A. M., CORDINER, M. A. & CHARNLEY, S. B. 2011. Formation of benzene in the interstellar medium. *Proceedings of the National Academy of Sciences,* 108**,** 452-457.

KAISER, R. I. 2002. Experimental investigation on the formation of carbon-bearing molecules in the interstellar medium via neutral− neutral reactions. *Chemical Reviews,* 102**,** 1309-1358.

KAISER, R. I. & HANSEN, N. 2021. An aromatic universe–A physical chemistry perspective. *The Journal of Physical Chemistry A,* 125**,** 3826-3840.

KAŇUCHOVÁ, Z., BODUCH, P., DOMARACKA, A., PALUMBO, M. E., ROTHARD, H. & STRAZZULLA, G. 2017. Thermal and energetic processing of astrophysical ice analogues rich in SO2. *Astronomy & Astrophysics,* 604**,** A68.

KAWAKITA, H. & MUMMA, M. J. 2011. Fluorescence excitation models of ammonia and amidogen radical (NH2) in comets: Application to Comet C/2004 Q2 (Machholz). *The Astrophysical Journal,* 727**,** 91.

KAWAKITA, H. & WATANABE, J.-I. 2002. Revised fluorescence efficiencies of cometary NH2: Ammonia abundance in comets. *The Astrophysical Journal,* 572**,** L177.

KELLY, N. J., BOYNTON, W. V., KERRY, K., HAMARA, D., JANES, D., REEDY, R., KIM, K. J. & HABERLE, R. M. 2006. Seasonal polar carbon dioxide frost on Mars: CO2 mass and columnar thickness distribution. *Journal of Geophysical Research: Planets,* 111.

KHAN, W., RAMACHANDRAN, R., GUPTA, S., MEKA, J., VENKATARAMAN, V., HILL, H., RAJASEKHAR, B., JANARDHAN, P., BHARDWAJ, A. & MASON, N. 2025. Infrared spectroscopy reveals ethylene glycol is an anti crystallizer in water-mixed astrochemical ices. *Life Sciences in Space Research*.

KIEFFER, H. H., CHASE JR, S. C., MARTIN, T. Z., MINER, E. D. & PALLUCONI, F. D. 1976. Martian north pole summer temperatures: Dirty water ice. *Science,* 194**,** 1341-1344.

KIM, T., LEE, J. & LEE, K.-H. 2016. Full graphitization of amorphous carbon by microwave heating. *RSC advances,* 6**,** 24667-24674.

KNACKE, R., MCCORKLE, S., PUETTER, R., ERICKSON, E. & KRÄTSCHMER, W. 1982. Observation of interstellar ammonia ice. *Astrophysical Journal, Part 1, vol. 260, Sept. 1, 1982, p. 141-146.,* 260**,** 141-146.

KOCHERIL, G., ZAGOREC-MARKS, C. & LEWANDOWSKI, H. 2025. Termination of bottom-up interstellar aromatic ring formation at C6H5+. *Nature Astronomy***,** 1-7.

KRASNOPOLSKY, V. A. 2001. Middle ultraviolet spectroscopy of Pluto and Charon. *Icarus,* 153**,** 277-284.

KROTO, H. W., HEATH, J. R., O'BRIEN, S. C., CURL, R. F. & SMALLEY, R. E. 1985. C60: Buckminsterfullerene. *nature,* 318**,** 162-163.

LACY, J., FARAJI, H., SANDFORD, S. & ALLAMANDOLA, L. 1998. Unraveling the 10 micron "silicate" feature of protostars: the detection of frozen interstellar ammonia. *The Astrophysical Journal,* 501**,** L105.

LEBOFSKY, L. A. & FEGLEY JR, M. B. 1976. Laboratory reflection spectra for the determination of chemical composition of icy bodies. *Icarus,* 28**,** 379-387.

LECASBLE, M., REMUSAT, L., VIENNET, J.-C., LAURENT, B. & BERNARD, S. 2022. Polycyclic aromatic hydrocarbons in carbonaceous chondrites can be used as tracers of both pre-accretion and secondary processes. *Geochimica et Cosmochimica Acta,* 335**,** 243-255.

LEE, K. L. K., CHANGALA, P. B., LOOMIS, R. A., BURKHARDT, A. M., XUE, C., CORDINER, M. A., CHARNLEY, S. B., MCCARTHY, M. C. & MCGUIRE, B. A. 2021. Interstellar detection of 2-cyanocyclopentadiene, C5H5CN, a second five-membered ring toward TMC-1. *The Astrophysical Journal Letters,* 910**,** L2.

LEROUX, K., GUILLEMIN, J.-C. & KRIM, L. 2021. Hydrogenation of glycolaldehyde to ethylene glycol at 10 K. *Monthly Notices of the Royal Astronomical Society,* 507**,** 2632-2642.

LINDAL, G. F. 1992. The atmosphere of Neptune-an analysis of radio occultation data acquired with Voyager 2. *Astronomical Journal (ISSN 0004-6256), vol. 103, March 1992, p. 967-982.,* 103**,** 967-982.

LINNARTZ, H., CAMI, J., CORDINER, M., COX, N., EHRENFREUND, P., FOING, B., GATCHELL, M. & SCHEIER, P. 2020. C60+ as a diffuse interstellar band carrier; a spectroscopic story in 6 acts. *Journal of Molecular Spectroscopy,* 367**,** 111243.

LINNARTZ, H., IOPPOLO, S. & FEDOSEEV, G. 2015. Atom addition reactions in interstellar ice analogues. *International Reviews in Physical Chemistry,* 34**,** 205-237.

LOEFFLER, M., BARATTA, G., PALUMBO, M., STRAZZULLA, G. & BARAGIOLA, R. 2005. CO synthesis in solid CO by Lyman-α photons and 200 keV protons. *Astronomy & Astrophysics,* 435**,** 587-594.

LÓPEZ-PUERTAS, M., DINELLI, B. M., ADRIANI, A., FUNKE, B., GARCÍA-COMAS, M., MORICONI, M., D'AVERSA, E., BOERSMA, C. & ALLAMANDOLA, L. J. 2013. Large abundances of polycyclic aromatic hydrocarbons in Titan's upper atmosphere. *The Astrophysical Journal,* 770**,** 132.

LORU, D., CABEZAS, C., CERNICHARO, J., SCHNELL, M. & STEBER, A. L. 2023. Detection of ethynylbenzene in TMC-1 and the interstellar search for 1, 2-diethynylbenzene. *Astronomy & Astrophysics,* 677**,** A166.

LUNA, R., SATORRE, M., SANTONJA, C. & DOMINGO, M. 2014. New experimental sublimation energy measurements for some relevant astrophysical ices. *Astronomy & Astrophysics,* 566**,** A27.

MARKS, J. H., WANG, J., SUN, B.-J., MCANALLY, M., TURNER, A. M., CHANG, A. H.-H. & KAISER, R. I. 2023. Thermal synthesis of carbamic acid and its dimer in interstellar ices: A reservoir of interstellar amino acids. *ACS central science,* 9**,** 2241-2250.

MASON, N. J., DAWES, A., HOLTOM, P. D., MUKERJI, R. J., DAVIS, M. P., SIVARAMAN, B., KAISER, R. I., HOFFMANN, S. V. & SHAW, D. A. 2006 spectroscopy and photo-processing of astrochemical ices: an experimental study. *Faraday discussions,* 133**,** 311-329.

MASON, N. J., NAIR, B., JHEETA, S. & SZYMAŃSKA, E. 2014. Electron induced chemistry: a new frontier in astrochemistry. *Faraday Discussions,* 168**,** 235-247.

MATÉ, B., TANARRO, I., ESCRIBANO, R., MORENO, M. & HERRERO, V. J. 2015. Stability of extraterrestrial glycine under energetic particle radiation estimated from 2 keV electron bombardment experiments. *The Astrophysical Journal,* 806**,** 151.

MATERESE, C. K., CRUIKSHANK, D. P., SANDFORD, S. A., IMANAKA, H. & NUEVO, M. 2015. Ice chemistry on outer solar system bodies: Electron radiolysis of N2-, CH4-, and CO-containing ices. *The Astrophysical Journal,* 812**,** 150.

MATERESE, C. K., CRUIKSHANK, D. P., SANDFORD, S. A., IMANAKA, H., NUEVO, M. & WHITE, D. W. 2014. Ice chemistry on outer solar system bodies: carboxylic acids, nitriles, and urea detected in refractory residues produced from the UV photolysis of N2: CH4: CO-containing ices. *The Astrophysical Journal,* 788**,** 111.

MAURY, A., BELLOCHE, A., ANDRÉ, P., MARET, S., GUETH, F., CODELLA, C., CABRIT, S., TESTI, L. & BONTEMPS, S. 2014. First results from the CALYPSO IRAM-PdBI survey-II. Resolving the hot corino in the Class 0 protostar NGC 1333-IRAS2A. *Astronomy & Astrophysics,* 563**,** L2.

MCCLURE, M. K., ROCHA, W., PONTOPPIDAN, K., CROUZET, N., CHU, L. E., DARTOIS, E., LAMBERTS, T., NOBLE, J., PENDLETON, Y. & PEROTTI, G. 2023. An Ice Age JWST inventory of dense molecular cloud ices. *Nature astronomy,* 7**,** 431-443.

MCGUIRE, B. A., BURKHARDT, A. M., KALENSKII, S., SHINGLEDECKER, C. N., REMIJAN, A. J., HERBST, E. & MCCARTHY, M. C. 2018. Detection of the aromatic molecule benzonitrile (c-C6H5CN) in the interstellar medium. *Science,* 359**,** 202-205.

MCGUIRE, B. A., LOOMIS, R. A., BURKHARDT, A. M., LEE, K. L. K., SHINGLEDECKER, C. N., CHARNLEY, S. B., COOKE, I. R., CORDINER, M. A., HERBST, E. & KALENSKII, S. 2021. Detection of two interstellar polycyclic aromatic hydrocarbons via spectral matched filtering. *Science,* 371**,** 1265-1269.

MCGUIRE, B. A., SHINGLEDECKER, C. N., WILLIS, E. R., BURKHARDT, A. M., EL-ABD, S., MOTIYENKO, R. A., BROGAN, C. L., HUNTER, T. R., MARGULÈS, L. & GUILLEMIN, J.-C. 2017. ALMA detection of interstellar methoxymethanol (CH3OCH2OH). *The Astrophysical journal letters,* 851**,** L46.

MEIER, R., EBERHARDT, P., KRANKOWSKY, D. & HODGES, R. 1994. Ammonia in comet P/Halley. *Astronomy and Astrophysics (ISSN 0004-6361), vol. 287, no. 1, p. 268-278,* 287**,** 268-278.

MELCHER, C., LEPOIRE, D., COOPER, B. & TOMBRELLO, T. 1982. Erosion of frozen sulfur dioxide by ion bombardment: Applications to Io. *Geophysical Research Letters,* 9**,** 1151-1154.

MENNELLA, V., BARATTA, G., COLANGELI, L., PALUMBO, P., ROTUNDI, A., BUSSOLETTI, E. & STRAZZULLA, G. 1997. Ultraviolet spectral changes in amorphous carbon grains induced by ion irradiation. *The Astrophysical Journal,* 481**,** 545.

MENNELLA, V., COLANGELI, L., PALUMBO, P., ROTUNDI, A., SCHUTTE, W. & BUSSOLETTI, E. 1996. Activation of an ultraviolet resonance in hydrogenated amorphous carbon grains by exposure to ultraviolet radiation. *The Astrophysical Journal,* 464**,** L191.

MERINO, P., ŠVEC, M., MARTINEZ, J., JELINEK, P., LACOVIG, P., DALMIGLIO, M., LIZZIT, S., SOUKIASSIAN, P., CERNICHARO, J. & MARTIN-GAGO, J. 2014. Graphene etching on SiC grains as a path to interstellar polycyclic aromatic hydrocarbons formation. *Nature Communications,* 5**,** 3054.

MIFSUD, D. V., HERCZKU, P., RAMACHANDRAN, R., SUNDARARAJAN, P., RAHUL, K., KOVÁCS, S. T., SULIK, B., JUHÁSZ, Z., RÁCZ, R. & BIRI, S. 2024. A systematic mid-infrared spectroscopic study of thermally processed H2S ices. *Spectrochimica Acta Part A: Molecular and Biomolecular Spectroscopy,* 319**,** 124567.

MODICA, P. & PALUMBO, M. 2010. Formation of methyl formate after cosmic ion irradiation of icy grain mantles. *Astronomy & Astrophysics,* 519**,** A22.

MOORE, M. & DONN, B. 1982. The Infrared Spectrum of a Laboratory-Synthesized Residue-Implications for the 3.4-MICRON Interstellar Absorption Feature. *Astrophysical Journal, Vol. 257, P. L47, 1982,* 257**,** L47.

MOORE, M., FERRANTE, R. & NUTH III, J. 1996. Infrared spectra of proton irradiated ices containing methanol. *Planetary and Space Science,* 44**,** 927-935.

MOORE, M. H. 1984. Studies of proton-irradiated SO2 at low temperatures: Implications for lo. *Icarus,* 59**,** 114-128.

MULLIKIN, E., ANDERSON, H., O'HERN, N., FARRAH, M., ARUMAINAYAGAM, C. R., VAN DISHOECK, E. F., GERAKINES, P. A., VASYUNIN, A. I., MAJUMDAR, L. & CASELLI, P. 2021. A new method for simulating photoprocesses in astrochemical models. *The Astrophysical Journal,* 910**,** 72.

MUMMA, M. J. & CHARNLEY, S. B. 2011. The chemical composition of comets—emerging taxonomies and natal heritage. *Annual Review of Astronomy and Astrophysics,* 49**,** 471-524.

NIXON, C. A., BÉZARD, B., CORNET, T., COY, B. P., DE PATER, I., ES-SAYEH, M., HAMMEL, H. B., LELLOUCH, E., LOMBARDO, N. A. & LÓPEZ-PUERTAS, M. 2025. The atmosphere of Titan in late northern summer from JWST and Keck observations. *Nature Astronomy***,** 1-13.

ÖBERG, K. I., GARROD, R. T., VAN DISHOECK, E. F. & LINNARTZ, H. 2009. Formation rates of complex organics in UV irradiated CH3OH-rich ices-I. Experiments. *Astronomy & Astrophysics,* 504**,** 891-913.

ÖBERG, K. I., MURRAY-CLAY, R. & BERGIN, E. A. 2011. The effects of snowlines on C/O in planetary atmospheres. *The Astrophysical Journal Letters,* 743**,** L16.

PAIGE, D. A., SIEGLER, M. A., HARMON, J. K., NEUMANN, G. A., MAZARICO, E. M., SMITH, D. E., ZUBER, M. T., HARJU, E., DELITSKY, M. L. & SOLOMON, S. C. 2013. Thermal stability of volatiles in the north polar region of Mercury. *Science,* 339**,** 300-303.

PALUMBO, M., CASTORINA, A. & STRAZZULLA, G. 1999. Ion irradiation effects on frozen methanol (CH_3OH). *Astronomy and Astrophysics, v. 342, p. 551-562 (1999),* 342**,** 551-562.

PALUMBO, M. & STRAZZULLA, G. 1993. The 2140/cm band of frozen CO-Laboratory experiments and astrophysical applications. *Astronomy and Astrophysics (ISSN 0004-6361), vol. 269, no. 1-2, p. 568-580.,* 269**,** 568-580.

PALUMBO, M. E., LETO, P., SIRINGO, C. & TRIGILIO, C. 2008. Detection of C3O in the low-mass protostar Elias 18. *The Astrophysical Journal,* 685**,** 1033.

PASCOLI, G. & POLLEUX, A. 2000. Condensation and growth of hydrogenated carbon clusters in carbon-rich stars. *Astronomy and Astrophysics, v. 359, p. 799-810 (2000),* 359**,** 799-810.

PAVITHRAA, S., METHIKKALAM, R., GORAI, P., LO, J.-I., DAS, A., SEKHAR, B. R., PRADEEP, T., CHENG, B.-M., MASON, N. & SIVARAMAN, B. 2017.

Qualitative observation of reversible phase change in astrochemical ethanethiol ices using infrared spectroscopy. *Spectrochimica Acta Part A: Molecular and Biomolecular Spectroscopy,* 178**,** 166-170.

PHILLIPS, R. J., DAVIS, B. J., TANAKA, K. L., BYRNE, S., MELLON, M. T., PUTZIG, N. E., HABERLE, R. M., KAHRE, M. A., CAMPBELL, B. A. & CARTER, L. M. 2011. Massive CO2 ice deposits sequestered in the south polar layered deposits of Mars. *Science,* 332**,** 838-841.

PILLING, S., MATEUS, M., OJEDA-GONZÁLEZ, A., FERRÃO, L., GALVÃO, B., BODUCH, P. & ROTHARD, H. 2024. Influence of temperature on the chemical evolution and desorption of pure CO ices irradiated by cosmic-rays analogues. *Monthly Notices of the Royal Astronomical Society,* 528**,** 6075-6098.

PIPES, J., ROUX, J., SMITH, A. & SCOTT, H. 1978. Infrared transmission of contaminated cryocooled optical windows. *AIAA Journal,* 16**,** 984-990.

POSTBERG, F., KHAWAJA, N., ABEL, B., CHOBLET, G., GLEIN, C. R., GUDIPATI, M. S., HENDERSON, B. L., HSU, H.-W., KEMPF, S. & KLENNER, F. 2018. Macromolecular organic compounds from the depths of Enceladus. *Nature,* 558**,** 564-568.

PROTOPAPA, S., RAUT, U., WONG, I., STANSBERRY, J., VILLANUEVA, G. L., COOK, J., HOLLER, B., GRUNDY, W. M., BRUNETTO, R. & CARTWRIGHT, R. J. 2024. Detection of carbon dioxide and hydrogen peroxide on the stratified surface of Charon with JWST. *Nature Communications,* 15**,** 8247.

RAHUL, K., SHIVAKARTHIK, E., MEKA, J., DAS, A., CHANDRASEKARAN, V., RAJASEKHAR, B., LO, J.-I., CHENG, B.-M., JANARDHAN, P. & BHARDWAJ, A. 2020. Residue from vacuum ultraviolet irradiation of benzene ices: Insights into the physical structure of astrophysical dust. *Spectrochimica Acta Part A: Molecular and Biomolecular Spectroscopy,* 231**,** 117797.

RAMACHANDRAN, R., HAZARIKA, A., GUPTA, S., NAG, S., MEKA, J., THAKUR, T. S., YASHONATH, S., VISHWAKARMA, G., CHOU, S.-L. & WU, Y.-J. 2024a. Amorphous 1-propanol interstellar ice beyond its melting point. *Monthly Notices of the Royal Astronomical Society,* 530**,** 1027-1034.

RAMACHANDRAN, R., MEKA, J., RAHUL, K., KHAN, W., LO, J.-I., CHENG, B.-M., MIFSUD, D., RAJASEKHAR, B., DAS, A. & HILL, H. 2024b. Ultraviolet spectrum reveals the presence of ozone on Jupiter's moon Callisto. *Icarus,* 410**,** 115896.

RAMACHANDRAN, R., RAHUL, K., MEKA, J., PAVITHRAA, S., ROY, A., RAJASEKHAR, B., JANARDHAN, P., BHARDWAJ, A., MASON, N. &

SIVARAMAN, B. 2023. Stability and morphology of cyanonaphthalene icy mantles on ISM cold dust analogues. *Journal of Chemical Sciences,* 135**,** 77.

RAMACHANDRAN, R., SIL, M., GORAI, P., MEKA, J., SUNDARARAJAN, P., LO, J.-I., CHOU, S.-L., WU, Y.-J., JANARDHAN, P. & CHENG, B.-M. 2024c. Experimental and Computational Study of Ethanolamine Ices under Astrochemical Conditions. *The Astrophysical Journal,* 975**,** 181.

REDING, F. & HORNIG, D. 1951. The Vibrational Spectra of Molecules and Complex Ions in Crystals. V. Ammonia and Deutero-Ammonia. *The Journal of Chemical Physics,* 19**,** 594-601.

REDING, F. & HORNIG, D. 1954. Vibrational Spectra of Molecules and Complex Ions in Crystals VII. The Raman Spectrum of Crystalline Ammonia and 3-Deutero-Ammonia. *Journal of Chemical Physics,* 22**,** 1926-1928.

REIZER, E., VISKOLCZ, B. & FISER, B. 2022. Formation and growth mechanisms of polycyclic aromatic hydrocarbons: A mini-review. *Chemosphere,* 291**,** 132793.

ROBERTSON, C. W., DOWNING, H. D., CURNUTTE, B. & WILLIAMS, D. 1975. Optical constants of solid ammonia in the infrared. *Journal of the Optical Society of America,* 65**,** 432-435.

ROCHA, W., VAN DISHOECK, E., RESSLER, M., VAN GELDER, M., SLAVICINSKA, K., BRUNKEN, N., LINNARTZ, H., RAY, T., BEUTHER, H. & O GARATTI, A. C. 2024. JWST Observations of Young protoStars (JOYS+): Detecting icy complex organic molecules and ions-I. CH4, SO2, HCOO−, OCN−, H2CO, HCOOH, CH3CH2OH, CH3CHO, CH3OCHO, and CH3COOH. *Astronomy & Astrophysics,* 683**,** A124.

RUBIN, M., ALTWEGG, K., BALSIGER, H., BERTHELIER, J.-J., COMBI, M. R., DE KEYSER, J., DROZDOVSKAYA, M., FIETHE, B., FUSELIER, S. A. & GASC, S. 2019. Elemental and molecular abundances in comet 67P/Churyumov-Gerasimenko. *Monthly Notices of the Royal Astronomical Society,* 489**,** 594-607.

SABBAH, H., BONNAMY, A., PAPANASTASIOU, D., CERNICHARO, J., MARTÍN-GAGO, J.-A. & JOBLIN, C. 2017. Identification of PAH isomeric structure in cosmic dust analogs: the AROMA setup. *The Astrophysical Journal,* 843**,** 34.

SCHMIDT, F., BORRMANN, T., MUES, M. P., BENTER, S., SWIDEREK, P. & BREDEHÖFT, J. H. 2022. Mechanisms of electron-induced chemistry in molecular ices. *Atoms,* 10**,** 25.

SCHMIDT, F., SWIDEREK, P. & BREDEHÖFT, J. H. 2018. Electron-Induced Formation of Ethyl Methyl Ether in Condensed Mixtures of Methanol and Ethylene. *The Journal of Physical Chemistry A,* 123**,** 37-47.

SCHMIDT, F., SWIDEREK, P. & BREDEHÖFT, J. H. 2019. Formation of formic acid, formaldehyde, and carbon dioxide by electron-induced chemistry in ices of water and carbon monoxide. *ACS Earth and Space Chemistry,* 3**,** 1974-1986.

SCHMIDT, F., SWIDEREK, P. & BREDEHÖFT, J. H. 2021a. Electron-induced processing of methanol ice. *ACS Earth and Space Chemistry,* 5**,** 391-408.

SCHMIDT, F., SWIDEREK, P., SCHEELE, T. & BREDEHÖFT, J. H. 2021b. Mechanisms of methyl formate production during electron-induced processing of methanol–carbon monoxide ices. *Physical Chemistry Chemical Physics,* 23**,** 11649-11662.

SCHOU, J., ELLEGAARD, O., BØGESEN, P. & SØRENSEN, H. The erosion of condensed gases by keV electron bombardment. Desorption Induced by Electronic Transitions DIET II: Proceedings of the Second International Workshop, Schloß Elmau, Bavaria, October 15–17, 1984, 1985. Springer, 170-176.

SCHOU, J. & PEDRYS, R. 2001. Sputtering of carbon monoxide ice by hydrogen ions. *Journal of Geophysical Research: Planets,* 106**,** 33309-33314.

SCHRIVER-MAZZUOLI, L., CHAABOUNI, H. & SCHRIVER, A. 2003. Infrared spectra of SO2 and SO2: H2O ices at low temperature. *Journal of molecular structure,* 644**,** 151-164.

SELIGMAN, D. & LAUGHLIN, G. 2020. Evidence that 1I/2017 U1 (‘Oumuamua) was composed of molecular hydrogen ice. *The Astrophysical Journal Letters,* 896**,** L8.

SHULENBERGER, K. E., ZHU, J. L., TRAN, K., ABDULLAHI, S., BELVIN, C., LUKENS, J., PEELER, Z., MULLIKIN, E., CUMBERBATCH, H. M. & HUANG, J. 2019. Electron-induced radiolysis of astrochemically relevant ammonia ices. *ACS Earth and Space Chemistry,* 3**,** 800-810.

SILL, G., FINK, U. & FERRARO, J. R. 1980. Absorption coefficients of solid NH3 from 50 to 7000 cm− 1. *Journal of the Optical Society of America,* 70**,** 724-739.

SIVARAMAN, B., JAMIESON, C. S., MASON, N. J. & KAISER, R. I. 2007. Temperature-dependent formation of ozone in solid oxygen by 5 keV electron irradiation and implications for solar system ices. *The Astrophysical Journal,* 669**,** 1414.

SIVARAMAN, B., RAHUL, K., AMBRESH, M., SAHU, D., MEKA, J., CHOU, S.-L., WU, Y.-J., GUPTA, D., DAS, A. & LO, J.-I. 2023. N-graphene synthesized in astrochemical ices. *The European Physical Journal D,* 77**,** 24.

SIVARAMAN, B., SEKHAR, B. R., NAIR, B., HATODE, V. & MASON, N. 2013. Infrared spectrum of formamide in the solid phase. *Spectrochimica Acta Part A: Molecular and Biomolecular Spectroscopy,* 105**,** 238-244.

SLAVICINSKA, K., TYCHONIEC, Ł., NAVARRO, M. G., VAN DISHOECK, E. F., TOBIN, J. J., VAN GELDER, M. L., CHEN, Y., BOOGERT, A. A., DRECHSLER, W. B. & BEUTHER, H. 2025. HDO ice detected toward an isolated low-mass protostar with JWST. *The Astrophysical Journal Letters,* 986**,** L19.

SLOBODKIN, L., BUYAKOV, I., CESS, R. & CALDWELL, J. 1978. Near infrared reflection spectra of ammonia frost: Interpretation of the upper clouds of Saturn. *Journal of Quantitative Spectroscopy and Radiative Transfer,* 20**,** 481-490.

SMITH, J.-D. T., DRAINE, B., DALE, D. A., MOUSTAKAS, J., KENNICUTT JR, R., HELOU, G., ARMUS, L., ROUSSEL, H., SHETH, K. & BENDO, G. 2007. The mid-infrared spectrum of star-forming galaxies: global properties of polycyclic aromatic hydrocarbon emission. *The Astrophysical Journal,* 656**,** 770.

SNOW, T. P. & MCCALL, B. J. 2006. Diffuse atomic and molecular clouds. *Annu. Rev. Astron. Astrophys.,* 44**,** 367-414.

STAATS, P., MORGAN, H. & GOLDSTEIN, J. 1959. THE INFRARED SPECTRA OF SOLID AMMONIA.

STECHER, T. & DONN, B. 1965. On graphite and interstellar extinction. *Astrophysical Journal, 142, p. 1681, 1965.,* 142**,** 1681.

STEGLICH, M., JÄGER, C., ROUILLÉ, G., HUISKEN, F., MUTSCHKE, H. & HENNING, T. 2010. Electronic spectroscopy of medium-sized polycyclic aromatic hydrocarbons: implications for the carriers of the 2175 Å UV bump. *The Astrophysical Journal Letters,* 712**,** L16.

STRAZZULLA, G., BRUCATO, J., PALUMBO, M. & SATORRE, M. 1997. Is it possible to detect frozen O_2_ and N_2_ on interstellar grains? *Astronomy and Astrophysics, v. 321, p. 618-624,* 321**,** 618-624.

STRUVE, W. S. 1989. *Fundamentals of molecular spectroscopy*, Wiley New York.

SULLIVAN, K. K., BOAMAH, M. D., SHULENBERGER, K. E., CHAPMAN, S., ATKINSON, K. E., BOYER, M. C. & ARUMAINAYAGAM, C. R. 2016. Low-energy (< 20 eV) and high-energy (1000 eV) electron-induced methanol radiolysis of astrochemical interest. *Monthly Notices of the Royal Astronomical Society,* 460**,** 664-672.

SWINGS, P. & ROSENFELD, L. 1937. Considerations regarding interstellar molecules. *Astrophysical Journal, vol. 86, p. 483-486,* 86**,** 483-486.

TAMAI, C., MATÉ, B., CAZAUX, S. & SATORRE, M. Á. 2023. Laboratory experiments on the sublimation of methane through ice dust layers and applications to cometary activity. *Astronomy & Astrophysics,* 675**,** A47.

THEULÉ, P., DUVERNAY, F., DANGER, G., BORGET, F., BOSSA, J., VINOGRADOFF, V., MISPELAER, F. & CHIAVASSA, T. 2013. Thermal

reactions in interstellar ice: A step towards molecular complexity in the interstellar medium. *Advances in Space Research,* 52**,** 1567-1579.

TIELENS, A. 2013. The molecular universe. *Reviews of Modern Physics,* 85**,** 1021-1081.

TIELENS, A. & HAGEN, W. 1982. Model calculations of the molecular composition of interstellar grain mantles. *Astronomy and Astrophysics, vol. 114, no. 2, Oct. 1982, p. 245-260. Research supported by the Nederlandse Organisatie voor Zuiver-Wetenschappelijk Onderzoek.,* 114**,** 245-260.

TOSI, F., MURA, A., COFANO, A., ZAMBON, F., GLEIN, C. R., CIARNIELLO, M., LUNINE, J. I., PICCIONI, G., PLAINAKI, C. & SORDINI, R. 2024. Salts and organics on Ganymede's surface observed by the JIRAM spectrometer onboard Juno. *Nature Astronomy,* 8**,** 82-93.

TROTTIER, A. & BROOKS, R. L. 2004. Carbon-chain oxides in proton-irradiated CO ice films. *The Astrophysical Journal,* 612**,** 1214.

VAN'T HOFF, M. L. & BERGNER, J. B. 2024. Protoplanetary disk chemistry and structure. *arXiv preprint arXiv:2410.23235*.

VAN DISHOECK, E. F., HERBST, E. & NEUFELD, D. A. 2013. Interstellar water chemistry: from laboratory to observations. *Chemical Reviews,* 113**,** 9043-9085.

WALSH, C., LOOMIS, R. A., ÖBERG, K. I., KAMA, M., VAN'T HOFF, M. L., MILLAR, T. J., AIKAWA, Y., HERBST, E., WEAVER, S. L. W. & NOMURA, H. 2016. First detection of gas-phase methanol in a protoplanetary disk. *The Astrophysical Journal Letters,* 823**,** L10.

WARNEKE, J., WANG, Z., SWIDEREK, P. & BREDEHÖFT, J. H. 2015. Electron-Induced Hydration of an Alkene: Alternative Reaction Pathways. *Angewandte Chemie International Edition,* 54**,** 4397-4400.

WATANABE, N. & KOUCHI, A. 2008. Ice surface reactions: A key to chemical evolution in space. *Progress in Surface Science,* 83**,** 439-489.

WENZEL, G., COOKE, I. R., CHANGALA, P. B., BERGIN, E. A., ZHANG, S., BURKHARDT, A. M., BYRNE, A. N., CHARNLEY, S. B., CORDINER, M. A. & DUFFY, M. 2024a. Detection of interstellar 1-cyanopyrene: A four-ring polycyclic aromatic hydrocarbon. *Science,* 386**,** 810-813.

WENZEL, G., SPEAK, T. H., CHANGALA, P. B., WILLIS, R. H., BURKHARDT, A. M., ZHANG, S., BERGIN, E. A., BYRNE, A. N., CHARNLEY, S. B. & FRIED, Z. T. 2024b. Detections of interstellar 2-cyanopyrene and 4-cyanopyrene in TMC-1. *arXiv preprint arXiv:2410.00670*.

WENZEL, G., SPEAK, T. H., CHANGALA, P. B., WILLIS, R. H., BURKHARDT, A. M., ZHANG, S., BERGIN, E. A., BYRNE, A. N., CHARNLEY, S. B. & FRIED,

Z. T. 2025. Detections of interstellar aromatic nitriles 2-cyanopyrene and 4-cyanopyrene in TMC-1. *Nature Astronomy,* 9**,** 262-270.

WHITTET, D., LONGMORE, A. & MCFADZEAN, A. 1985. Solid CO in the Taurus dark clouds. *Monthly Notices of the Royal Astronomical Society,* 216**,** 45P-50P.

WHITTET, D. C., BODE, M., LONGMORE, A., ADAMSON, A., MCFADZEAN, A., AITKEN, D. & ROCHE, P. 1988. Infrared spectroscopy of dust in the Taurus dark clouds: ice and silicates. *Monthly Notices of the Royal Astronomical Society,* 233**,** 321-336.

WILSON, R., JEFFERTS, K. & PENZIAS, A. 1970. Carbon monoxide in the Orion nebula. *Astrophysical Journal, vol. 161, p. L43,* 161**,** L43.

WOLFF, H., ROLLAR, H. G. & WOLFF, E. 1971. Infrared spectra and vapor pressure isotope effect of crystallized ammonia and its deuterium derivatives. *The Journal of Chemical Physics,* 55**,** 1373-1378.

YAN, W., HE, W.-Y., CHU, Z.-D., LIU, M., MENG, L., DOU, R.-F., ZHANG, Y., LIU, Z., NIE, J.-C. & HE, L. 2013. Strain and curvature induced evolution of electronic band structures in twisted graphene bilayer. *Nature communications,* 4**,** 2159.

ZANCHET, A., RODRÍGUEZ-LAZCANO, Y., GÁLVEZ, Ó., HERRERO, V. J., ESCRIBANO, R. & MATÉ, B. 2013. Optical constants of NH3 and NH3: N2 amorphous ices in the near-infrared and mid-infrared regions. *The Astrophysical Journal,* 777**,** 26.

ZEICHNER, S. S., APONTE, J. C., BHATTACHARJEE, S., DONG, G., HOFMANN, A. E., DWORKIN, J. P., GLAVIN, D. P., ELSILA, J. E., GRAHAM, H. V. & NARAOKA, H. 2023. Polycyclic aromatic hydrocarbons in samples of Ryugu formed in the interstellar medium. *Science,* 382**,** 1411-1416.

ZHANG, F., JONES, B., MAKSYUTENKO, P., KAISER, R. I., CHIN, C., KISLOV, V. V. & MEBEL, A. M. 2010. Formation of the phenyl radical [C6H5 (X2A1)] under single collision conditions: a crossed molecular beam and ab initio study. *Journal of the American Chemical Society,* 132**,** 2672-2683.

ZHANG, F., PARKER, D., KIM, Y. S., KAISER, R. I. & MEBEL, A. M. 2011. On the formation of ortho-benzyne (o-C6H4) under single collision conditions and its role in interstellar chemistry. *The Astrophysical Journal,* 728**,** 141.

ZHAO, L., PRENDERGAST, M. B., KAISER, R. I., XU, B., ABLIKIM, U., AHMED, M., SUN, B. J., CHEN, Y. L., CHANG, A. H. & MOHAMED, R. K. 2019. Synthesis of polycyclic aromatic hydrocarbons by phenyl addition–dehydrocyclization: The third way. *Angewandte Chemie,* 131**,** 17603-17611.

ZHENG, W., JEWITT, D. & KAISER, R. I. 2007. Electron irradiation of crystalline and amorphous D2O ice. *Chemical physics letters,* 435**,** 289-294.

ZHENG, W., JEWITT, D., OSAMURA, Y. & KAISER, R. I. 2008. Formation of nitrogen and hydrogen-bearing molecules in solid ammonia and implications for solar system and interstellar ices. *The Astrophysical Journal,* 674**,** 1242.

ZHENG, W. & KAISER, R. I. 2007. An infrared spectroscopy study of the phase transition in solid ammonia. *Chemical physics letters,* 440**,** 229-234.

ZHU, C., FRIGGE, R., BERGANTINI, A., FORTENBERRY, R. C. & KAISER, R. I. 2019. Untangling the formation of methoxymethanol (CH3OCH2OH) and dimethyl peroxide (CH3OOCH3) in star-forming regions. *The Astrophysical Journal,* 881**,** 156.

List of Publications:

Publication included in the thesis

1."Infrared spectroscopy reveals ethylene glycol is an anti-crystallizer in water mixed astrochemical ices," W. Khan, R Ramachandran, S Gupta, JK Meka, V Venkatraman, H Hill, BN Rajasekhar, P Janardhan, Anil Bhardwaj, NJ Mason, B Sivaraman , *Life Sciences in Space Research*, 2025.

doi- https://doi.org/10.1016/j.lssr.2025.01.006

2."Irradiation of condensed CO reveals a new pathway for the formation of aro matic molecules in astrochemical ices," W. Khan, R Ramachandran, S Gupta, JK Meka, V Venkatraman, BN Rajasekhar, P Janardhan, Anil Bhardwaj, NJ Mason, B Sivaraman , *Life Sciences in Space Research*, 2025.

doi- https://doi.org/10.1016/j.lssr.2025.09.007

3. "Water ice formation above its sublimation temperature in astrochemical conditions" W. Khan, R Ramachandran, S Gupta, JK Meka, P Janardhan, Anil Bhardwaj, NJ Mason, B Sivaraman- Under preparation

4. "Revisiting Ammonia ice: Resolving the Phase Debate Using Mid-IR Spectroscopy"- Ganapathy S, R Ramachandran, **W Khan**, S Gupta, J K Meka, B N Rjasekhar, P Janardhan, Anil Bhardwaj, N J Mason, B Sivaraman - **Under Preparation**

Other publications (not included in the thesis)

1. "Ultraviolet spectrum reveals the presence of ozone on Jupiter's moon Callisto", R Ramachandran, JK Meka, KK Rahul, W. Khan, J-I Lo, B-M Cheng, DV Mifsud,

BN Rajasekhar, A Das, H Hill, P Janardhan, Anil Bhardwaj, NJ Mason, B Sivaraman Icarus 410 (2024)115896

doi- https://doi.org/10.1016/j.icarus.2023.115896

International scientific visit

1. DLR Planetary Spectroscopy Laboratory, Berlin, Germany." to carry out spectroscopy of shock processed planetary analogues mimicking impact events on the surface of Mercury- 9-13 October 2023

2. National Synchrotron Radiation Research don (NSRRC),Taiwan." to carry out VUV and electron irradiation experiments on astrochemical ices, 18 May-10 June 2024

Papers presented in conferences

1. Oral presentation titled "Understanding the Effects of Ethylene Glycol on Cometary Water" in 53rd Lunar and Planetary Science Conference (LPSC) 2022, in Texas, USA, 7-11 March 2022, organised by Lunar and Planetary Institute and NASA jointly at The Woodlands, Texas (online mode).
2. Oral presentation titled "EFFECT OF ETHYLENE GLYCOL ON COMETARY WATER" in 3rd Indian Planetary Science Conference (IPSC-2022) in PRL, Ahmedabad 14-16 March 2022, organised by Physical Research Laboratory at Ahmedabad (online mode).
3. Poster presentation titled "An anti-crystallizer in the solar system and in the ISM – icy ethylene glycol" Spectroscopy and Dynamics of Molecules and Clusters (SDMC 2022) in Malpe, Karnataka, 10-13 November 2022 organised by IIIT Hyderabad, IIT Hyderabad, TIFR Hyderabad (offline mode).

4. Poster presentation titled “Physico-chemical investigation of ethylene glycol at low temperatures and its astrophysical implications” in XXXXI conference of the Indian Council of Chemists (ICC), in Agra, 27-29 December - 2022 at Dr. Bhimrao Ambedkar University, Agra (offline mode).
5. Poster presentation titled “THE ROLE OF ETHYLENE GLYCOL AS AN ANTICRYSTALLIZER IN ASTROCHEMICAL CONDITIONS” in National Conference on Atomic and Molecular Physics (NCAMP 23), in IIST Thirvananthapuram, 20-23 February 2023, organised by IIST Thiruvananthapuram (offline mode).
6. Oral presentation titled “Mid-IR spectroscopy of pure phenylacetylene at low temperature” in Meteoroid, Meteor, Meteorites: Messenger from Space (MetMeSS), in PRL, Ahmedabad, 1-3 November 2023, organised by PRL Ahmedabad (offline mode).
7. Poster presentation titled “Dirty cometary nucleus containing diols can carry water ice close to the Sun” in 60th Annual Convention of Chemists 2023, in IIT Delhi, 20-21 December 2023, organised by IIT Delhi (offline mode).
8. Poster presentation titled “Molecules containing two OH ends prevent water ice from crystallizing -implications to cometary and ISM ices” in National Space Science Symposium 2024, in Goa, 25 February-1 March 2024, organised by the University of Goa (offline mode).
9. Poster presentation titled “Mid-IR spectroscopy of phenylacetylene at low temperature -implications to cometary and ISM ices” in National Space Science Symposium 2024, in Goa, 25 February-1 March 2024, organised by the University of Goa (offline mode).

10. Oral presentation titled “FORMATION OF WATER ICE AT 200 K AS A RESULT OF HYDROGEN BONDING BETWEEN DIOLS AND WATER.” in Meteoroid, Meteor, Meteorites: Messenger from Space (4th MetMeSS), in PRL Ahmedabad, 20-22 November 2024, organised by PRL Ahmedabad (offline mode).
11. Oral presentation titled “FORMATION OF WATER ICE AT 200 K - A RESULT OF HYDROGEN BONDING BETWEEN DIOLS AND WATER” in National Conference on Atomic and Molecular Physics (NCAMP 25), in IIT Dhanbad, 08-11 January 2025, organised by IIT (ISM) Dhanbad (offline mode).
12. Oral presentation titled “Energetic processing of CO reveals a new pathway fot the formation of aromatic molecules at low temperature” in 6th Indian Planetary Science Conference (IPSC-2025), in IIT Roorkee, 4-7 March 2025, organised by Indian Institute of Technology (IIT) Roorkee (offline mode).

Awards

Early Career researcher award by the Indian Planetary Science Association (IPSA) for the oral presentation “Energetic processing of CO reveals a new pathway fot the formation of aromatic molecules at low temperature” in 6th Indian Planetary Science Conference (IPSC-2025), in IIT Roorkee, 4-7 March 2025, organised at Indian Institute of Technology (IIT) Roorkee.